Faculty of Engineering – Porto University

Production of solid lipid nanoparticles (SLN) and nanostructured lipid carriers (NLC) containing antitumoral drug (saquinavir)

FINAL VERSION

Ana Rita dos Santos Azevedo

Dissertation presented according to the requirements for the degree in
MASTER IN BIOMEDICAL ENGINEERING

Supervisor: Prof. Paulo Jorge Costa
Co-supervisor: Prof. Domingos Ferreira

October 21, 2015

U.PORTO
FEUP FACULDADE DE ENGENHARIA UNIVERSIDADE DO PORTO

MEB - MESTRADO EM ENGENHARIA BIOMÉDICA | **2014/2015**

A Dissertação intitulada

"Production of Solid Lipid Nanoparticles (SLN) and Nanostructured Lipid Carriers (NLC) containing antitumoral drug (saquinavir)"

foi aprovada em provas realizadas em 21-10-2015

o júri

Presidente Professor Doutor Jorge Alves da Silva
Professor Auxiliar do Departamento de Engenharia Informática da Faculdade de Engenharia da U. Porto

Doutor Bruno Filipe Carmelino Cardoso Sarmento
Investigador do Instituto de Engenharia Biomédica da U. Porto

Professor Doutor Paulo Jorge Cardoso da Costa
Professor Associado do Departamento de Ciências do Medicamento da Faculdade de Farmácia da U. Porto

O autor declara que a presente dissertação (ou relatório de projeto) é da sua exclusiva autoria e foi escrita sem qualquer apoio externo não explicitamente autorizado. Os resultados, ideias, parágrafos, ou outros extratos tomados de ou inspirados em trabalhos de outros autores, e demais referências bibliográficas usadas, são corretamente citados.

Autor - Ana Rita dos Santos Azevedo

Faculdade de Engenharia da Universidade do Porto

Abstract

The blood-brain barrier (BBB) is a limiting barrier to the passage of a large number of drugs, particularly antitumoral drugs. This is mainly due to the tight junctions between the endothelial cells lining the blood vessels of the brain. Inevitably, this barrier makes these drugs ineffective on the treatment of brain tumors, since they cannot diffuse freely across this barrier. Glioblastoma (GBM) is the most common and most malignant form of primary brain tumors, with relatively short survival rate (9-12 months). There have been several attempts to overcome the BBB and nanotechnology emerges as leading solution. By developing colloidal delivery systems such as solid lipid nanoparticles (SLNs) and nanostructured lipid carriers (NLCs), new boundaries have been opened to improve the delivery of drugs. These nanoparticles are non-toxic, biodegradable, with high loading capacity of lipophilic drugs and increased bioavailability in target cells.

The main goal of this Master's thesis project was to develop, characterize and optimize SLNs and NLCs containing saquinavir (SQV-SLNs and SQV-NLCs). SQV is a lipophilic and poorly water soluble HIV protease inhibitor, also used as a potent antitumoral agent efficient against numerous tumor cell lines *in vitro* and *in vivo*.

The nanoparticles were produced by hot high-pressure homogenization and ultrasonication techniques with different lipid (5% and 10%), surfactant (1%, 2% and 3%) and drug (0.05% and 0.1%) concentrations and physically characterized in order to assess which ones are the most efficient and that best meet the desired requirements. The size, polydispersity, zeta potential and stability (LD, DLS and ELS), encapsulation efficiency (HPLC) and thermodynamic behavior (DSC) of SLNs and NLCs were also tested. The formulations with lipid 5%, polysorbate 2% and drug 0.05%, produced by ultrasonication, were the most promising. The final diameter and zeta potential of the tested SQV-SLNs and SQV-NLCs were ~ 200 nm and ~ -24 mV, respectively. Encapsulation efficiency greater than 90% was obtained for the two types of nanoparticles. The drug was solubilized in the lipid both in SQV-SLNs and the SQV-NLCs, because there were not any drug fusion events as showed by the DSC technique.

In order to assess the cell response to a drug and the vehicle carrying it, cell viability and cytotoxicity assays were performed. NLC showed better behavior, with a low cytotoxicity compared with SLN.

If on one hand the SLNs showed a good stability of the suspension while keeping the same size throughout the investigation period, the NLCs showed good stability of matrix with high encapsulation efficiency and fewer losses of the drug over time. Furthermore, cytotoxicity and viability studies also showed the most promising results for this type of lipid nanoparticles.

Key words: Brain Tumor, Glioblastoma, Blood-Brain Barrier, HIV Protease Inhibitors, Saquinavir, Lipid Nanoparticles, Solid Lipid Nanoparticles, Nanostructured Lipid Carriers

Resumo

A barreira hematoencefálica (BHE) é uma barreira que limita a passagem de um grande número de fármacos, particularmente fármacos anti-tumorais. Isto deve-se, principalmente, às junções apertadas entre as células endoteliais que revestem os vasos sanguíneos do cérebro. Inevitavelmente, esta barreira faz com que esses fármacos sejam ineficazes no tratamento de tumores cerebrais, uma vez que não se conseguem difundir livremente através desta barreira. O glioblastoma (GBM) é a forma mais comum e maligna dos tumores cerebrais primários, com uma taxa de sobrevivência relativamente curta (9-12 meses). Houve já várias tentativas de superar a BHE e a nanotecnologia surge como uma solução promissora. Através do desenvolvimento de formas farmacêuticas coloidais, como são as nanopartículas lipídicas sólidas (NLS) e os transportadores lipídicos nanoestruturados (TLN), novas fronteiras foram abertas para melhorar a libertação de fármacos. Estas nanopartículas são não-tóxicas, biodegradáveis, com alta capacidade de carga de drogas lipofílicas e a sua biodisponibilidade é aumentada para as células alvo.

O principal objetivo deste projeto de tese de mestrado foi desenvolver, caracterizar e otimizar NLS e TLN contendo saquinavir (SQV-NLS e SQV-TLN). O SQV é um inibidor de protease de VIH lipofílico e pouco solúvel em água, também usado como um potente agente anti-tumoral eficaz contra várias linhas celulares *in vitro* e *in vivo*.

As nanopartículas foram produzidas pelas técnicas de homogeneização de alta pressão a quente e ultrassonicação, com diferentes concentrações de lípido (5% e 10%), tensioactivo (1%, 2% e 3%) e fármaco (0,05% e 0,10%) e caracterizadas fisicamente de modo a avaliar quais as mais eficientes e que melhor atendem aos requisitos desejados. O tamanho, índice de polidispersão, potencial zeta e estabilidade (LD, DLS e ELS), eficiência de encapsulação (HPLC) e comportamento termodinâmico (DSC) das NLS e TLN, também, foram testados. As formulações com 5% de lípido, 2% de polissorbato e 0,05% de fármaco, produzidas por ultrassonicação, foram as mais promissoras. O diâmetro e potencial zeta finais das SQV-NLS e SQV-TLN testadas foi de ~200 nm e ~24 mV. Uma eficiência de encapsulação maior do que 90% foi obtida para os dois tipos de nanopartículas. O fármaco foi solubilizado na matriz lipídica, tanto nas SQV-NLS como nas SQV-TLN, uma vez que não houve quaisquer eventos de fusão de droga na técnica DSC.

A fim de avaliar a resposta celular a um fármaco e ao "veículo" que a transporta, foram realizados ensaios de viabilidade e citotoxicidade celular. As TLNs apresentaram melhor comportamento, com uma baixa citotoxicidade em comparação às NLSs.

Se por um lado, as NLSs mostraram uma boa estabilidade de suspensão, mantendo o mesmo tamanho durante todo o período de investigação, as TLNs mostraram boa estabilidade de matriz com alta eficiência de encapsulação e menos perdas de droga ao longo do tempo. Além disso, os

estudos de citotoxicidade e de viabilidade também mostraram resultados mais promissores para este tipo de nanopartículas lipídicas.

Palavras-chave: Tumores cerebrais, glioblastoma, barreira hematoencefálica, inibidores de protease de VIH, saquinavir, nanopartículas lipídicas, nanopartículas lipídicas sólidas, transportadores lipídicos nanoestruturados

Agradecimentos

Durante o desenvolvimento desta tese várias foram as pessoas que, de forma direta ou indireta, contribuíram para que o trabalho fosse proveitoso, quer ao nível científico quer pessoal.

Em primeiro lugar, um agradecimento muito especial ao professor Paulo Costa pela ajuda incansável na compreensão teórica e prática dos diversos equipamentos e *software*, necessários ao desenvolvimento do trabalho. Obrigada pelos conselhos, disponibilidade e ajuda na resolução de problemas próprios de uma investigação científica. Obrigada, ainda, pela dedicação e tempo disponibilizados na leitura deste documento.

Ao professor Domingos Ferreira agradeço o acolhimento, boa disposição, ajuda e incentivo. Muito agradecida por ter sido incansável na resolução de problemas primordiais para o sucesso deste trabalho.

À Doutora Cláudia Marques agradeço a hospitalidade recebida, os conselhos dados e o conhecimento partilhado em várias áreas.

Um muito obrigada às meninas do laboratório, Marlene, Gabriela, Verónica, Rita, Ana Cláudia e Rachel, pelos momentos de boa disposição e descompressão necessários em alturas de maior *stress*.

Às minhas amigas de todos os momentos, Vanessa, Maria, Rita e especialmente à Paula, agradeço pelos momentos de incentivo, diversão e por serem muitas vezes um escape. Vocês são especiais. Obrigada ao Nuno e à Tânia pela sua amizade e por saber que posso contar sempre com eles.

Um agradecimento especial à minha irmã, a minha inspiração, por ser a personificação de persistência, determinação, profissionalismo e sacrifício. É, de facto, o exemplo a seguir.

Finalmente aos meus pais pelo apoio incondicional e pela confiança que depositam em mim todos os dias. Por serem o meu pilar na vida e durante este percurso, que nem sempre foi fácil. Obrigada pela paciência e incentivo extra, muitas vezes fundamental.

A todos aqueles que de alguma forma me ajudaram nesta viagem e que, por algum motivo, me tenha esquecido, obrigada!

Index of contents

x

Index of figures

Index of tables

Abbreviations

ABC	adenosine triphosphate-binding cassette
ACN	acetonitrile
AIDS	acquired immunodeficiency syndrome
Akt	protein kinase B (PKB)
AMT	adsorption-mediated transcytosis
ApoE	apolipoprotein E
BBB	blood-brain barrier
BCRP	breast cancer resistance protein
BCS	Biopharmaceutical Classification System
bFGF	basic fibroblasts growth factor
BMEC	brain microvascular endothelial cells
CMT	carrier-mediated transport
CNS	central nervous system
CP	cetyl palmitate
CV	coefficient of variation
DAD	diode array detector
DLS	dynamic light scattering
DMEM	dulbecco's modified eagle's medium
DMSO	dimethyl sulfoxide
DPBS	dulbecco's phosphate buffered saline
DSC	differential scanning calorimetry
EAAT	excitatory amino acid transporters
ECM	extracellular matrix
EDTA	ethylenediamine tetraacetic acid
EE	encapsulation efficiency
ELS	electrophoretic light scattering
EPR	enhanced permeability and restraint
FBS	fetal bovine serum
FDA	US Food and Drug Administration
GBM	glioblastoma multiforme
GLUT	glucose transporter
GRAS	generally recognized as safe
HAART	highly active antiretroviral therapy
HIV	human immunodeficiency virus
HIV-PI	HIV protease inhibitor
HPH	high pressure homogenization
HPLC	high performance liquid chromatography
ICH	International Conference on Harmonisation
IFN	interferon
IκBα	nuclear factor of kappa light polypeptide gene enhancer in B-cells inhibitor, alpha
IL	interleukin
IV	intravenous
KS	Kaposi's sarcoma
LAT	L-system for large neutral amino acids transporter
LD	Laser diffraction
LDL	low density lipoprotein
LN	lipid nanoparticle
M	miglyol 812
MDR	multidrug resistance protein
MCP	monocyte chemoattractant protein
MMP	matrix metalloproteinases
MOAT	multi-organic anion transporters
MRP	multidrug resistance-associated protein family
NFκB	nuclear factor kappa-light-chain-enhancer of activated B cells

NLC	nanostructured lipid carriers
OAT	organic anion transporter
OATP	organic anion transport polypeptides
P-gp	P-glycoprotein
PI	polydispersity index
PI	propidium iodide (cell culture)
PKC	protein kinase C
RES	reticuloendothelial system
RI	recrystallization index
RMT	receptor-mediated transcytosis
RSS	residuals squared sum
SC	subcutaneous
SEM	scanning electron microscopy
SLN	solid lipid nanoparticles
SM	supercooled melts
SQV	saquinavir
SQV-NLC	saquinavir-loaded nanostructured lipid carriers
SQV-SLN	saquinavir-loaded solid lipid nanoparticles
T	tween 80
TEER	transendothelial electrical resistance
TJ	tight junctions
TNF	tumor necrosis factor
VEGF	vascular endothelial growth factor
WHO	World Health Organization
ZP	zeta potential

Chapter I - Motivation and objectives

Saquinavir, in addition to its function as an HIV protease inhibitor, in the last decades has shown its vast potential in combating various types of cancer. Its effect on important diseases such as cancer and HIV, increase its interest in the scientific research. However, this drug administered in its free form has a poor bioavailability, low solubility and is rapidly metabolized losing its therapeutic activity. Considering this, saquinavir shown to be ineffective in the treatment of brain cancers and neurological complications associated with HIV, due to the fact that blood-brain barrier almost impermeable to this drug.

In this context, the aim of this work was to develop saquinavir-loaded lipid nanoparticles able to overcome the blood-brain barrier (BBB), taking advantage of the anti-tumor effects of this drug. Lipid nanoparticles were used in this study, because are known to be promising delivery systems for some drugs enhancing theirs brain uptake. To reach this goal, these nanoparticles were optimized to obtain particles with diameters in the order of 200 nm, optimal size for penetration through the BBB. The size, zeta potential, encapsulation efficiency and thermal behavior were studied and changes of its properties evaluated over several weeks. In addition, *in vitro* assays to assess the cytotoxicity of nanoparticles were made.

Chapter II – Introduction

2.1. Glioblastoma multiforme

Brain tumor includes a diverse set of intracranial neoplasms and is the leading cause of cancer-related death in patients younger than 35 years. Half of all primary brain tumors arise from cells in the brain (intrinsic injuries), while the remaining originate in the meninges or nerves (extrinsic injuries). A larger part of primary intrinsic tumors arise from glial cells (astrocytes, oligodendrocytes and ependymal cells) [1]. These tumors are classified as glioma. According to the *World Health Organization* (WHO) the gliomas are organized in different levels, based on histopathologic features [2, 3], ranging from the grade I which is the variant with slower growth until grade IV which is the most malignant form characterized by cellular atypia, high mitotic index, growth and infiltration diffuse, apoptosis resistance, high genomic instability, tendency for recurrence, necrosis and neovascularization [2-4].

Glioblastoma multiforme (GBM) is a grade IV malignant glioma originating from astrocytes. These tumors are associated with a poor prognosis due to its rapid growth, it is locally aggressive inside the central nervous system (CNS), tumor cells infiltrate deep into the brain itself. However, very rarely metastasizes outside the brain, unlike most of other types of tumors, although it has highly robust angiogenic and invasive capacities [2, 5]. Another distinctive feature is the histopathology and genetic heterogeneity within the tumor itself [5].

GBM is the most common central nervous system (CNS) primary neoplasms in adults (40% [6]) and the most deadly. Patients rarely live more than two years, even with aggressive treatment which often involves devastating neurological consequences [2]. The median survival of GBM patients is known to be about 4 months without therapy, 15 months with standard therapy and with 3 to 5% of patients with GBM surviving five years after diagnosis [3, 7]. It is a disease with a rapid clinical progression, which relapses almost in all cases [8].

2.1.1. Conventional treatment

Despite advances and extensive research on new approaches, current treatments are limited and include the maximum safe surgical removal followed by radiotherapy and chemotherapy to treat infiltrative peripheral tumor mass not removed [2, 9, 10]. Chemotherapy and radiotherapy may be more effective when the minimal residual disease is present. However, the complete neurosurgical resection of these tumors is impossible due to its infiltrating nature [3]. On the other hand, the impressive cellular and genetic heterogeneity within the GBMs, limits the treatment and most of the cells appear to be resistant to radiotherapy [3, 5]. Also, systemic chemotherapy is not fully effective, due to several factors: (i) aggressive local spread of the tumor and high risk of relapse [10]; (ii) non-selective therapy, in addition to the invading cells the healthy brain tissue is also damaged [11]; (iii) most antitumor agents cannot cross the BBB,

which regulates trafficking of substances between the blood flow and the CNS [4]; (iv) very short-range diffusion of drugs in the brain, distant brain areas cannot be reached [4]; (v) drug resistance [9, 11]; (vi) bioavailability of drugs in the tumor tissue is limited and larger doses are required, leading to increased toxicity to normal cells [9, 11]. Additionally, (vii) BBB efflux proteins across, such as p-glycoprotein and ABC, known to actively pump chemotherapeutic agents outside the CNS, affect the therapeutic [5].

2.2. Tumor effects of HIV protease inhibitors

Sir James W. Black, pharmacologist and Nobel Prize for Medicine (1988), said that *the most fruitful basis of the discovery of a new drug is to start with an old drug* [12]. The development of new treatments for cancer is slow (on average 15 years) and extremely costly (on average $800 million) and so it is with great enthusiasm that researchers look for anti-HIV drugs as potential anticancer drugs [12].

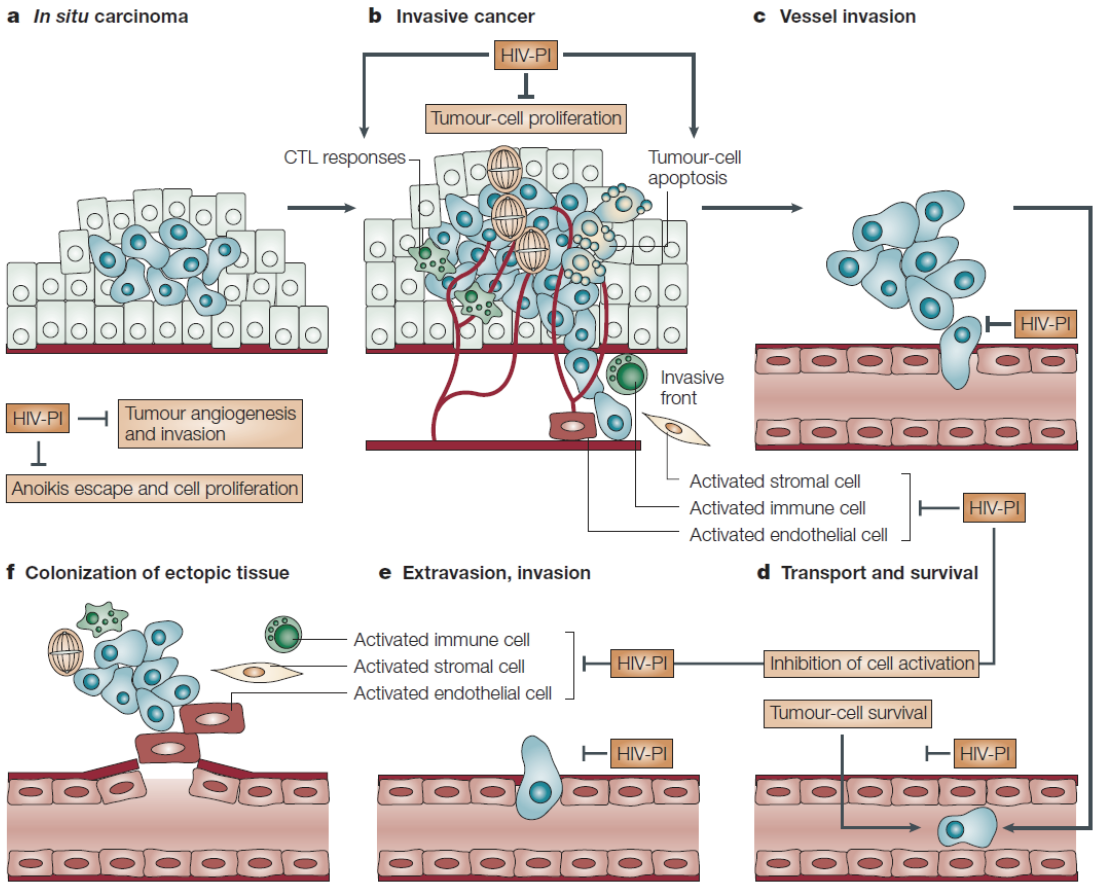

Figure 2.1 – Main steps in tumor progression and metastases affected by HIV protease inhibitors. The carcinoma *in situ* (a) progress to invasive cancer (b) and then metastases and dissemination through a set of mechanisms occurs (c-f) [13].

Infection by the human immunodeficiency virus (HIV) leads to increased incidence of certain tumors (e.g., Kaposi's sarcoma, non-Hodgkin lymphoma and cervical cancer). However, with the widespread use of highly active antiretroviral therapy (HAART) the appearance of these tumors in infected patients by HIV decreased significantly. But this effect cannot be explained only by the ability of these drugs to suppress HIV replication and restore normal

immune function. Studies have shown that HIV protease (e.g., HIV aspartyl protease) inhibitors (HIV-PIs) (such as ritonavir, saquinavir, indinavir and nelfinavir), which are widely used in HAART, have non-virological actions. As result, it was found that the HIV-PIs directly affect various stages of tumor development. They inhibit the proliferation and survival of tumor cells, the production of inflammatory cytokines, the proteasome activity and the tumor immunity in HIV free models. They also induce apoptosis in cancer cells, and have direct anti-angiogenic, anti-invasive, anti-metastic and anti-tumor effects that are not related to their antiviral activity [12, 13]. These data indicate that HIV-PIs directly block tumor development and progression (figure 2.1) [13].

2.2.1. Saquinavir mesylate – antitumor

There are several studies that prove the viability of saquinavir mesylate, as an anti-cancer drug. The ability of saquinavir mesylate (SQV) to prevent progression and tumor growth may be mediated by their ability to inhibit proteasome function and matrix metalloproteinases activity (MMPs) [13]. Studies clearly show that the SQV differentially affects various tumor ways, depending on the concentration of drug used [12].

The proteasome controls a variety of cellular pathways and its main function is the degradation of unused proteins or proteins with production errors. The proteasome also controls the proteolytic maturation and activation of the transcription factor NFκB, the degradation of apoptotic factors, and the degradations of tumor suppressor genes products, among other functions.

Thus, proteasome inhibitors have become a new strategy in fighting cancer. The SQV has shown ability to block these activities of the proteasome and, thus, increase the apoptosis, sensitize the tumor cells to ionizing radiation (prostate cancer, lymphoblastoid leukemia and glioblastoma) [12, 14], the production and/or release of tumor-associated inflammatory cytokines and chemokines (TNF-α, IL-6, IL-8 and IFNγ) and endothelial cells activation. Tumor cells often exhibit high constitutive activity of the anti-apoptotic transcription factor NFκB, resulting in its enhanced survival. NFκB activation depends classically on the degradation of its inhibitor IκBα by the 26S proteasome. Thus, with the inhibition of the proteasome by SQV the activation of NFκB is compromised [15]. This effect occurs at a relatively wide range of drug concentrations (5-100 μM), that are similar or above of the pharmacokinetic peak level present in the serum of treated patients [13, 16]. However, no effect on the proliferation or survival was observed with non-tumor cells [13].

In drug concentrations that are too low to affect cell proteasome, but are similar to the lower peak level current in the serum of treated patients (0.1-1.0 μM), a different mechanism of action is observed. At these lower concentrations, the SQV inhibits angiogenesis and cell invasion through its effects on the matrix metalloproteinases (MMPs) activity, especially MMP2 [13]. MMP2 is highly expressed in tumor cells and endothelial cells, and is required to degrade the basement membrane allowing the endothelial cell migration and metastases [12, 16]. The expression of MMP2 is regulated by various cytokines and growth factors [17], such as, basic fibroblasts growth factor (bFGF) and vascular endothelial growth factor (VEGF), which mediate angiogenesis and studies demonstrate the SQV potential of its inhibition [13]. Although the exact mechanism for the inhibition of MMP2 activation by SQV is not yet entirely clear, the

effect of these drugs on MMPs, cell invasion, angiogenesis, tumor growth and metastasis is proven [13].

SQV also can inhibit the production and/or release of MMP zymogen (pro-MMP). These SQV effects can block angiogenesis and tumor cells invasion, and may also affect the cell survival and inflammation [13].

The SQV effects (direct and indirect) as antitumor drug are shown in table 2.1 and 2.2.

Table 2.1 - Direct effects of saquinavir on tumors [adapted from [13]].

Effect	Experimental model	Drug dose/ concentration	Mechanism(s) of action	Molecular target(s)
Necrosis of KS lesions	Primary (non-immortalized) KS cells transplanted into immunodeficient mice	HIV therapeutic dose	Blocks neoangiogenesis	MMPs, possibly integrins
Inhibition of growth and metastasis of tumors of various origin	Human or syngeneic tumor grafts in immunodeficient mice	HIV therapeutic dose	Blocks angiogenesis, tumor-cell invasion, ECM remodeling	MMPs, possibly integrins
Inhibition of cell invasion (with no effects on cell viability/proliferation)	Human endothelial cells and tumor cell lines	Patient's steady-state plasma concentration (0.1-1 μM)	Blocks MMPs proteolytic activation	MMP2, MT1-MMP, possibly $\alpha_v\beta_3$-integrin
Tumor-cell apoptosis and radiosensitization	Human tumor cell lines	Above patient's peak plasma concentration (50–100 μM)	Inhibition of NFκB function	Proteasome

Table 2.2 - Indirect effects of saquinavir on tumors [adapted from [13]].

Effect	Experimental model	Drug dose/ concentration	Mechanisms(s) of action (molecular targets)	Potential antitumor action
Modulation of dendritic-cell maturation (that is, expression of co-stimulatory surface molecules) and function	Monocyte-derived dendritic cells	Similar to peak plasma concentration (10–20 μM)	Unknown (cell aspartic proteases, MMPs?)	Modulation of antitumor immunity
Restoration of T-cell responsiveness to antigens	Cultured CD34+ cells T cells, PBMCs	Similar or below patient's steady-state plasma concentration (5 nM to 10 μM)	Unknown (cell aspartic proteases, MMPs?)	Decreased tumor immune evasion
Radiosensitization in bladder cancer and others	Bladder, head and neck, pancreas and lung cancer cell line and rat model	25 μM	Inhibition of p-Akt	Proteasome

As the SQV is erased with a very fast kinetics in patients, plasma concentrations of these drugs will be sufficient to block MMPs during most of the time, affecting proteasome function

only at an early stage. Therefore, the antitumor effects of SQV will be more evident in blocking cell invasion and angiogenesis by MMP inhibition [13].

In conclusion, SQV has pleiotropic cellular effects that lead to antitumor activity, including inhibition of MMP2 activation, NFκB activation, activity of the 20S and 26S proteasome, Akt phosphorylation, production of pro-angiogenic factors. Their direct anti-tumor effects have been documented in several tumor cell lines such as human prostate carcinoma, glioblastoma, leukemia and, non-small cell lung cancer [12, 16, 18].

2.3. Saquinavir mesylate - general characteristics

Saquinavir mesylate (SQV) is classified as a Class IV drug (low permeability, low solubility) [19] in accordance with the terms of the Biopharmaceutical Classification System (BCS) [20].

SQV, the first protease inhibitor approved by the FDA in 1995 [12, 21, 22], is used conventionally in the clinical treatment of acquired immunodeficiency syndrome (AIDS), which stems from infection by the human immunodeficiency virus (HIV). Proteases are enzymes that cleave protein molecules in smaller fragments [23]. HIV aspartyl protease is essential for viral replication within the cell and the release of mature viral particles from an infected cell [23]. During the infectious stage, the cleavage position of precursor protein of HIV can only be recognized by specific viral proteases [24]. Thus, SQV is designed as a peptide similar to the cleavage position which binds to the active site of the viral protease and prevents cleavage of viral polyprotein, resulting in formation of immature and noninfectious virus particles (figure 2.2) [22, 24]. SQV inhibits both HIV-1 and HIV-2 proteases [23]. As already mentioned, SQV is also referred as an efficient anti-tumor agent against numerous tumor cell lines *in vitro* and *in vivo*, although the exact way it is processed is still somewhat obscure.

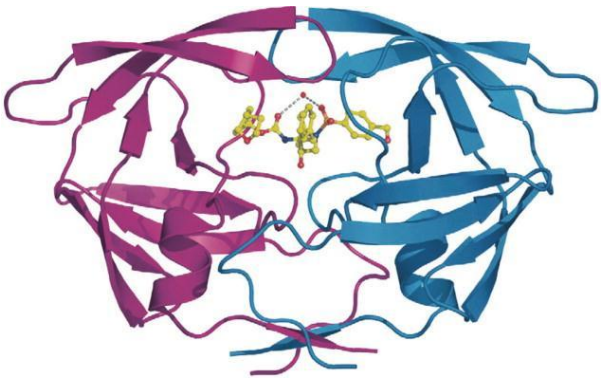

Figure 2.2 - HIV-1 protease structure connected to a protease inhibitor. The protease dimer with an inhibitor molecule (yellow) bound at the active site [12].

Molecular formula is $C_{38}H_{50}N_6O_5 \cdot CH_4O_3S$ (figure 2.3) and the molecular weight is 766.95 g/mol [25]. The molecular weight of the free base is 670.841 g/mol [23]. SQV is an anti-HIV agent rather lipophilic with the log P (octanol/water partition coefficient) at pH 7.4 of 4.51 [24, 26, 27]. This protease inhibitor undergoes extensive first pass metabolism (liver) [27], has poor oral bioavailability (1-12%) [28] and is poorly permeable across the BBB [22, 26]. The metabolism of SQV is mediated by cytochrome P450, with the specific enzyme CYP3A4, responsible for 90% of the hepatic metabolism. Furthermore, SQV is a substrate for P-glycoprotein (P-gp), which explains its reduced penetration into the brain [15, 21, 27, 29].

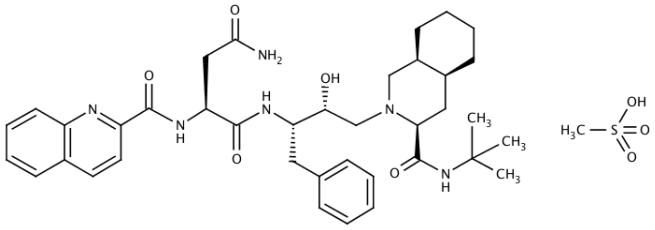

Figure 2.3 - Chemical structure of saquinavir mesylate [25].

Other important SQV properties are the resident period in the blood of 1 hour, 98% plasma protein binding, and 13.2 hour half-life of elimination [24].

As result, there is a need to develop strategies to improve its bioavailability [22, 28].

2.4. Blood-brain barrier

The central nervous system (CNS) is a unique and complex environment with restricted anatomical access, mainly due to blood-brain barrier (BBB). This barrier is an active, dynamic and complex interface between the blood and the CNS, which has neuroprotectors; regulates the transport inside and outside of the brain of different metabolic elements, molecules and cells (e.g., leukocytes), protects the brain against infiltration of hazardous compounds and maintains the homeostasis of the brain microenvironment [30, 31]. The BBB is also an insurmountable obstacle for the supply of a large number of drugs for the CNS, preventing the drugs from reaching effective concentrations in the brain [32].

The BBB is formed by endothelial cells to level of brain capillaries. These endothelial cells interact with perivascular elements, such as the basal lamina and end-feet of astrocytes processes intimately associated, perivascular neurons (represented in figure 2.4 for an interneuron), and pericytes to form a functional BBB.

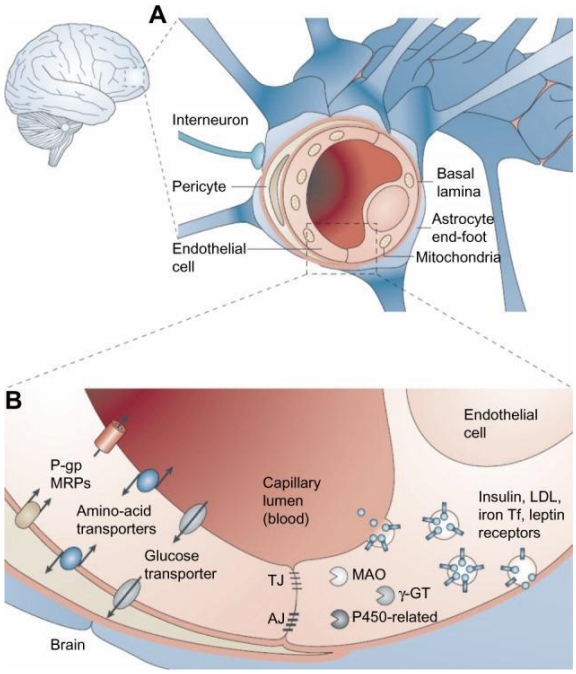

Figure 2.4 - Blood-brain barrier [31].

Brain microvascular endothelial cells (BMEC) play a crucial role in the neuronal activity and in the proper functioning of the CNS, as well as in the BBB characteristics [26, 32]. The BMEC are supported by adhesions and interactions with brain pericytes, neurons and the basement membrane which is surrounded by the end-feet of astrocytes (figure 2.4) [2, 32]. In the BBB, the joints that connect the BMEC are very tight and continuous. As result, this endothelium exhibits a very high transendothelial electrical resistance (TEER) (> 1500 Ω.cm2) [32]. This tightness is apparently related to the specific protein composition of the BBB tight junctions (TJ), including occludin, claudin 3 and claudin 5 [32].

So, the limited access of drugs to the brain is due to these TJ between the endothelial cells lining the blood vessels of the brain, as well as the existence of various very active drugs efflux transporters systems on the luminal membrane of these cells. The TJ avoid the paracellular transport of drugs [33] while the efflux pumps immediately to carry the drug that had partitioned in the endothelial cell membranes back into the blood stream [4].

The BBB is, therefore, a severe restriction to the transport of anti-cancer drugs.

2.4.1. Transport across of the BBB

The BBB limits the transport of endogenous and exogenous compounds. There are different types of pathways for molecules to cross the BBB (figure 2.5), and some of them can be strategically used for drug delivery purposes.

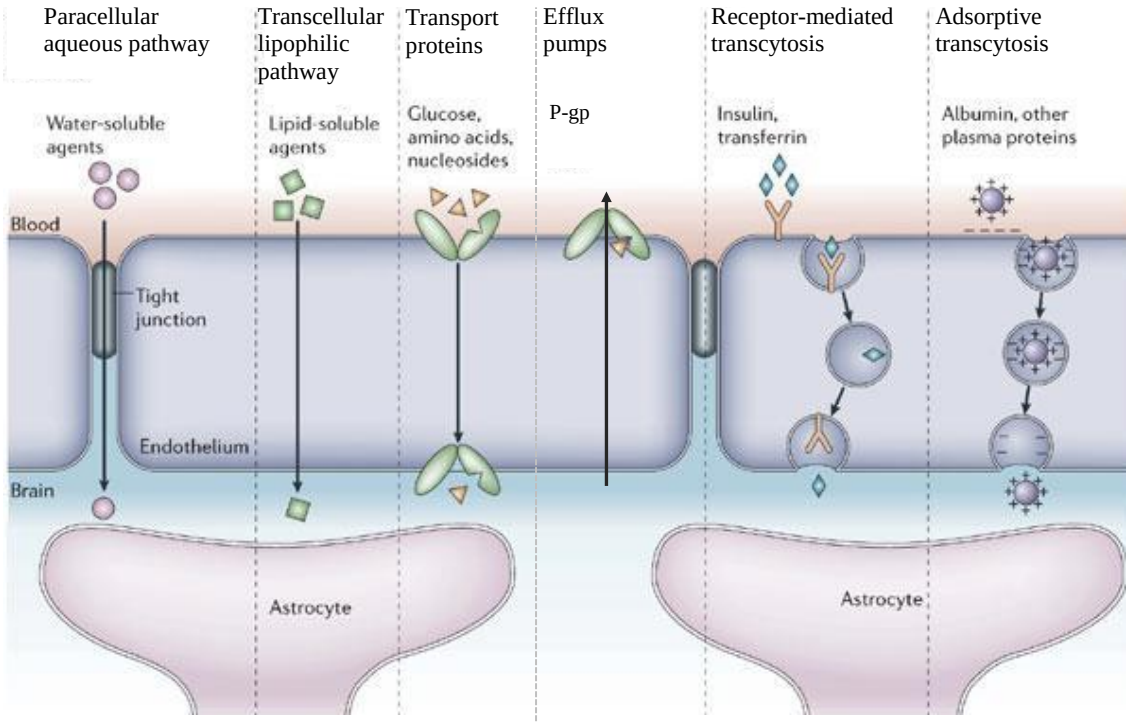

Figure 2.5 - Pathways through of the BBB [adapted from [34]].

For the transport of low molecular weight molecules, there are two possibilities. The first one is the diffusive transport, in which passage of molecules through the BBB can be done between adjacent cells (paracellular pathway) or through the cells (transcellular pathway) [31]. For polar compounds (e.g., H_2O, O_2, CO_2, NH_3, ethanol), the main factor that hinders its entrance is the TJ that occlude the paracellular pathway [32]. For compounds with more favorable lipid solubility properties, penetration in the CNS depends on a number of chemical

factors, including the degree of lipophilicity (octanol/water partition coefficient – log P), the surface charge, the molecular weight, and the ability to bind to proteins or red blood cells, as well as other factors inherent to vascular and choroid systems, such as local cerebral blood flow and the surface area available for exchange [32, 33]. Although the large surface area of the lipid membranes of endothelial offer an effective way for the diffusion of lipophilic agents, these molecules are subject to be pumped back into the bloodstream by extremely effective efflux pumps (discussed later in this section) [33-35].

While some small molecules (<400 Da) relatively lipophilic, can diffuse freely through the BBB, studies suggest that 90% of small molecules and almost all large molecules are unable to passively cross this barrier [2]. That is how the second possibility of transport for small substrates arises, which is the active transport that is mediated by carriers, such as proteins (carrier-mediated transport - CMT) [31]. The brain is dependent on the blood to provide substrates as well as to remove metabolic waste. For this reason, CMT systems allow the entry or removal of a variety of compounds, including hydrophilic substances such as hexoses, amino acids, glucose and purine compounds, compounds which are essential for brain homeostasis [33]. Some examples of CMT: excitatory amino acid transporters 1–3 (EAAT1–3); glucose transporter 1 (GLUT1); L-system for large neutral amino acids transporter (LAT1) (figure 2.6) [34].

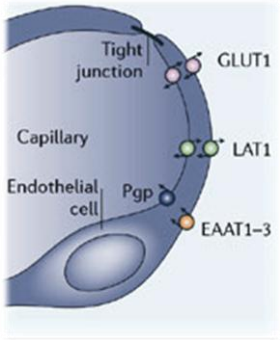

Figure 2.6 - The cells express a number of transporters, some of which are shown [adapted from [34]].

On the other hand, the transport of macromolecules, includes receptor-mediated transcytosis (RMT), nonspecific adsorption-mediated transcytosis (AMT) and cell-mediated transcytosis. RMT involves the endocytosis of macromolecules (e.g. insulin, transferrin, immunoglobulin, epidermal growth factor, low-density lipoprotein (LDL) and nanoparticles) that bound specifically to a receptor on the endothelial surface of BBB. Then it is diffused across the endothelium and, finally, exocytosed on the opposite side [34]. AMT, also known as pinocytosis, is mediated by electrostatic interactions between positively charged ligands (e.g., albumin) and negatively charged membranes of the BBB. Cell-mediated transcytosis refers only to the transport mediated by immune cells [31].

The active efflux transport is another important type of molecular transfer across the BBB that limits the brain penetration. This latter mechanism involves drugs extruding from the CNS back to the blood, which is a major impediment to drug therapy. Examples of efflux pumps, are the known ABC transporters (ATP – binding cassette transporter), such as P-glycoprotein (P-gp), breast cancer resistance protein (BCRP), and multidrug resistance-associated protein (MRP) and so-called multi-organic anion transporters (MOAT), such as organic anion transporter (OAT) and organic anion transport polypeptides (OATP) [4, 29, 32, 33]. P-gp sometimes referred to as multidrug resistance protein 1 (MDR1), has high affinity for a wide range

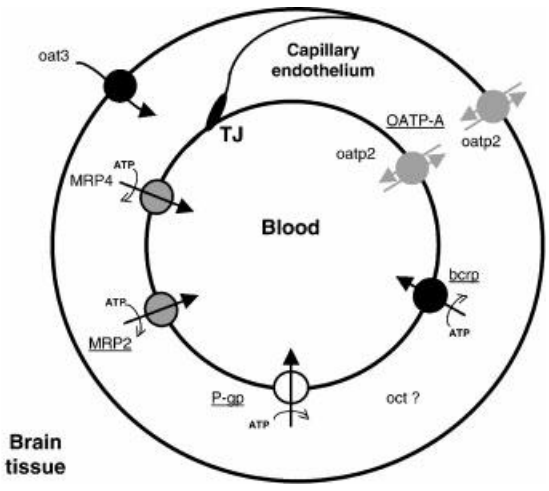

Figure 2.7 - Drug efflux transporters in the brain-blood [32].

of cationic and lipophilic compounds, and therefore limits the transport of many drugs, including cytotoxic anticancer drugs, antibiotics, hormones and HIV-PIs [31, 33].

Figure 2.7 shows several genes or proteins that have been located in the BBB and that can potentially modulate the drug efflux.

2.4.2. HIV-PIs vs BBB

There are several reasons that may explain the poor brain penetration by the HIV-PIs. First of all, the HIV-PIs bind strongly to proteins in the blood, which reduces their bioavailability [31] and the inflow rate in the CNS. Indeed, the binding of proteins to drugs has a key influence in the diffusion process, once that only the concentration of free drug (unbound) is the driving force for the influx. Thus, a compound that is highly bound to proteins (mainly albumin and/or alpha-1-acid glycoprotein) or red blood cells have a very small rate entry for the brain. However, this entry rate into the brain also depends on the affinity between the protein and the drug (association or dissociation constant). If the diffusion inflow rate is fast and the dissociation rate is high, a significant portion of the drug bound to the protein may become free and enter in the brain [32].

The second reason for the poor penetration of these drugs is related to the fact that several HIV-PIs are very lipophilic drugs and have very high log P, above +4. It is believed that molecules that have a very high hydrophobicity are not easily distributed throughout the BBB, possibly because of their inability to distribute in the opposite extracellular compartment [32].

Finally an increasing number of trials highlight the importance of efflux transport proteins to restrict HIV-PIs from entering the CNS [32]. SQV is a substrate of efflux transporter P-gp and MRP2 [24, 32].

Other studies have demonstrated the involvement of different host cellular factors, such as cytokines and chemokines (TNF-α, IL-6, CCL2/MCP-1, etc.) in the P-gp regulation of different types of human cells. In brain tumor, inflammation alters the expression of MDR1 in the brain and many chemokines are believed to be inflammatory mediators. It was observed that the chemokine release in humans can increase the P-gp expression on endothelial cells of the BBB through different signaling pathways, especially the path of protein kinase C (PKC) [36].

2.5. Nanotechnology

The development of more effective therapeutic strategies for the treatment of CNS tumors has become a focus area in recent years. The most recently discovered chemical drugs are poorly soluble in water. The improvement of the bioavailability of these lipophilic compounds is a main goal of the pharmaceutical research. One of the strategies most studied in this respect is nanotechnology, because of the ability of the nanoparticles to pass various biological barriers and release the therapeutic compound to specific cells within the optimum dose range [19]. This is due to their small size, typically in the range of 10-1000 nm [37]. The nanocarriers can be classified according to the material used for its manufacture. Liposomes, dendrimers, polymeric nanoparticles, solid lipid nanoparticles, micelles, gold nanoparticles and metallic nanoparticles appear to be promising tools for delivery of poorly soluble drugs, however, few have reached the market (see section 2.5.1) [19, 37, 38]. Nanotechnology which is progressing consistently can be used to restrain the limitations of the conventional chemotherapeutic method available for the cancer treatment [11].

Targeting the drugs to the tumor microenvironment is one of the great advantages of using nanoparticles. Thus, their anti-tumor effects are increased while its toxicity and side effects are decreased. Targeting will allow the anticancer drug to have the ability to selectively kill cancer cells, preventing the healthy ones, leading to an improved quality of life and survival of the patient [11]. This targeting can be active or passive (figure 2.8).

Passive targeting

This type of transport explores the anatomical and pathophysiological characteristics of the tumor vasculature [11].

Tumor cells divide at a rapid and uncontrollable rate significantly faster than other cells. This overgrowth leads to hypoxic conditions, due to restrictions of oxygen and nutrients to the tumor environment. Angiogenesis is therefore a key step for the cell survival and function, involving the creation of new blood vessels from pre-existing ones, to deliver oxygen and nutrients to the newly formed tissue. Thus, tumors are able to survive independently. Abnormal proliferation of endothelial cells has some effects on microvascular network newly formed, giving rise to a defect in the architecture of these new vessels, in contrast with the neovasculature in normal tissues. These vessels become more permeable due to the large gaps between endothelial cells. In addition, proliferative cancer cells are capable of intratumoral lymphatic vessels collapse by compression. This poor lymphatic drainage, together with increasing permeability of the newly formed tumor blood vessels is known as Enhanced Permeability and Retention (EPR) effect [11, 39-41].

The EPR effect allows the nanoparticles loaded with drugs to spill of permeable tumor blood vessels and accumulate in tumor tissues and not in healthy tissue. The normal vasculature is provided with TJ that are impermeable to molecules of size > 2-4 nm, thus keeping the nanoparticles within the circulation; however, the leaky vasculature of tumor tissue enables that macromolecules with a diameter of 100-600 nm spill over for tumor tissues [11, 41].

Active targeting

The overexpressed receptors on the surface of a tumor cell membrane have been studied to achieve selective delivery to target sites [9]. Active targeting is based on a combination of receptors for specific ligands, such as peptides, carbohydrates or monoclonal antibodies, which are located on the surface of the nanoparticles [11]. Nanoparticles recognize and bind to their target in the cells with subsequent uptake through the receptor-mediated endocytosis. Once internalized, the drug is released into the cytoplasm or in the nucleus. For example, over-expression of transferrin (known to be expressed on the luminal membrane of the capillary endothelium of the BBB [31]) and folate in some types of tumors has been exploited to deliver nanoparticles conjugated with these ligands [9].
This targeting will allow, thereby, to increase drug accumulation in the cancer tissue [39, 41].

Another promising mechanism of drug targeting is when nanoparticles release their load at the target site when exposed to a stimulus: pH change, chemical stimulation, applying a magnetic field or applying a heat source (hyperthermia). The main disadvantage of these types of nanoformulations is that they are not easy to prepare and in addition, they can release drugs without being triggered or even not release its load when exposed to the stimuli [11].

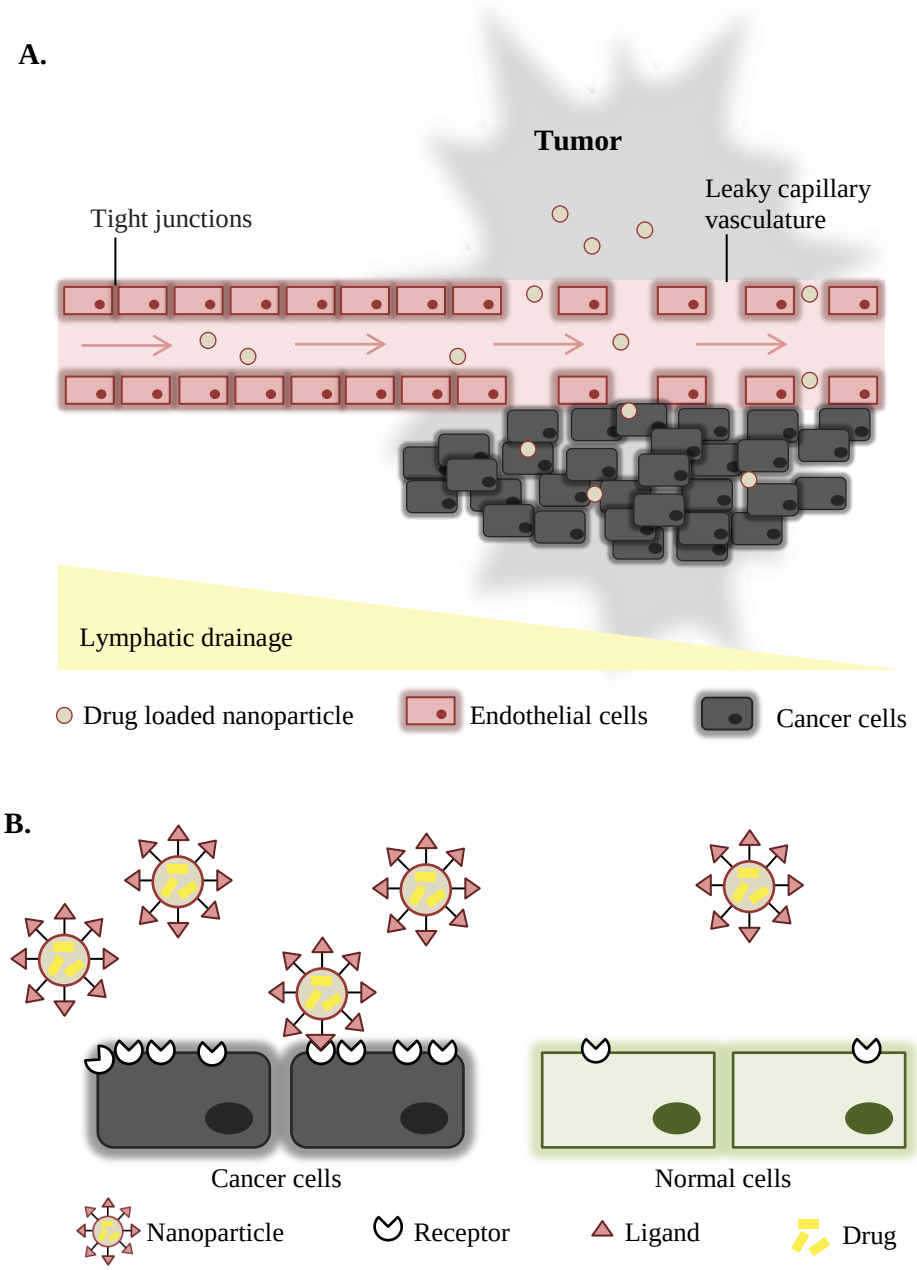

Figure 2.8 - Representation of (A) passive (EPR effect) and (B) active (receptor-mediated) targeting utilized for targeting nanoparticles to tumors [adapted from [42]].

As mentioned before, the tumor microenvironment characteristics are important for an effective nanoparticles delivery. However, this efficiency is also dependent on factors inherent to nanoparticles themselves, such as size, charge and surface properties [9, 41]. In order to nanoparticles reach target sites and make use of targeting, they should be able to remain long enough in the bloodstream with minimal loss of activity or load. The nanoparticles must be able to hide from the phagocytic immune cells as neutrophils or monocytes/ macrophages from the reticuloendothelial system (RES), responsible for the destruction of foreign bodies. The two main factors affecting recognition by the RES and until the uptake by the tumor cells are the size and particles surface [11].

In short, the use of nanoparticles loaded with cytotoxic drugs for cancer treatment offers many advantages over conventional formulations: (i) reducing the cytotoxic effects of

anticancer active drugs by increasing targeting to cancer cells [39]; (ii) reduction of side effects of short and long term [9, 39]; (iii) required less drug to obtain the same therapeutic effect [39]; (iv) protection of the drug against degradation [37]; (v) increased cellular uptake of poorly permeable drugs [37]; (vi) reduction in cell and tissue clearance of drugs [37]; (vii) delivery sustained drug [37]; (viii) reduction of the immune response [37]; (ix) selective and controlled release of drugs in their target sites [11]; (x) superior features pharmacokinetic [9] and prolonged blood circulation time [9]; (xi) volume of distribution [9], half-life [9] and increased bioavailability of the drug [31] and finally, (xii) nanoparticles overcome the BBB more efficiently preventing the efflux pumps [4, 22, 31].

2.5.1. Nanoformulations on the market

Some of the nanoformulations are already on the market. Table 2.3 shows the most important ones used for cancer treatment.

2.5.2. Solid lipid nanoparticles

The solid lipid nanoparticles (SLNs) concept emerged in the early 90's of the last century [43, 44], and they have been establishing over the years as stable drug vectors, reliable and easy to produce [45].

SLNs consists in a solid lipid core at room and body temperature (i.e., with melting point ≥ 40 °C), which serves as matrix to the bioactive substance. The particle is stabilized by a surfactant layer which may be single or composed of a mixture of surfactants (figure 2.10) [43, 46]. The size of these nanocarriers varies between 50 and 1000 nm [43].

2.5.2.1. Stability of SLNs

The physical and chemical stability of the SLNs is influenced by two different factors. The first one is the ability of the SLNs suspension to remain homogeneous (suspension stability). The second one is the ability of the crystal matrix to resist recrystallization (matrix stability) [46].

Suspension stability

Instability in the suspension is caused by flocculation and coalescence processes.

Flocculation occurs when two or more nanoparticles are associated but retain their individual integrity. This process may lead to an increased viscosity of the dispersion and sometimes can lead to the formation of a gel. The flocculation usually happens due to insufficient repulsive interaction forces between the particles. This failure can be caused by changes in the ionic strength or pH of the system, which affects the adsorbed surfactants rate on the nanoparticles surface. Flocculation can also occur due to increased collisions between the nanoparticles, due to agitation or high temperatures. As result of flocculation and driven by gravitation, there may be sedimentation [46].

On the other hand, coalescence is the process in which two or more liquid droplets (nanoemulsions) join to form a single larger drop. This process requires a liquid lipid matrix and, so, it is generally not a problem of SLNs. However, this phenomenon can occur during the production of SLNs or when the previously formed SLNs are heated above their melting temperature (for example, sterilization or drying). During the heating and above of the melting

temperatures the "melted" SLNs (nanoemulsions) can coalesce. After cooling, significantly different matrix structures are formed, with increasing particle size and creaminess [46].

Table 2.3 - Some selected nanomedicine products currently on the market [adapted from [47-50]].

Brand-name	Drug	Indication	Approval date
Lipossomes			
Daunoxome®	Daunorubicin citrate	Kaposi sarcoma in AIDS (IV)	FDA 1996
Depocyt®	Cytarabine	Lymphomatous malignant meningitis (IV)	FDA 1999/2007
Doxil®	Doxorubicin hydrochloride	AIDS-related KS, multiple myeloma, ovarian cancer (IV)	FDA 1995
Marqibo®	Vincristine sulfate	Acute lymphoid leukemia, Philadelphia chromosome-negative, relapsed or progressed (IV)	FDA 2012
Mepact™	Mifamurtide	Non-metastasizing resectable osteosarcoma (IV)	Europe 2009
Myocet®	Doxorubicin	Metastatic breast cancer (IV)	Europe 2000
PEGylated proteins, polypeptides, aptamers			
Neulasta®	Filgrastim	Febrile neutropenia, In patients with nonmyeloid malignancies; prophylaxis (SC)	FDA 2002
Oncaspar®	Pegasparginase	Acute lymphoblastic leukemia (SC)	FDA 1994
Polymer-based nanoformulation			
Eligard®	Leuprolide acetate	Advanced prostate cancer (SC)	FDA 2002
Genexol®	Paclitaxel	Metastatic breast cancer, pancreatic cancer (IV)	South Korea 2001
Opaxio®	Paclitaxel	Glioblastoma	FDA 2012
Zinostatin stimalamer®	antitumor protein NCS	Primary unresectable hepatocellular carcinoma	Japan 1994
Protein-drug conjugates			
Kadcyla®	DM1	Metastatic breast cancer	FDA 2013
Ontak®	Denileukin diftitox	Primary cutaneous T-cell lymphoma, CD25-positive, persistent or recurrent disease (IV)	FDA 1994/2006
Metal-based nanoformulations			
NanoTherm®	Aminosilane	Local ablation in glioblastoma, prostate, and pancreatic cancer (intratumoral)	Europe 2013
Virosomes			
Gendicine®	P53 gene	Head and neck squamous cell carcinoma	People's Republic of China 2003
Rexin-G®	G1 gene	For all solid tumors	Philippines 2007

The SLNs, however, have good suspension stability. The very small particle size and density close to unity of SLNs means that gravity has little effect on the particles in dispersion, and Brownian motion is sufficient to maintain colloidal dispersion without creaming or sedimentation [51].

Matrix stability

Because of the crystalline nature of the solid lipids, the polymorphism is a typical characteristic of SLNs. The heating/melting and cooling/recrystallization of most lipids can lead to the occurrence of transitions between its various polymorphic states: unstable (α), metastable (β') and stable (β) (figure 2.9) [52]. The more unstable configurations have a lower density and so a greater ability to incorporate drug molecules. During the storage, the rearrangement of the crystal structure may occur in favor of thermodynamically stable configurations (polymorphic transition), with expulsion of drug molecules [53, 54]. This rearrangement of the lipid matrix influences the drug loading capacity, and also the matrix stability. The fact is that recrystallization of the lipid matrix destabilizes the suspension by transforming the initial spherical particles into needle-shaped particles (β structure) that are highly ordered and thermodynamically more stable. This transformation results in an increased surface area, and surfactants are not able to diffuse fast enough to cover the newly formed surfaces, leading to the destabilization and flocculation of the suspension due to the hydrophobic attraction between the lipophilic lipid nanoparticles [46, 53].

The matrix instability can lead to instability of the suspension and, therefore, these two parameters are linked.

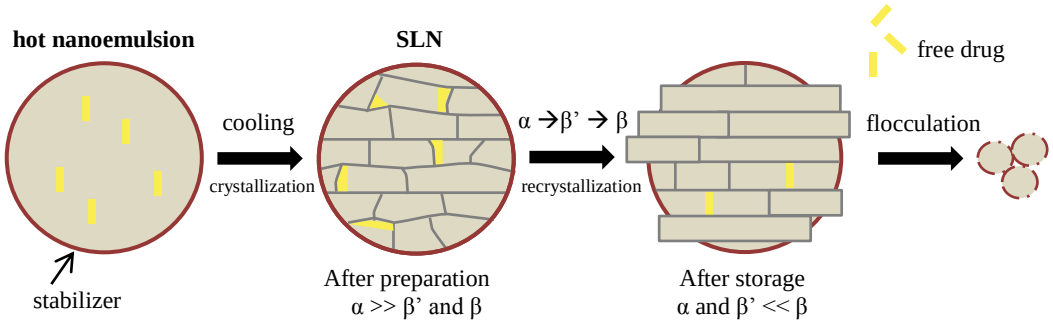

Figure 2.9 – Recrystallization (α → β' → β) and drug release of SLNs by cooling a hot nanoemulsion [adapted from [55]].

2.5.2.2. Advantages and disadvantages of SLNs

SLNs combine the advantages of various colloidal carriers (e.g., liposomes, polymeric nanoparticles, micro- and nanoemulsions), avoiding some of their disadvantages [56]. The main disadvantage of liposomes and emulsions is that they cannot protect chemically labile drugs [43]. On the other hand, SLNs make use of an excellent physical and chemical stability, which provides greater protection against degradation of labile drugs [57]. In general, the use of crystallized lipids (SLNs) instead of liquid lipids (lipid nanoemulsions and liposomes) has been shown to increase control over the release and stability of the incorporated bioactive substances [46]. Contrary to what occurs in the production of polymeric nanoparticles, it is not necessary to use potentially harmful organic solvents during the production of SLNs [43, 58].

Compared to traditional colloidal systems, lipid particles have the following advantages: (i) lipids are physiological, biodegradable and biocompatible, and generally are recognized as safe (GRAS) which reduces the danger of acute and chronic toxicity [51]; (ii) surfactants used to produce lipid nanoparticles are also GRAS [43]; (iii) avoiding of organic solvents in production methods [56]; (iv) fast, efficient and inexpensive production process, including the possibility of

large scale production [53]; (v) good suspension stability [51]; (vi) possibility to freeze and/or sterilize, allowing more comprehensive routes of administration [56]; (vii) have a solid matrix at room and body temperature, allowing the development of modified release systems as well as chemical protection of incorporated drugs [43]; (viii) can be used in all administration routes due to their small size (50-1000 nm) and are biocompatible [57]; (ix) can incorporate lipophilic and hydrophilic drugs [53, 59].

However, these nanoparticles also have some disadvantages: (i) little drug incorporation capacity [56]; (ii) instability in the lipid matrix due to polymorphic transitions of the lipids that transforms a little ordered lipid matrix in a highly ordered during storage [56]; (iii) high water content of the dispersions (70.0 to 99.9%) [56]; (iv) coexistence of alternative colloidal structures (micelles, liposomes, drug nanocrystals, supercooled melt (see section 2.5.3.)) [46, 53].

2.5.3. Nanostructured lipid carriers

At the beginning of the new millennium, and in order to overcome the problems associated with conventional SLNs, the nanostructured lipid carriers (NLCs) were developed, which constituted the second generation of lipid nanoparticles [43, 60].

NLCs have a solid matrix (melting point of the solid lipid ≥ 40 ° C) mixed with liquid lipids to form an unstructured matrix with many imperfections that help to increase the drug loading capacity of nanoparticles and to prevent or reduce the expulsion of drug from the matrix during storage [19, 61, 62]. On the contrary, as already mentioned, for the production of SLNs only solid lipids are used with a high degree of crystallinity, resulting in very ordered lipid matrices [43].

In figure 2.10 are represented the lipid matrix structures of the SLNs and NLCs, highlighting the differences between an "almost perfect" crystalline lipid structure (SLNs) and a lipid structure with many imperfections (NLCs) [43].

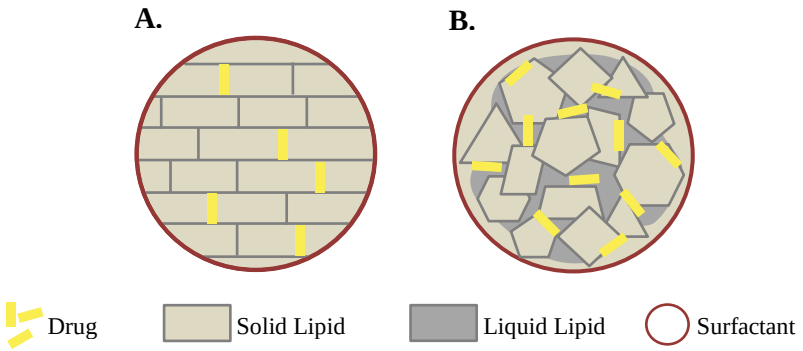

Figure 2.10 - Schematic description of SLNs (A) and NLCs (B) [adapted from [2]].

2.5.4. Supercooled melts

Supercooled melts (SM) describes the phenomenon in which the lipid crystallization cannot occur while the sample is stored at a temperature below the melting point of the lipid and they are not uncommon in SLNs systems. Special attention should be given to SM because the potential benefits of SLNs against the nanoemulsions are attached to the solid state of the lipid. The main reason for the formation of SM is the liability between size and crystallization processes. Crystallization requires a critical number of crystallization cores to start. This critical

number of molecules is less likely to be formed in small particles and, therefore, the tendency of SM formation increases with decreasing size of the nanoparticles. In addition to size, crystallization can be affected by surfactant, incorporated drug, and other factors. The supercooling range (temperature difference between the melting and crystallization points) can reach 30° - 40°C in lipid dispersions [53, 63].

SM have lower thermodynamic stability and degree of lipid packaging that the polymorphic forms (α, β', β) and, therefore, cannot immobilize the drug molecules as strongly as the solid particles [63].

The stability of colloidal dispersions of SLNs is also conditioned by the occurrence of supercooled melts in addition to the other factors mentioned above.

2.6. Lipid nanoparticles, BBB and SQV

The SLNs have been studied to overcome biological barriers such as the BBB. The use of SLNs for drug delivery to the brain was first proposed by Yang et al [64] and Zara et al [65] in the late 1990s, in their studies on the pharmacokinetics of two anti-tumor agents, camptothecin and doxorubicin, respectively. The drug accumulation in the brain was observed after oral and systemic administration of drug-loaded SLNs in mice. Since then, several studies were conducted on the ability of SLNs to improve the drugs delivery into the brain. Kuo and Su [30] prepared SLNs loaded with stavudine, delavirdine, and SQV, independently, and evaluated their ability to cross the BBB *in vitro* using human brain microvascular endothelial cells. The drug entrapment efficiency depended of its lipophilicity. SQV which is more lipophilic had the maximum entrapment efficiency, which indicates a better match of SLNs for more lipophilic drugs. The drug permeability was improved 4-11 times when incorporated in SLNs [37]. SQV is a substrate of some drug efflux transporters such as P-gp. The activity of these efflux transporters results in a lower intracellular accumulation of SQV [29]. The authors suggest that the SLNs bypass P-gp-mediated efflux and mask the drug from the membrane attached to the P-gp efflux transporter, thus facilitating its intracellular accumulation [37].

Also the NLCs have shown potential as a drug carrier for the CNS [31].

Recently it was demonstrated that, once in the bloodstream, lipid nanoparticles coated with polysorbate 80 (nonionic surfactant) adsorb different apolipoproteins in particular apolipoprotein E (ApoE) [4]. ApoE is involved in the transport of lipids in the brain via low density lipoprotein receptors, which are essential for the maintenance of cholesterol homeostasis in the brain [31]. The nanoparticles thus appear to mimic the natural lipoprotein particles (low density - LDL) and interact with the LDL receptor family located on brain capillary endothelial cells, followed by endocytic uptake, favoring their absorption by endothelial cells. After endocytosis two mechanisms are possible: one is the transcytosis into the brain and the other mechanism is the simple release of the drug within the endothelial cells and spread to the brain. Since ABC transporters are located primarily on the luminal membrane this diffusion in the brain would not be obstructed [4].

2.7. Cell culture

The cell culture has been asserting itself as a very useful and important tool in fulfillment of cytotoxicity tests in the investigation and development of new drug delivery systems [66, 67]. To pass the *in vitro* cytotoxicity test, nanoparticles should not lead to cell death or affect their cellular functions. The cytotoxic effects, when causing severe cell damage, may compromise the

cell viability disrupting the structural integrity and/or metabolic of the cells and its reproductive integrity, leading to a series of destructive effects. Thus, with the use of cell culture techniques, tests, it is possible to detect the occurrence of cell lysis, inhibition of cell growth and other effects that can be triggered in the cells [68].

In vitro tests are, thus, a very important tool because they offer the possibility to reduce the number of animals used and hence the reduction of pain and suffering that *in vivo* tests can cause. The parameter further investigated by cytotoxicity assays is cell viability, determined by several cellular processes. There are several tests for evaluation of cytotoxicity/viability, as the neutral red dye test, the reduction test of 3-(4,5-dimethylthiazol-2-yl)-2,5-diphenyltetrazolium bromide (MTT), the release assay of cytoplasmic enzymes such as lactate dehydrogenase (LDH), or incorporation test of propidium iodide for dead cells (PI) [69].

Chapter III - Materials and methods

3.1. Materials

Nanoparticles

For the nanoparticles production, saquinavir (more than 98.0% pure) was purchased from Glentham Life Sciences (Corsham, Wiltshire, United Kingdom), the solid lipid cetylpalmitate was provided by Gattefossé SA(St Priest, France), the liquid lipid miglyol 812 and polysorbate 80 (Tween® 80) were ordered from Acofarma (Spain).

HPLC

For high performance liquid chromatography (HPLC), the organic solvents (acetonitrile, methanol) were supplied by Merck KgaA (Darmstadt, Germany). For the preparation of pH 5.0 phosphate buffer solutions, potassium phosphate monobasic was obtained from Sigma-Aldrich and potassium hydroxide from Riedel-de Haën (Seelze, Germany).

Cell culture

Dulbecco's Modified Eagle's Medium (DMEM); Dulbecco's Phosphate Buffered Saline (DPBS) modified, without calcium chloride and magnesium chloride; Fetal Bovine Serum (FBS); penicillin-streptomycin; trypan blue (0.4%) and trypsin-EthyleneDiamineTetraacetic Acid (EDTA) were provided by Gibco (Invitrogen Corporation, USA). Triton-X 100 was provided by Sigma-Aldrich (Portugal), vybrant® MTT cell proliferation assay kit and propidium iodide were obtained by LifeTechnologies (Invitrogen Corporation, USA). Lastly, Dimethyl Sulfoxide (DMSO) was supplied by Merck KgaA (Darmstadt, Germany).

The water used in all experiments during this project was purified water by Direct-Q® Water Purification System (Merck Millipore, Darmstadt, Germany), and was obtained from a reverse osmosis process.

3.2. Methods

3.2.1. Preparation of SLNs and NLCs

There are different approaches to the production of lipid nanoparticles (SLNs and NLCs). The choice often depends on the purpose for which they are manufactured, like the type of drug, route of administration, among others [46]. For this project, two different production methods were chosen: hot high pressure homogenization and ultrasonication. Both methods have been preceded by high shear homogenization [70] (figure 3.1).

The ingredients of the SLNs and NLCs produced contained cetyl palmitate (solid lipid at room and physiological temperature), miglyol 812 (liquid lipid at room and physiological

temperature, used only for NLCs), polysorbate 80, saquinavir to be encapsulated and milli-Q water. Lipid nanoparticles (LN) were produced with different lipid (10% and 5%), surfactant (3%, 2% and 1%) and drug (0.1% and 0.05%) concentrations in order to pick the best formulation. Based on the results of the unloaded LN, the most promising formulations with regard to the size were reproduced incorporating saquinavir anticancer drug. Eight drug-loaded formulations (most promising unloaded nanoparticles) were studied.

Throughout the LN production phase, the temperature was about 5-10 °C above the melting point of the cetyl palmitate (54 °C).

3.2.1.1. High shear homogenization

It is a widely used technique for the production of micro-dispersion. Melted lipid mixture and hot aqueous surfactant solution were homogenized in a high-shear mixing device (Ultra-Turrax T25, IKA Labortechnik, Alemanha) at 8000 rpm for 40 seconds. Although it is easy to handle, the quality of dispersion is often poor [71]. In order to obtain the best results, this technique was combined with ultrasonication or hot high pressure homogenization in order to reduce the microparticles (hot pre-emulsion) to nanometer range (nanoemulsion), see figure 3.1.

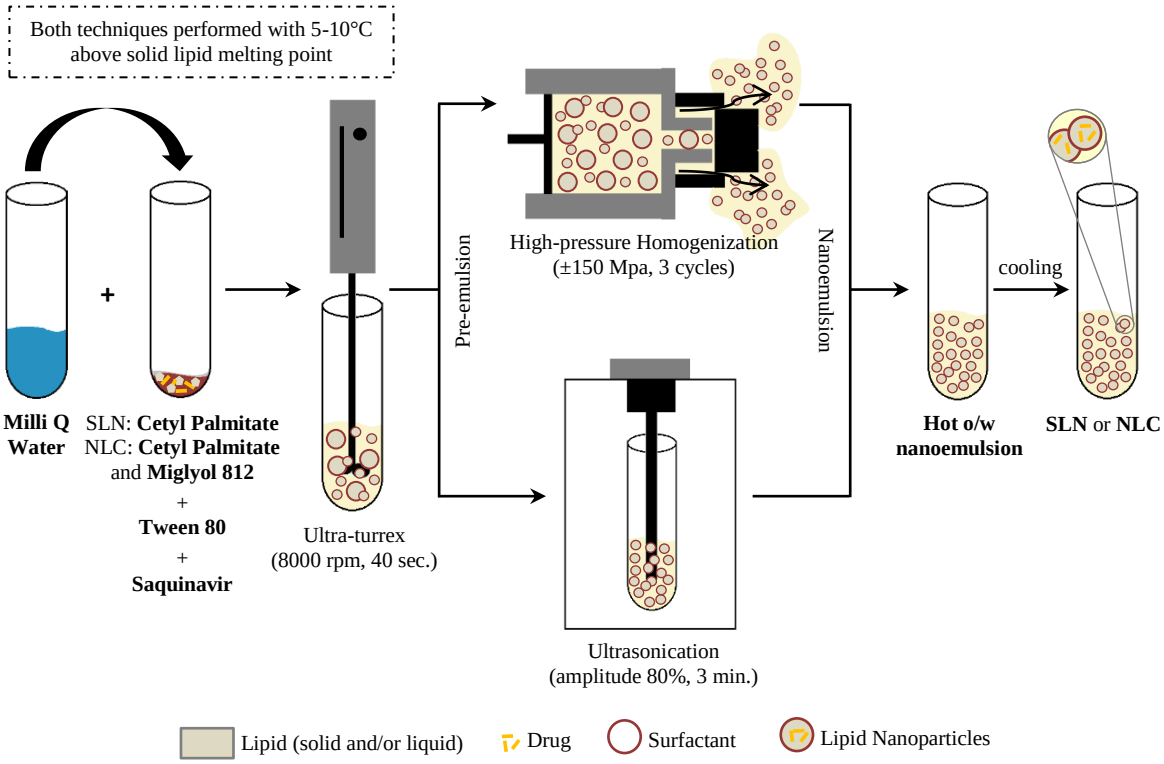

Figure 3.1 - Schematic overview of the production of lipid nanoparticles (SLNs and NLCs) by hot HPH and ultrasonication.

3.2.1.2. Hot high-pressure homogenization

In the hot high-pressure homogenization (hot HPH) (High Pressure Homogenizer SPCH-10, Stansted Fluid Power, UK), the hot pre-emulsion (obtained by high shear homogenization) was pushed under high pressure (±150 Mpa) through a narrow opening (in the range of a few microns) (figure 3.1) [56]. This process was repeated three times (3 cycles). As product resulted

in a hot oil-in-water nanoemulsion and its cooling gave rise to crystallization of cetylpalmitate and formation of SLNs and NLCs [53].

3.2.1.3. Ultrasonication

In this technique (VibraCell VCX130, Sonics & Materials, Inc. & Newtown, CT. USA), the hot pre-emulsion was converted into a nanoemulsion using a sonication probe (6mm) at amplitude 80% for 3 minutes (figure 3.1). Powerful ultrasonication caused acoustic cavitation, leading to disintegration of the lipid phase into smaller particles [71]. The solidification of the nanoemulsion after cooling led to the SLNs and NLCs.

3.2.2. Evaluation of storage stability

The dispersions were stored, after production, in closed falcon tubes at 4 °C and its size examined on the day of production. The most promising nanoformulations were then evaluated after 60 and 120 days of storage for the unloaded nanoparticles, and 45 and 90 days for the loaded nanoparticles. Indicators of storage stability were average particle size, polydispersion, zeta potential, among others.

3.2.3. Characterization of SLNs and NLCs

The proper and correct characterization of LN is necessary for its quality control. Characterization of SLNs and NLCs is often challenging due to its complexity and dynamic nature. The important parameters to be evaluated in the LN are: particle size, zeta potential, degree of crystallinity and lipid modification (polymorphism), drug encapsulation, the surface morphology and cytotoxicity [53, 56]. This project is mainly focused on determining these properties. It is important to point out that the particle characterization techniques use a subsampling and, therefore, this should be as representative as possible of the whole sample [72]. There is a wide range of techniques for characterizing particles commercially available that can be used to measure the particle samples. Each one has its strengths and limitations and there is no universally applicable technique for all samples and all situations [72]. Some of these techniques will be described in the course of this work.

3.2.3.1. Particle size measurement

The particle size is, by far, the most important physical property of particle samples and it has a direct influence on the physical stability of SLNs and NLCs [56]. The measurement of the particle size and understanding of how this will affect their properties is significant and fundamental [72].

The dynamic light scattering and laser diffraction are some of the most powerful techniques for determining the size of these particles [56].

Dynamic light scattering

Dynamic sight scattering (DLS) (also known as photon correlation spectroscopy (PCS) or quasi-elastic light scattering (QELS)) measures the variation of the intensity of scattered light, which is caused by the movement of the particles. If the particles are illuminated with a laser, the intensity of the scattered light varies in very short time scales at a rate that depends on the

particle size (figure 3.2). Smaller particles have a higher diffusion in solvent, move faster and have a greater variation of intensity of the scattered light. Thus, the analysis of these intensity fluctua tions depends on the speed of the Brownian motion and consequently the particle size using the Stokes-Einstein relation [72].

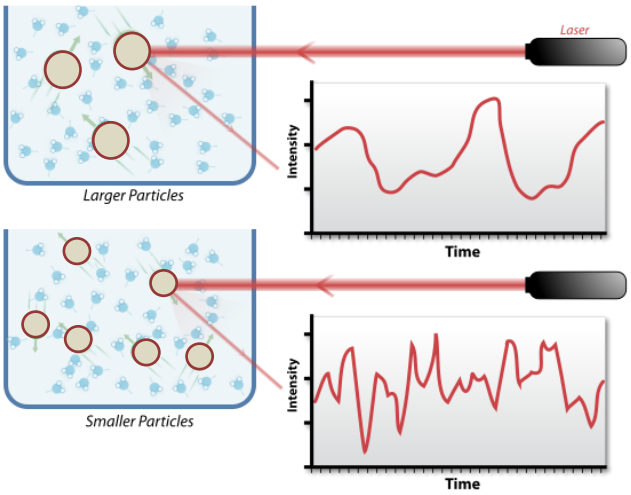

Figure 3.2 - Representation of the effect of particle size on the variation of the intensity of scattered light [73].

The particle diameter measured by the DLS method is called hydrodynamic diameter and refers to how a particle diffuses within a fluid (figure 3.3). The hydrodynamic diameter will depend not only on the "core" particle size, but also of any surface structure as well as the concentration and type of ions in the environment. It is not measured the particle diameter but all that moves with it (e.g. counter-ions). This means that the size will be greater than that measured by electron microscopy, for example, when the particle is removed from its native environment [72].

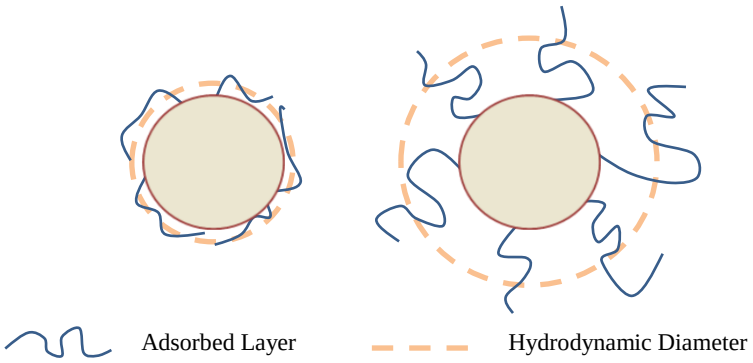

Figure 3.3 - Illustration of the reported hydrodynamic diameter in DLS being larger than the 'core' diameter**.**

This technique besides allowing measuring the mean particle size (Z-average) can measure the size distribution (polydispersity index – PI). The polydispersity index of 0 corresponds to a completely homogeneous monodisperse sample, whereas a polydispersity index of 1 indicates a very wide size distribution. Typically, a sample with a polydispersity index <0.25 is considered monodispersed [74].

The advantages of this method are the speed of analysis, the lack of required calibration and the sensitivity to submicron particles. This method covers a size range of a few nanometers to few microns. This means that DLS is a useful tool for characterizing nanoparticles, but is not able to detect larger microparticles. These can be seen using the LD method [53, 56].

To analyze the size of the LN via the DLS technique a ZetaPALS (Brookhaven Instruments, Holtsville, NY, USA) was used. Before the measurements, samples were diluted (1:1000) using milli-Q water to obtain an intensity adequate dispersion. The diluted samples were analyzed at 25 °C, with a fixed light incidence angle of 90°. The refractive index (lipid) used was 1.59. The mean hydrodynamic diameter (Z-average) and polydispersity index (PI) were obtained by

calculating the average of five runs, with two minutes each. Measurements were performed in three or more samples [75].

Laser diffraction

Laser diffraction (LD) is other technique widely used for particle sizing [72]. This method, also known as static light scattering (SLS) or Fraunhofer diffraction, is based on dependence between the diffraction angle and the particle diameter when a laser beam passes through of dispersed particles sample. The smaller particles cause increased light scattering and so higher angle values when compared with larger particles (figure 3.4) [53, 56, 72]. The data of angular scattering intensity is then analyzed to calculate the particle size responsible for creating the dispersion pattern using the Mie theory of light scattering. The particle size is reported as an equivalent volume to the diameter of a sphere [72].

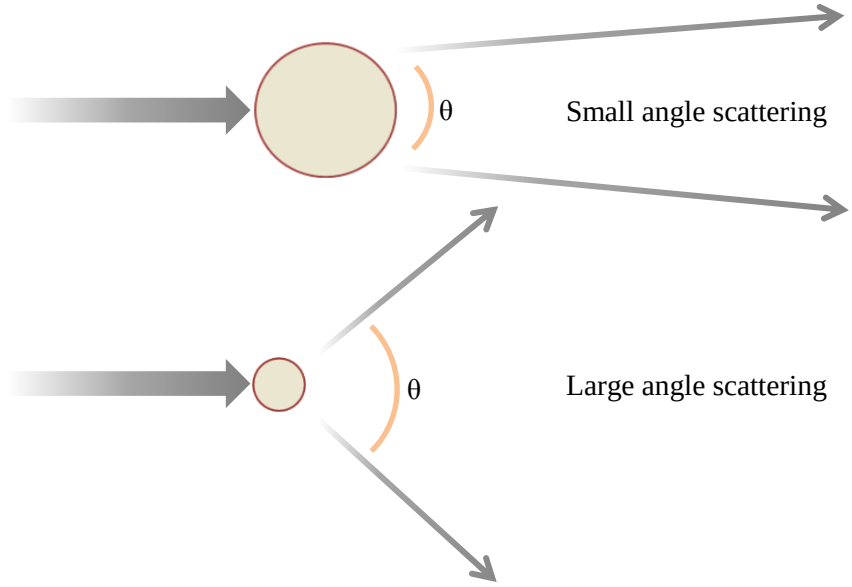

Figure 3.4 - Light scattering for small and large particles.

In this technique, the results are presented in accordance with the maximum particle size for a given percentage of sample volume.

Percentiles are set to XaB where:

X = parameter, generally D for diameter

a = distribution coefficient, for example, n for the number, v for the volume, i for the intensity

B = percentage of sample below this particle size e.g. 50%.

For example, the Dv50 would be the maximum particle diameter below which 50% of the sample volume exists - also known as the median particle size by volume. The most common percentiles reported are the Dv10, Dv50 and Dv90. Span refers to the bandwidth of the size distribution [76] and it is determined by the following equation (equation 3.1):

$$Span = \frac{Dv90 - Dv10}{Dv50} \quad (\boldsymbol{equation\ 3.1})$$

This is a fast and robust method, but requires more cleaning than the DLS, and prior knowledge of the optical qualities of the particles [56]. A clear advantage of LD is to cover a wider range of sizes, ranging from several hundred nanometers to several millimeters in size [53].

To analyze the size of SLNs and NLCs through the LD technique, it was used a Mastersizer 3000 (Malvern, Worcestershire, UK). In this technique, the deionized water was used as a dispersant. The optical properties of the lipid (cetyl palmitate) considered for the test were a refractive index of 1.1 and absorption index of 0.01. The sample was added to the dispersant until reaches 5-10% of obscuration (preferably 6%). The Dv10, Dv50, Dv90 and Span were obtained by calculating the average of five runs. Only the measurements with residuals and weighted residuals near and below 2% were considered. Measurements were performed using three or more independent samples.

It is strongly recommend the use of DLS and LD simultaneously. It should be borne in mind that both methods do not "measure" the particle size. Instead, they detect light scattering effects, which are used to calculate the particle size. In both methods uncertainties arise which may result in non-spherical particle shapes. Furthermore, difficulties may arise both in LD and DLS measurements for samples containing various populations of different sizes [53]. Therefore, additional techniques, as cryoSEM, may be useful.

3.2.3.2. Morphology determination

Scanning electron microscopy (SEM) is a microscopic technique that became very popular in nanotechnology due to its ability to obtain three dimensional images of the surfaces of the particles on a nanometer to micrometer scale [74].

The SEM is confronted with the inescapable fact that the liquid is an essential part of practically all the specimens (samples). Cryo-SEM is a fast, reliable and effective way to overcome the limitations of SEM found in liquid samples [77]. The cryo-SEM is a conventional SEM, which has been fitted with specific equipment which allows samples appear in the frozen state. This is particularly useful for viewing directly hydrated samples (wet), delicate biological samples, hydrogels, food, biofilms, foams, fats and waxes, suspensions, pharmaceutical products and nanoparticles [78]. Using this technique eliminates the need for conventional preparation techniques, such as, the critical point of drying or freeze-drying (which may probably cause nanoparticles shrinkage), and allows observation of the sample in its "natural" hydrated state [77]. This technique allows the frozen samples to be fractured or cut during preparation to reveal internal structures [78].

To characterize the morphology of SLNs and NLCs, the nanosystems were observed by cryo-SEM using a JEOL JSM 6301F (Tokyo, Japan), an Oxford Instruments INCA Energy 350 (Abingdon, UK), and a Gatan Alto 2500 (Pleasanton, CA, USA). The dispersions of nanoparticles were placed in an appropriate support, which was then mounted on a cleverly designed freezing/vacuum transfer rod. The samples were then rapidly cooled in a liquid nitrogen slush (−210°C), and transferred under vacuum to the cold stage of the preparation chamber. Here, the samples were fractured, sublimated (2 minutes, −90°C) to reveal greater detail, and coated with a gold-palladium alloy. Finally, the specimens were moved under vacuum into the SEM chamber where they were observed at −150°C [77]. The

nanoformulations were then photographed using both secondary electrons (SE) as backscattered electrons (BSE) [78].

3.2.3.3. Zeta potential determination

The liquid layer surrounding the particle is composed of the stern layer (where ions bind strongly to the particle) and a more diffuse outer zone (where ions are less strongly bound). In this diffuse layer ends the limit of the particle as a charged isolated entity. The potential in this limit is the zeta potential (figure 3.5).

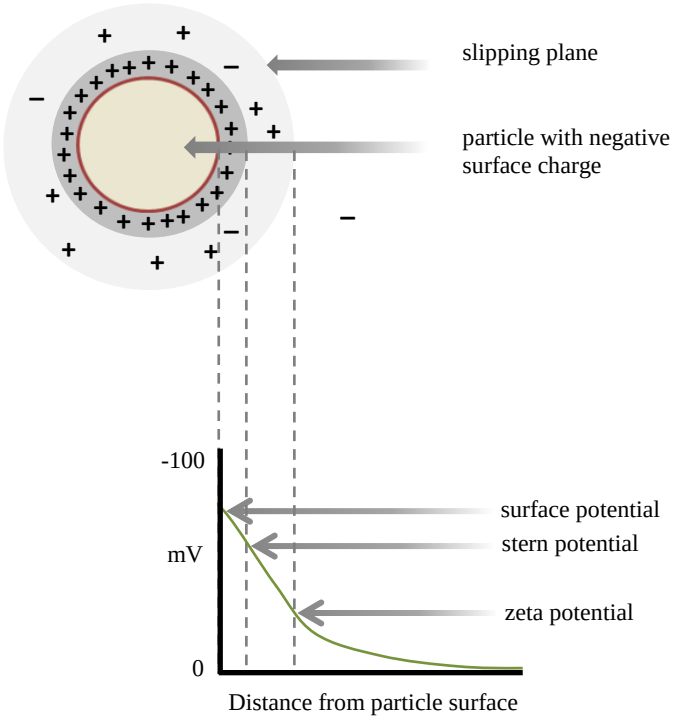

Figure 3.5 - Schematic representation of zeta, stern and surface potential.

Zeta potential (ZP) is then a measure of the magnitude of repulsion or attraction electrostatic charge between particles in liquid suspension and can help to understand and control colloidal suspensions [72, 79]. It is one of the key parameters known that affect the stability of a colloidal dispersion [53]. In general, the particles can be considered stably dispersed when the absolute value of the zeta potential is above 30 mV due to electrical repulsion between particles, while potential of 5 mV to 15 mV results in limited flocculation and potential of 0 mV and 5 mV at maximum flocculation [75].

The electrophoretic light scattering was the technique used to evaluate this parameter.

Electrophoretic light scattering

Electrophoretic light scattering (ELS) is a technique used to measure the electrophoretic mobility of the dispersed particles or molecules in solution. This mobility is usually converted into Zeta Potential. The fundamental physical principle is electrophoresis. The dispersion is introduced into a cell containing two electrodes. An electric field is applied to the electrodes and any charged particles/molecules migrate towards the electrode of an opposite charge. The speed they migrate is known as the electrophoretic mobility and is related to the zeta potential (figure 3.6). This speed is measured by Laser Doppler technique [72].

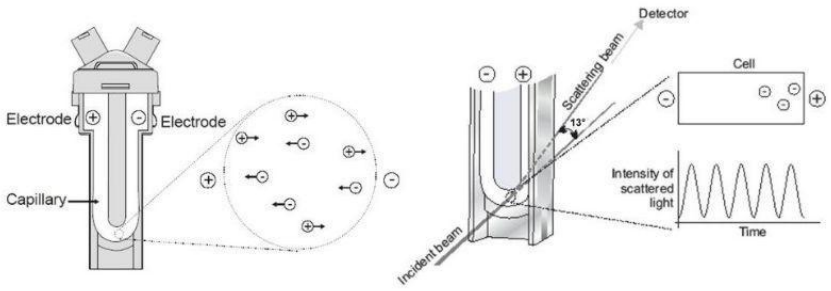

Figure 3.6 - Illustration of the operation of electrophoretic light scattering [80].

In the case of DLS, Brownian motion causes movement of particles. In the case of ELS, the oscillation of the electric field performs the same function. It often combines the DLS and ELS techniques in a single instrument which gives the ability to measure both the particle size and zeta potential [72].

The zeta potential was determined by measuring the electrophoretic mobility using a ZetaPALS (Brookhaven Instruments, Holtsville, NY, USA). Samples were diluted (1:1000) with milli-Q water and analyzed at 25 °C. The zeta potential of the samples was obtained by calculating the average of six runs, each with ten cycles. Measurements were performed in three or more samples.

3.2.3.4. Thermodynamic behavior

The determination of particle size and zeta potential are necessary conditions, but not an enough step to characterize the quality of LN. Special attention should be given to characterize the degree of crystallinity and lipid modification of the lipid profile, since these parameters are strongly correlated with the drug incorporation and release rates [53].

As referred to in chapter II, section 2.2.1.1., the lipid molecules can cross several thermodynamic configurations, from the most unstable (α), after production, to the more stable (β), during the shelf life. During storage the lipid nanoparticles, especially the SLNs, lose some of its load capacity (having drug expulsion) due to rearrangement of the crystal structure and the acquisition of a more organized structure [53].

These characteristics have been evaluated by differential scanning calorimetry.

<u>Differential scanning calorimetry</u>

Differential scanning calorimetry (DSC) is a thermal analysis technique that analyzes how the heat capacity (C_p) of a material is changed by temperature. A sample of known mass is heated or cooled and the changes in its thermal capacity are controlled as well as changes in heat flow. This allows the detection of transitions, such as melts, crystallization, glass transition, phase changes, and curing (figure 3.7) [81]. In addition, the DSC is helpful to understand the drug and lipid interactions within the SLNs and NLCs [74].

In DSC analysis, the sample is placed in an aluminum pan (sample pan) and an empty pan is used as reference (reference pan) (figure 3.8). Both pans are placed into the DSC chamber under which there are thermocouples sensors [82]. The temperatures of both pans are increased identically over time. The difference in energy input required to equalize the temperature of the sample and reference would be the amount of excess heat absorbed or released by the sample (during an endothermic or exothermic process, respectively) [83]. This technique allows then to

measure enthalpy changes (ΔH) [82]. ΔH is obtained by integration of the peak (peak area) of DSC thermograms [74].

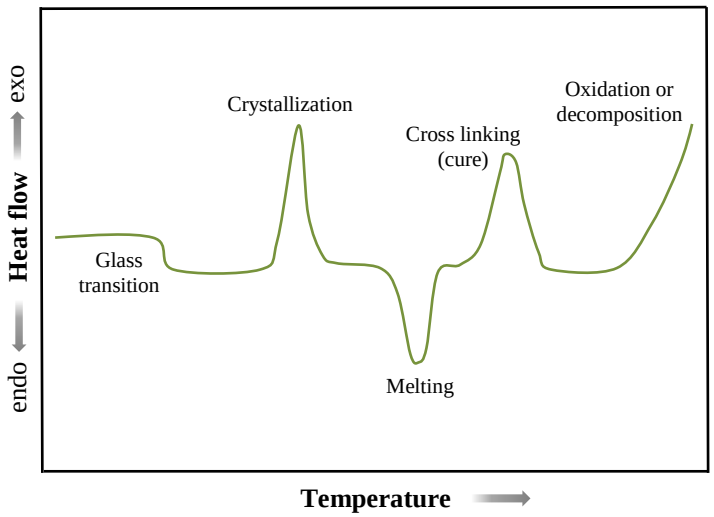

Figure 3.7 - A schematic DSC thermogram. This graph presents four critical points: the glass transition temperature (Tg), the crystallization temperature (Tc), the melting temperature (Tm), and the curing temperature [82].

The biggest advantage of DSC is the ease and speed with which can be used to see transitions in materials. Speaking of LN, in particular, the DSC utilizes the fact that different lipid modifications have different melting points and fusion enthalpies [53]. The DSC is the most common technique of thermal analysis [53, 56, 81].

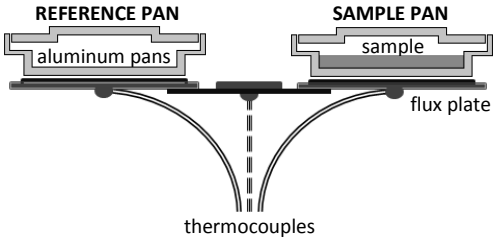

Figure 3.8 - Based scheme of the differential scanning calorimetry.

The study of the degree of crystallinity and polymorphism of lipids was performed using a DSC 200F3 Maia (Netzsh–Gerätebau GmbH). DSC analyzes were performed on the lipid nanoparticles under investigation, as well as the bulk materials used in the preparation of nanoparticles. The SLNs and NLCs were placed in an oven at 34 °C for 12 hours in order to evaporate the water (this treatment is not necessary in the bulk material). The samples were weighed (5-10 mg) directly into aluminum pans. The sample was scanned between -30°C and 270°C (samples with drug) or -30°C and 120°C (samples without drug) at a heating rate of 10°C/min under nitrogen gas (40 mL/min). An empty aluminum pan was used as reference. The onset temperature and melting enthalpy (ΔH) were calculated using Proteus Analysis software. The degree of crystallinity or recrystallization index (RI) was calculated by the following equation [75] (equation 3.2):

$$RI\ [\%] = \frac{\Delta H\ \text{SLN/NLC}\ [J/g]}{\Delta H\ \text{bulk material}\ [J/g] \text{x Concentration CP}\ [\%]}\ x\ 100\ (\boldsymbol{equation\ 3.2})$$

wherein ΔH is the molar melting enthalpy given by J/g and concentration is determined by the percentage of lipid phase.

3.2.3.5. Encapsulation efficiency

The encapsulation efficiency (EE) of nanoformulations was determined by high-performance liquid chromatography.

High-performance liquid chromatography

High-performance liquid chromatography (HPLC) is used in analytical chemistry and biochemistry to separate chemical compounds in mixtures for analysis or purification (figure 3.9). A small volume of liquid sample is injected into a column filled with silica-based particle (stationary phase). The sample individual components are separated in the column by pumping (high pressure) of a solvent (mobile phase) through this column. Depending on the affinity that each single component (analyte) has with mobile and stationary phase, the different components will migrate down the column at different speeds and times, so there will be a separation of the components. The analytes with greater affinity for the mobile phase migrate faster through the column and the opposite happens with the analytes with higher affinity for the stationary phase which migrate more slowly. This migration time (retention time) is somehow unique for each component, which will allow its separation and identification. As well as a qualitative method, it is also a quantitative method. With the suitable use of a detection method after the column, each analyte can be quantified by analysis of the area under the peak [84].

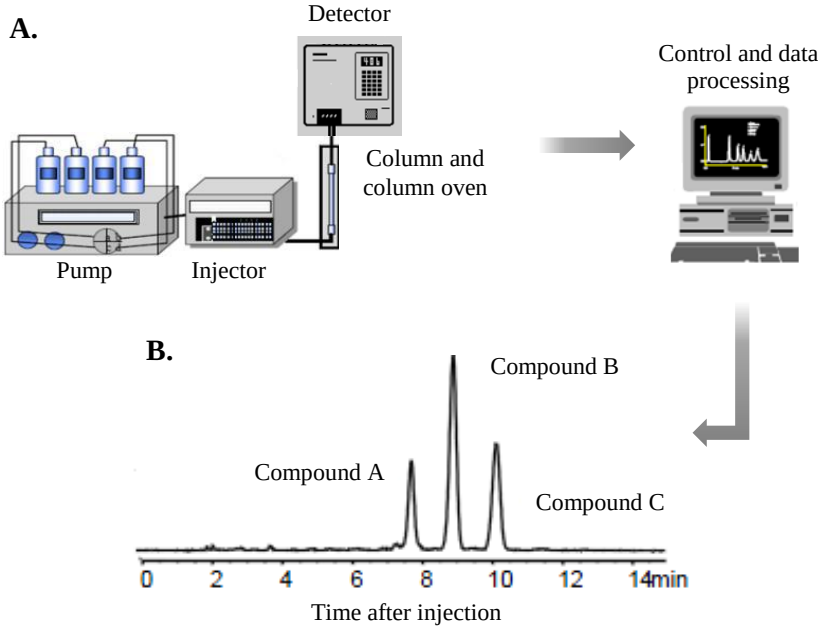

Figure 3.9 – A. Basic components of an HPLC system are a solvent delivery pump, sample injection port, column, detector and data system (computer). **B.** Presentation of a chromatogram obtained by HPLC in which are displayed three chromatographic peaks and each one represents a separated compound.

Validation of the HPLC method to saquinavir

To be able to determine the encapsulation efficiency of LN it was necessary to validate the HPLC method for saquinavir. To this end, an UltiMate 3000 Standard HPLC Systems (Dionex Corporation, Sunnyvale, USA) was used.

Having regard to methodology already developed and described in the literature and were conducted reproduction tests under the analytical conditions described [19, 38], with slight changes. The tests were performed using a Diode Array Detector (DAD). To set the wavelength where the readings were made, SQV absorption spectra was performed using a

spectrophotometer (Jasco V-650 UV-VIS Spectrophotometer, Tokyo, Japan) to find the maximum aborption wavelength (240 nm). The chromatographic analysis was performed at 30 °C in reversed-phase Mediterranea™ Sea18 column (150 mm × 4.0 mm, 5 µm, Teknokroma, Spain). Mobile phase contained 55% acetonitrile (phase A) and 45% (v/v) of 70 mM KH_2PO_4 was adjusted to pH 5 with 1 M KOH (phase B). The flow rate was 1 mL/min in isocratic elution and the injected sample volume was 40 µL. Each run lasted 8 minutes, with retention times in the order of 2.9 minutes.

SQV stock solution was prepared in ACN (55%) and KH_2PO_4 (45%) (eluent solution) with a concentration around 100 µg/mL. Through independent dilutions of the stock solution with the eluent solution five standard solutions with concentrations ranging from 1.2 µg/mL and 1.8 µg/mL were obtained. With these concentrations and areas under the peak corresponding, the calibration curve was obtained. These steps were repeated to obtain three similar calibration curves in order to avoid the error to obtain the stock solution (appendix – figures A.1-15).

System suitability

To assess whether the system used for the analysis is capable of providing acceptable quality data, system suitability experiments were performed. Some of the parameters being measured and their recommended limits, in accordance with US-FDA, are the capacity factor ($k' > 2$), number of column plates ($N > 2000$) and asymmetry (f.s. ≤ 2). Typically, at least two of these criteria are required to ensure system suitability. However, in this analysis all these requirements have been met by ensuring that HPLC is able to generate results of acceptable accuracy and precision [85, 86].

The chromatographic method was validated for specificity, linearity, accuracy and precision following the recommendations of ICH Harmonised Tripartite Guideline [87].

Specificity

The specificity is the ability of an analytical method to distinguish and quantify the analyte in the presence of other components attached to the samples (excipients) [74]. To verify the chromatographic purity of the principal peak, "sliced-up" the peak to get the UV spectra of each part [88]. Another way to evaluate the specificity was to compare the matrix free of active substance (eluent solution and empty LN) and the matrix added with SQV [85].

Linearity

Linearity was assessed taking into account the correlation between the measured signal (peak area) and SQV concentration - calibration curve ($y = ax + b$). The correlation coefficient (R), y-intercept (b), regression line slope (a) and residual sum of squares (RSS) allowed an estimation of the quality of the obtained curve [85, 87]. Furthermore, an analysis of the deviation of the real data points from the regression line, may also be useful for evaluating the linearity (residual plot) [87]. A third approach was to divide the signal data by their respective concentrations by providing the relative responses (response graph vs log concentration) [85].

Precision

- Repeatability

The repeatability corresponds to precision of detector response. The repeatability was verified from a minimum of nine determinations covering the range of expected concentrations: 3 injections of 3 different concentrations (1.35, 1.50 e 1.65 µg/mL) [85, 86].

Results of method precision were presented through the coefficient of variation (CV), calculated by the ratio to the standard deviation with mean values obtained [89].

- Intermediate precision

It indicates the effect of changes in a laboratory due to events such as different days, analysts, equipment, etc. [85]. So, after 48 hours the response of the detector with the same solution under the same conditions was checked again, restarting the whole system. The same solutions (1.35, 1.50 e 1.65 µg/mL) were injected three times and the detector response results were compared with results obtained previously [86].

The number of trials needed to assess the intermediate precision followed the same recommendation of ICH for the calculation of repeatability described above. The intermediate precision was expressed by coefficient of variation (CV) [85].

Accuracy

It is the degree of agreement between individual results obtained in a particular test and a reference value accepted as true. It is important to note that an accurate or true value is the value obtained by a perfect measurement and this value is indeterminate by nature [85]. The ICH provides that at least nine determinations involving a minimum of three different concentration levels must be obeyed. Standards were used in triplicate for three concentration levels (1.35, 1.50 e 1.65 µg/mL) [85]. In addition, and in order to study the overall accuracy, lipid nanoparticles with known SQV concentration were exposed to direct method (without the first filter - see next section), in order to account the influence of the losses associated to sample preparation in the determining the concentration.

The accuracy results were obtained from the ratio in percentage of the difference between the obtained value and the theoretical value in relation to theoretical value [89].

Encapsulation efficiency - direct method

As described by Das et al [90], the freshly prepared formulation, diluted with milliQ water (1:5), was filtered through a 5 µm nitrocellulose membrane filter (Millipore, Ireland) to remove unencapsulated drug crystals. The saquinavir have high solubility in methanol, whereas the lipids are insoluble in methanol. Hence, 9 mL methanol was added to a 1 mL filtered formulation and thoroughly mixed to extract the drug from the lipid matrix. The mixture was then centrifuged at 4620 g for 15 min (ThermoScientific Heraeus Multifuge X1R Refrigerated Benchtop Centrifuge) and supernatant was filtered through a 0.45 µm PTFE syringe filter (Millipore, Ireland). The supernatant was again diluted 1:6 with eluent solution to the HPLC assay calibration range. The amount of drug in the filtered supernatant was measured by HPLC (HPLC Systems Standard UltiMate 3000, Dionex Corporation, Sunnyvale, USA). EE, determined in six separate lots, was calculated as follows (equation 3.3), considering the dilution factor:

$$EE\ (\%) = \frac{Amount\ of\ SQV\ in\ the\ filtered\ formulation}{Total\ amount\ of\ SQV}\ x\ 100\ (\boldsymbol{equation\ 3.3})$$

3.2.4. Cell culture

3.2.4.1. Cell description

The human astrocytoma U-87 MG cell line is a commercial cell line sold by American Type Culture Collection (U-87 MG (ATCC® HTB-14™). It derived from a human glioblastoma (astrocytoma), classified as grade IV as of 2007 with adherent properties [91].

3.2.4.2. Cell line culture conditions

The human glioma U-87 MG cell line was maintained in complete Dulbecco's Modified Eagle's Medium (DMEM) supplemented with 10% fetal bovine serum (FBS) and 1% antibiotic-antimycotic (10,000 units/mL penicillin G sodium, 10,000 mg/mL streptomycin sulphate) in 25 cm^2 or 75 cm^2 flasks. Cells were subcultured every 2-3 days using trypsin-EDTA [91].

3.2.4.3. Routine laboratory procedures

Cell subculture

The culture was visually examined for macroscopic evidence of any microbial contamination. Using an inverted microscope (Motic AE2000 Inverted Microscope) the presence of any microbial contamination (bacteria, mold and yeast) and cell confluency was inspected. When cells reached 70/80% confluence, they were subcultured to prevent cell death [92]. Initially, the culture medium was aspirated and the cells washed with PBS without Ca^{2+}/Mg^{2+}. Then the cells were suspended by adding trypsin-EDTA [92]. Trypsin, cuts the adhesive proteins in the cell cell and cell-matrix interactions. After cell detaching (5-10 minutes), medium was added in order to block the action of trypsin. Cell suspension

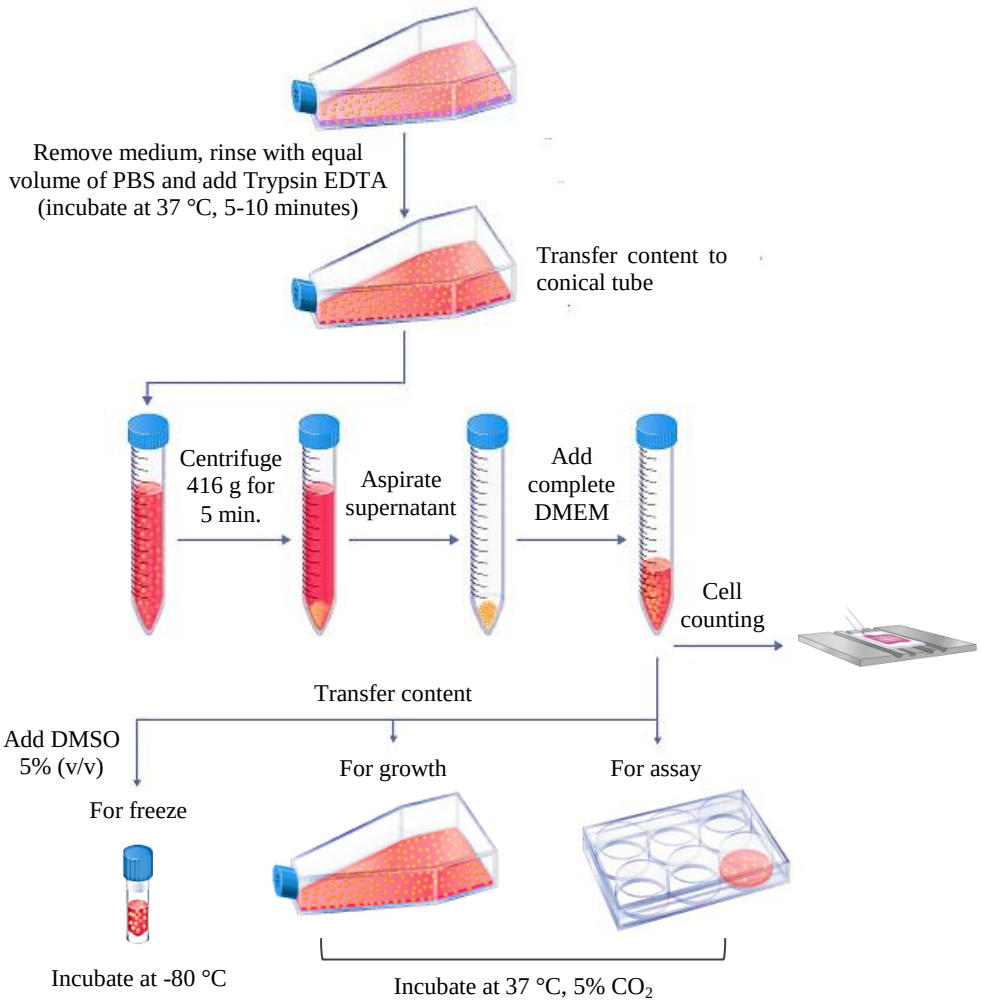

Figure 3.10– Expansion, subculture and freezing of U-87 MG cell line.

was then centrifuged at 416 g and 21 °C for 5 minutes. The supernatant was removed and the formed pellet was ressuspended in new medium. Cells were counted, the concentration adjusted and cultured in new culture flasks. The flasks were incubated at 37 °C, 5% CO_2 in air atmosphere (Heraeus HeraCell 150 Air-Jacketed CO_2 Incubator). This cell suspension were also frozen or used for a cellular assay (figure 3.10) [93].

Cell counting

10 µL of cell suspension was added to 90 µl of 0.4% trypan blue vital dye (1:10) and placed in a Neubauer chamber. Using an inverted microscope, viable cells were then counted [93]. The number of cells in the total volume [93] was calculated with the following equation (equation 3.4):

$$\frac{n}{4}\ x\ \frac{1}{d^{-1}}\ x\ 10^4 = number\ of\ \ cells/mL\ (\boldsymbol{equation\ 3.4})$$

where n is the number of cells counted and d is the proportion of dilution.

Cell thawing

The cryovial was thawed by gentle agitation in a 37 °C water bath (figure 3.11). The content thawed (thawing should be quick, approximately 2 min.) was ressuspended in complete DMEM medium and then centrifuged at 416 g for 5 minutes, at room temperature. The suspension was discarded and the pellet resuspended in complete DMEM. The cell suspension was transferred to a 25 cm^2 culture flask and incubated at 37 °C and 5% CO_2 in air atmosphere [93].

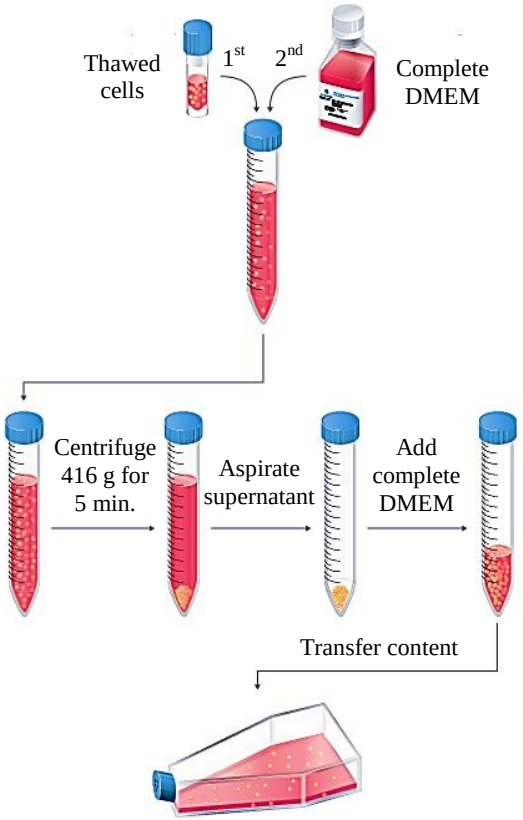

Figure 3.11 - Thawing of U-87 MG cell line.

Cell freezing

Some of the cells used in subculture can be frozen in order to prevent phenotypic and genotypic degeneration, consequence of high passage number [93]. Thus, 5% (v/v) DMSO was added to cell suspension, a cryo-preservative which prevents the formation of crystals during the storage phase [93]. $5x10^5$ cell per ml (or more) were transferred to 1 mL or 2 mL cryovials and stored at -80 °C.

3.2.4.4. In vitro assays

Determination of cell viability by MTT

The viability of the U-87 MG glioma cell line exposed to SQV-SLN and SQV-NLC was assessed using the MTT assay. The 3-(4,5-dimethylthiazol-2-yl)-2,5-diphenyltetrazolium bromide, or simply tetrazolium bromide (MTT) can be used to measure metabolic activity of viable cells. The MTT is reduced to formazan (precipitated of violet coloring) by mitochondrial succinate dehydrogenase, an enzyme which is active in cells with intact respiratory chain metabolism. Thus, the formazan is quantified in a plate reader at 570 nm and has a positive correlation with the number of viable cells [94].

Before performing the tests, a standard curve was obtained to meet the most appropriate cell concentration for measurements. To optimize the method, 100 µL of cell suspension were seeded in 96 well tissue culture plates at different cell concentrations (*0*, $5x10^4$, $1x10^5$, $2x10^5$ and $4x10^5$ cell/mL). A 12 mM MTT stock solution was prepared by adding 1 mL of sterile PBS at 5 mg of MTT, and mixed by vortex until dissolved. Then, 9 mL of incomplete DMEM was added to stock solution. This solution was protected from light and prepared on the day of use. After 48 hours of cell incubation at 37 °C and an atmosphere of 5% CO_2 (with change of medium after 24 hours) 100 µL per well of the MTT solution prepared were added. The culture plate was incubated at 37 °C and 5% CO_2, in the dark. After labeling the cells for 2 hours with MTT, the contents of the wells were aspirated and 100 µL of DMSO were added to each well. After 15 minutes at 37 °C incubation in the dark, the released formazan was then quantified by reading its absorbance at 570 nm on a plate reader (BioTek, Synergy HT multi-mode microplate reader).

Using the optimized method, cells were seeded (100 µL per well) according to the most appropriate cell density and incubated at 37 °C, 5% CO_2. After 24 hours of incubation, the cells were placed with the different formulations (SQV, SLN, NLC, SQV-SLN e SQV-NLC). The cells in complete DMEM were used as positive control, and cells with Triton X-100 (2%) or DMSO (10%) were used as negative control.

For SQV solution, SQV was dissolved in DMSO (5 mg/mL) and then diluted in complete medium to the concentrations of 2.5 and 25 µM. The other conditions (SLN, NLC, SQV-SLN e SQV-NLC) were also diluted in complete DMEM to the desired concentrations. The plate was incubated for 24 hours at 37 °C under an atmosphere of 5% CO_2. On the third day, the procedure was the same as used for optimization of the method. The assay was repeated 3 times in independent experiments.

Determination of cell viability by propidium iodide exclusion

To verify the integrity of the plasma membrane, the incorporation technique of propidium iodide (PI) staining was used. The PI is a red dye that is generally excluded from viable cells and stain dead cells. This dye does not pass through intact cell membranes, but freely penetrate

cells with compromised cell membranes. Upon entering dead cells, PI binds to double-stranded DNA by intercalating between base pairs. As this intercalation is mediated by non-covalent forces, these dyes must remain present in the buffer used to resuspend cells for data acquisition so that dead cells will remain labeled. PI is excited at 488 nm and, with a relatively large Stokes shift, emits in the maximum wavelength of 617 nm [95]. Therefore, the method used to quantify the amount of PI into dead cells was flow cytometry,a rapid and reliable technique to quantify the viable/dead cells in a cell suspension. Flow cytometry is a technology which measures and analyzes various physical properties of individual particles (relative size, granularity and fluorescence intensity), usually cells, as they flow in a fluid stream through a light beam. An optical- to-electronic coupling system records as the cell or particle scatters the incident laser light and emits fluorescence [96].

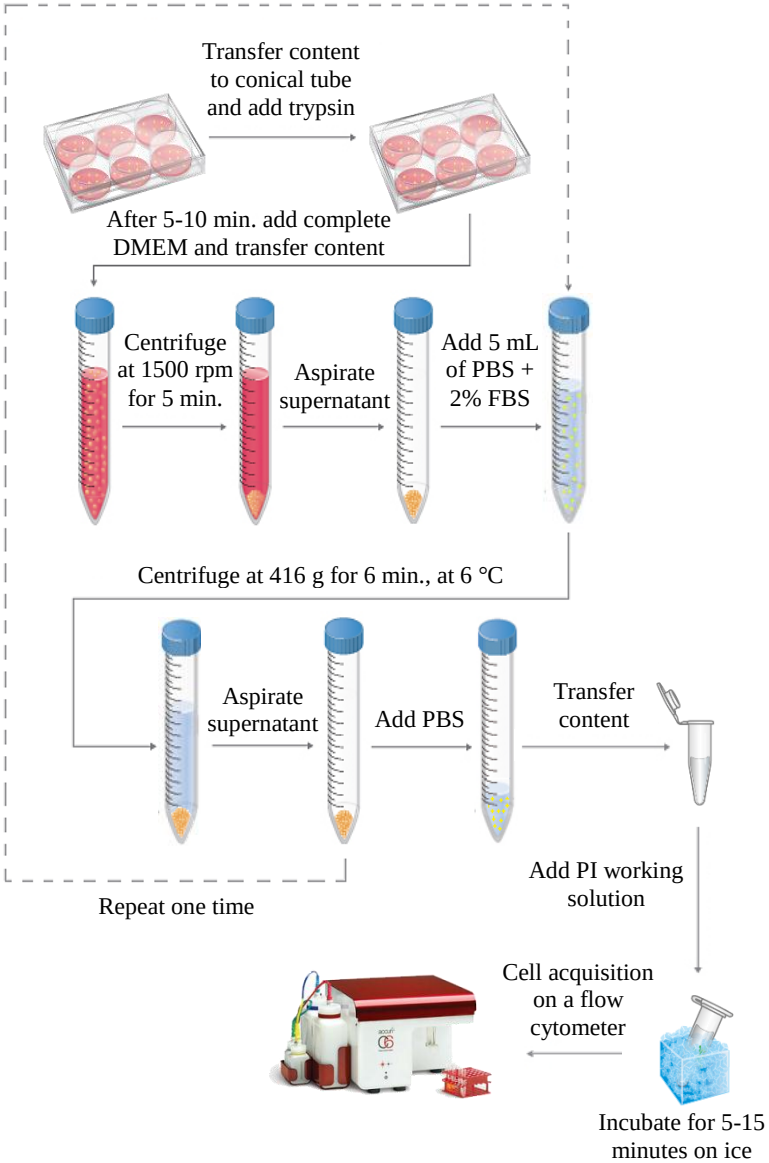

Figure 3.12- PI staining assay procedure.

Briefly, U-87 MG cells were seeded at $1.0x10^5$ cell per well in 12-well culture plates (1 mL per well) [97, 98]. Culture plates were incubated at 37 °C and 5% CO_2 for 24 hours.

Then, the cells were placed in the presence of the formulations under study: SQV, SLN, NLC, SQV-SLN e SQV-NLC. SQV in free form was dissolved in DMSO (5 mg/mL). All formulations were then diluted in complete DMEM to a concentration of 25 µM of SQV. Wells with DMSO (10%) and Triton X-100 (2%) were used as positive cell controls.

The plates were incubated for 24 hours (37 °C and 5% CO_2). By the third day (figure 3.12), the contents of the wells were transferred into conical tubes and the cells were detached from the bottom of the wells by the action of trypsin. After 5-10 minutes, complete DMEM was added to stop the action of trypsin and the content was centrifuged at 416 g for 5 minutes at room temperature. The supernatant was discarded and the cells washed two times by addition of 5 ml of PBS (1X) + 2% FBS (at a temperature of 6 °C), centrifuging at 416 g for 6 minutes at a temperature of 6 °C. Then, the supernatant was aspirated and the cells were ressuspended in 100 µL of PBS. Content was transferred to eppendorfs and, finally, stained with 5 µL of PI working solution [10 µL of stock solution (10 mg of PI + 10 mL of Milli Q water) in 1 mL of PBS] 5 minutes before starting the analysis. Cells were acquired on the flow cytometer BD Accuri C6 and the fluorescence of PI (using the FL-2 channel) was determined. Data were acquired to unstained cells to determine the number of positive events. At least 20000 events per sample were acquired by flow cytometry.

3.2.5. Statistical analysis

The t-test and the one-way analysis of variance (ANOVA) were performed to compare two or multiple groups, respectively. Differences between more than two groups were compared within a post hoc test (Tukey HSD), after confirming normality and homogeneity of variance with Shapiro-Wilk and Levene tests. Results are reported as a mean ± SD from a minimum of three independent experiments. Differences were considered statistically significant at $p < 0.05$. All statistical analyses were performed with the SPSS software (v 23.0; IBM, Armonk, NY, USA).

Chapter IV - Results and Discussion

A unique code was selected in order to identify the quantitative composition of the several lipid formulations. For example, **$SQV_{0.05}$- $CP_3M_2T_2$** where **SQV** stands for saquinavir, **subscript 0.05** for 0.05% drug; **CP** stands for cetyl palmitate, **subscript 3** for 3% solid lipid; **M** stands for miglyol 812, **subscript 2** for 2% liquid lipid; and **T** for tween 80, **subscript 2** for 2% surfactant. All the formulation codes are depicted in table 4.1.

4.1. Optimization of empty nanoparticles

The main objective of this work was to produce lipid nanoparticles (LN) loaded with SQV with homogeneous sizes in the range of 200 nm. This is the ideal nanoparticle size to effectively cross the BBB and reach the tumor tissue (EPR effect) [9, 11]. Another advantage of this size is that the nanoparticles are large enough to prevent the elimination of first pass through the kidney (renal clearance < 6 nm), and are small enough to prevent the filtration in the spleen and absorption in the liver (> 250 nm). Particles larger than 250 nm are quickly captured and excreted [9]. On the other hand, nanoparticles in the range of 200nm can be used for systemic use (e.g., intravenous (IV)) without risk of causing coagulation and aggregation in blood and subsequent embolism, since the size of particles administered by this route must be less than 5 µm to avoid blockage of capillaries [43].

With this provost, various formulations were tested with different proportions of lipid (5 and 10%), surfactant (1, 2 and 3%) and drug (0.10 and 0.05%). The parameters inherent to the high-shear homogenization (rpm and time), ultrasonication (time and amplitude) and hot homogenizing (pressure and cycles) were fixed, not being the subject of study.

4.1.1. Preliminary study of empty nanoparticles

At an initial phase of work only formulations without drug were tested and characterized. The size of the dispersions was assessed, on day 0, by laser diffraction technique. The results of this pre-assessment can be seen in the table 4.1 and figures 4.1 e 4.2.

4.1.1.1. Influence of lipid and surfactant

Analyzing the results, it is observed that the concentration of lipid and surfactant have a direct influence on the final size of the LN [53]. When the percentage of lipid decreases and surfactant increases, SLNs and NLCs acquire a smaller size. This can be explained by the high surfactant concentration that decreases the surface tension and stabilizes the newly formed surfaces during manufacture, forming small droplets [46]. The opposite was observed when the lipid concentration increases and the of surfactant decreases. In this case, the increased lipid

content results in an increase of the pre-emulsion viscosity, making more difficult its emulsification in the aqueous phase [63]. In addition, an insufficient amount of surfactant may have led to increased instability, forming larger droplets [46]. Thus, the $\mathbf{CP_{10}T_1}$ and $\mathbf{CP_7M_3T_1}$ nanoformulations correspond to dispersions with a higher sizes range, within of the corresponding LN type (SLN and NLC, respectively), both in hot homogenization and in ultrasonication. In contrast, the $\mathbf{CP_5T_3}$ and $\mathbf{CP_3M_2T_3}$ formulations have the lowest size (Dv50 ~200nm), from all corresponding LN studied. In $\mathbf{CP_5T_2}$ suspension, despite the mean

Table 4.1 - Mean Dv10, Dv50 and Dv90 of the drug-free nanoformulations tested on day 0.

Formulation			Mean Dv10 ± SD [nm]	Mean Dv50 ± SD [nm]	Mean Dv90 ± SD [nm]	Mean Span ± SD
Ultrasonication	SLN	$\mathbf{CP_{10}T_1}$	309.0 ± 44.2	661.0 ± 71.4	1596.7 ± 115.0	1.955 ± 0.119
		$\mathbf{CP_{10}T_2}$	204.7 ± 31.6	477.3 ± 69.2	1373.3 ± 204.0	2.447 ± 0.023
		$\mathbf{CP_{10}T_3}$	184.7 ± 56.6	450.7 ± 159.7	1298.7 ± 595.8	2.368 ± 0.437
		$\mathbf{CP_5T_1}$	142.7 ± 7.6	313.3 ± 18.7	718.3 ± 60.5	1.833 ± 0.081
		$\mathbf{CP_5T_2}$	92.2 ± 6.9	205.5 ± 12.8	511.8 ± 74.8	1.985 ± 0.238
		$\mathbf{CP_5T_3}$	93.3 ± 8.3	204.5 ± 27.2	529.5 ± 163.5	2.080 ± 0.488
	NLC	$\mathbf{CP_7M_3T_1}$	517.3 ± 195.7	1179.7 ± 305.6	3360.0 ± 661.9	2.451 ± 0.236
		$\mathbf{CP_7M_3T_2}$	214.3 ± 52.2	689.0 ± 280.7	2543.3 ± 665.6	3.561 ± 0.658
		$\mathbf{CP_7M_3T_3}$	157.3 ± 43.0	460.7 ± 242.0	2543.3 ± 711.5	5.609 ± 1.531
		$\mathbf{CP_3M_2T_1}$	174.3 ± 59.7	458.3 ± 232.8	1813.3 ± 795.1	3.651 ± 0.292
		$\mathbf{CP_3M_2T_2}$	100.7 ± 6.9	230.8 ± 8.7	1208.7 ± 468.9	4.334 ± 1.561
		$\mathbf{CP_3M_2T_3}$	94.6 ± 6.7	219.1 ± 23.8	1390.4 ± 698.9	5.667 ± 2.723
Hot HPH	SLN	$\mathbf{CP_{10}T_1}$	141.0 ± 5.3	324.0 ± 17.3	1176.7 ± 141.5	3.179 ± 0.245
		$\mathbf{CP_{10}T_2}$	127.3 ± 4.7	297.0 ± 9.8	1063.7 ± 99.7	3.145 ± 0.245
		$\mathbf{CP_{10}T_3}$	124.0 ± 3.5	281.7 ± 9.8	726.7 ± 22.3	2.138 ± 0.016
		$\mathbf{CP_5T_1}$	129.0 ± 6.2	308.0 ± 21.0	1223.3 ± 70.9	3.544 ± 0.104
		$\mathbf{CP_5T_2}$	99.2 ± 4.7	221.0 ± 11.6	618.1 ± 62.4	2.348 ± 0.228
		$\mathbf{CP_5T_3}$	92.5 ± 10.7	211.2 ± 35.2	529.5 ± 115.6	2.021 ± 0.208
	NLC	$\mathbf{CP_7M_3T_1}$	153.7 ± 12.1	373.0 ± 36.0	1793.3 ± 162.0	4.400 ± 0.245
		$\mathbf{CP_7M_3T_2}$	119.7 ± 3.5	280.0 ± 11.5	1640.0 ± 170.6	5.403 ± 0.420
		$\mathbf{CP_7M_3T_3}$	117.7 ± 1.5	269.7 ± 4.7	1045.7 ± 132.1	3.437 ± 0.452
		$\mathbf{CP_3M_2T_1}$	125.0 ± 4.0	302.7 ± 12.6	1896.7 ± 109.7	5.847 ± 0.206
		$\mathbf{CP_3M_2T_2}$	103.7 ± 1.2	242.3 ± 4.0	1503.3 ± 37.9	5.743 ± 0.038
		$\mathbf{CP_3M_2T_3}$	96.2 ± 3.6	220.2 ± 6.5	955.3 ± 142.6	3.672 ± 0.794

*To calculate the mean and standard deviation (Dv10, Dv50 and Dv90) of the tabulated formulations three or more lots were used. The values of individual sizes of each batch are in appendix (tables A.1-4).

Dv50 exceeds the **CP_5T_3**, the differences are not significant ($p > 0.05$, appendix – table B.1). The same happens between **$CP_3M_2T_2$** and **$CP_3M_2T_3$** formulations.

4.1.1.2. Influence of production technique

The choice of the LN production method is often influenced by the type of study drug, in particular, by its solubility and stability. Hot HPH and ultrasonication have already proven its effectiveness in encapsulation of poorly water soluble drugs [99]. As the SQV is a very lipophilic drug [19] these were the two chosen production methods.

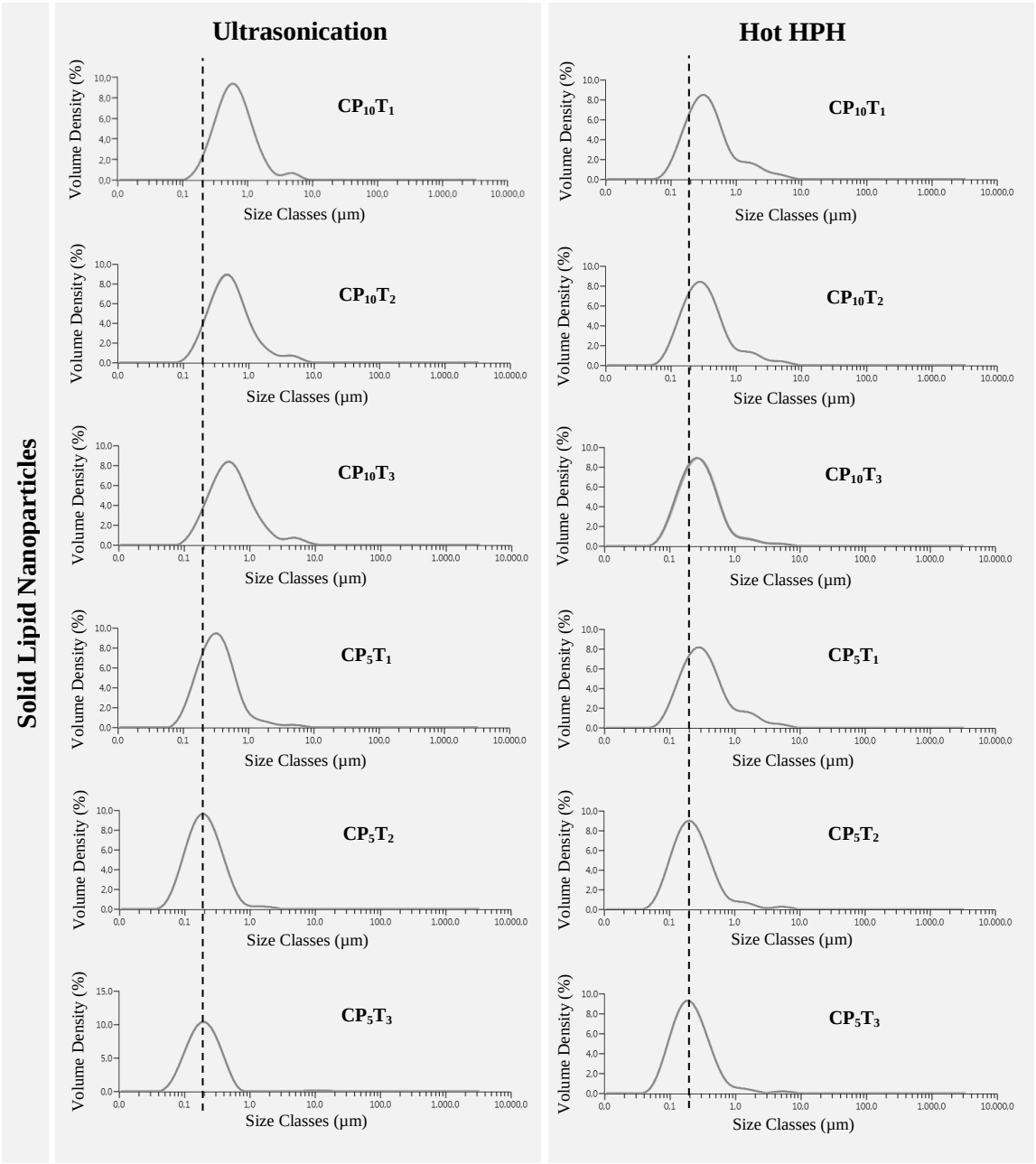

Figure 4.1 - Size distribution (day 0) of drug-free SLNs for the different proportions of lipid and surfactant in both production methods (characterization technique: laser diffraction).

By comparing the percentiles (Dv10, Dv50 and Dv90) obtained by the two techniques, for formulations with the same characteristics - type of lipid nanoparticles (SLNs or NLCs) and

lipid and surfactant ratios -, it was found that in the dispersions with highest lipid percentage (10%) there are significant differences ($p < 0.05$, appendix – tables B.2 e B.4). The means size (Dv10, Dv50 and Dv90) were lower for nanoparticles produced by hot HPH. Unlike ultrasonication, in the hot HPH the energy distribution is more homogeneous, due to the small size of the homogenization gap, which contributed to lower percentile values [99]. However, when evaluating the LN with lower lipid percentage (5%), it does not occur, there being no significant differences ($p > 0.05$, appendix - tables B.1 e B.3), except for the formulation **$CP_3M_2T_1$**. A lower lipid percentage contributes to a lower dispersion viscosity. This fact may have led to greater dispersion movement making the cavitation more efficient during ultrasonication, by contributing to a more uniform energy distribution across the sample, such as in homogenization.

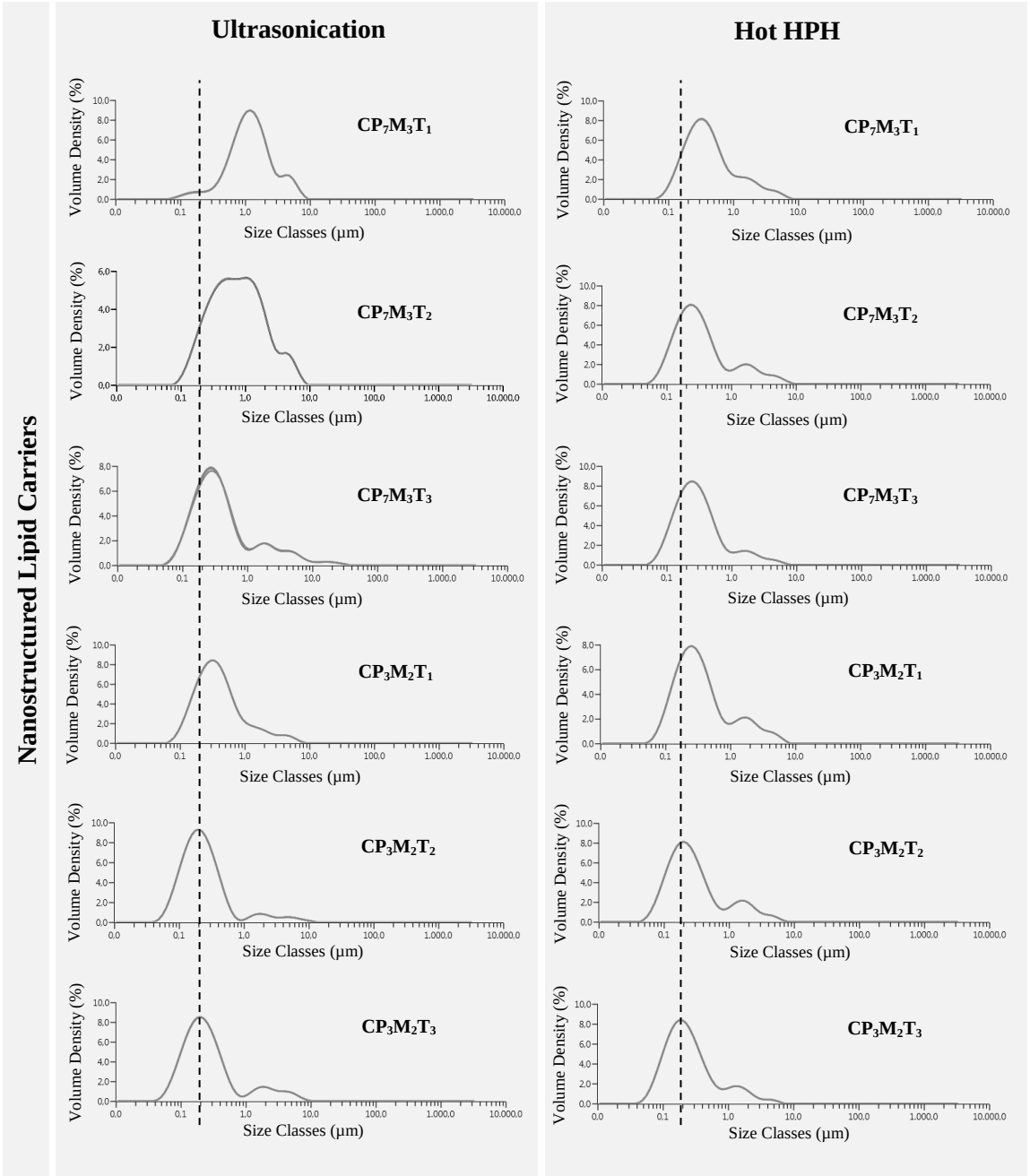

Figure 4.2 - Size distribution (day 0) of drug-free NLCs for the different proportions of lipid and surfactant in both production methods (characterization technique: laser diffraction).

4.1.1.3. Influence of type of LN (SLNs vs NLCs)

In hot HPH, the difference between the SLNs and their respective NLCs (same technique of production and the same proportion of ingredients) was not significant ($p > 0.05$, appendix – table B.5). On the other hand, in the ultrasonication these differences were more evident, having NLCs a relatively higher sizes range compared with the corresponding SLNs, but no significant difference in most formulations ($p > 0.05$, appendix – tables B.6).

Taking into account all these factors, the **CP_5T_2**, **CP_5T_3**, **$CP_3M_2T_2$** and **$CP_3M_2T_3$** dispersions, in both techniques, (eight formulations) were considered the most promising and, therefore, subject to more rigorous characterization. Before loading the nanoparticles with saquinavir, eight drug-free formulations were characterized according to its average size (by DLS technique), polydispersity index and zeta potential (figures 4.1 e 4.2 e tables 4.1 e 4.2).

4.1.2. More detailed study of most promising formulations

As in LD technique (table 4.1), in the DLS method the average of the most promising nanoparticle mean size was circa 200 nm (table 4.2). However, in this latter technique the sizes were slightly lower, with no significant differences ($p > 0.05$, appendix – table B.7) to ultrasonication and with significant differences to hot HPH ($p < 0.05$, appendix - table B.8). These differences exist because the two techniques follow different principles. While the LD technique applies based on the principle that particles passing through a laser beam scatter light with an angle which is directly related to its size, the DLS technique determines the particles size based on the Brownian motion of the same in suspension. Furthermore, the DLS reports the mean particle size of the entire population, while LD indicates the 10, 50 and 90 percentile (10%, 50% and 90% of the population lies below of the size of particle obtained) [100]. Furthermore it must be noticed that the DLS results are shown in intensity function and in the LD the results are in volume function, which leads to differences in size obtained between both techniques.

Table 4.2 - Mean size (Z-average), polydispersity index and zeta potential of the most promising nanoformulations without drug, on day 0.

Formulation			Z-average ± SD [nm]	PI ± SD	ZP ± SD [mV]
Ultrasonication	SLN	CP_5T_2	197.7 ± 8.8	0.117 ± 0.044	-32.61 ± 1.13
		CP_5T_3	200.1 ± 12.5	0.127 ± 0.060	-34.78 ± 4.17
	NLC	$CP_3M_2T_2$	215.5 ± 12.0	0.094 ± 0.053	-34.78 ± 2.83
		$CP_3M_2T_3$	210.5 ± 8.0	0.090 ± 0.047	-30.44 ± 6.28
Hot HPH	SLN	CP_5T_2	185.6 ± 6.2	0.129 ± 0.058	-33.60 ± 2.03
		CP_5T_3	167.1 ± 10.4	0.148 ± 0.039	-30.82 ± 3.62
	NLC	$CP_3M_2T_2$	195.3 ± 4.7	0.154 ± 0.041	-35.79 ± 5.00
		$CP_3M_2T_3$	183.8 ± 11.3	0.172 ± 0.030	-36.86 ± 7.44

*To calculate the mean and standard deviation (Z-average, PI, ZP) of the tabulated formulations were used three lots. The values of individual sizes of each batch are in appendix (table A.5)

The DLS technique, in addition to the Z-average, allows the determination of the size distribution. The polydispersity index (PI) obtained for the eight "chosen" formulations were satisfactory. In all the suspensions the PI value was below 0.2 (table 4.2), indicating that the samples under study are monodisperse. The SLNs that showed a lower PI were the $\mathbf{CP_5T_2}$ produced by ultrasonication. On the other hand, the NLC with improved PI were $\mathbf{CP_3M_2T_3}$, also produced by ultrasonication. Contrary to expectations, the nanoformulations obtained by Hot HPH resulted in a larger sizes distribution. Normally, a more uniform energy distribution (as in Hot HPH), results in lower PI. However, an inadequate homogenization pressure or number of cycles can lead to an increase in the size dispersion as a result of particle coalescence, which occurs due to the high kinetic energy of the particles [56, 60].

In addition to the size and polydispersity index, the zeta potential is another important factor when trying to characterize a suspension. According to literature, when the absolute value of the zeta potential is greater than 30mV for colloidal formulation, the particles are likely to be electrochemically stable under storage conditions, because the surface charge prevents particle aggregation [101]. In the eight tested formulations, the zeta potential was always lower than -30 mV (table 4.2). These values were relatively better for NLCs than for SLNs, although with no significant differences ($p > 0.05$, appendix – table B.9).

4.1.3. Stability

The stability of the eight formulations was assessed over 4 months (days 0, 60, 120). The samples remained during storage at 4 °C. The stability parameters evaluated were the mean size (by LD and DLS), polydispersity index and zeta potential. The results obtained for each component are shown in figures 4.3, 4.4 and 4.5.

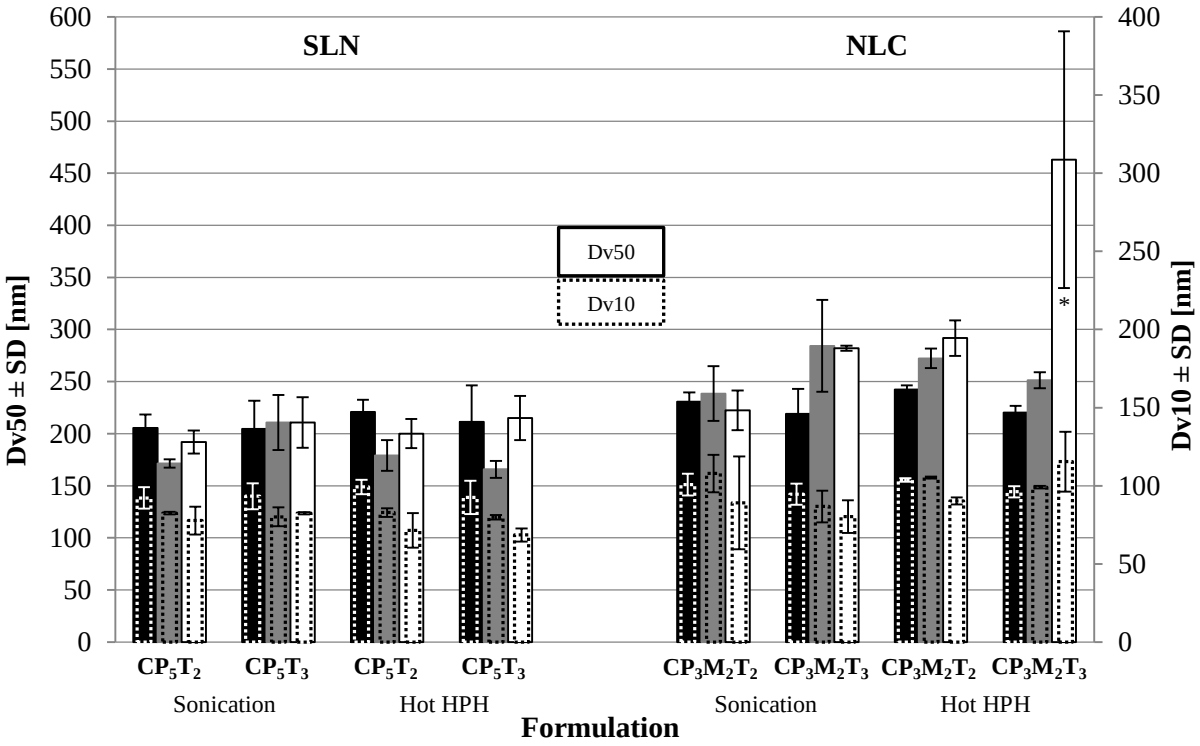

Figure 4.3 - Effect of time of storage (at 4°C) on particle size of empty SLNs and NLCs at different concentrations of lipid and surfactant, in ultrasonication and hot HPH. **Notes**: Dv10 and Dv50 on the production day (■), after 2 months (■), and 4 month (□). All data represent the mean ± standard deviation (n = 3). * Formulation data are statistically different ($p < 0.05$, appendix – tables B.10 and B.11) compared with the production day.

The figures 4.3 and 4.4 show the percentiles 10, 50 and 90, obtained by LD of the drug-free SLNs and NLCs at different times over the 4 months of investigation. The results show that, despite some variations, the Dv10 and Dv50 were kept constant throughout the observation period for both types of LN ($p > 0.05$, appendix – tables B.10 and B.11). In a global review of varying sizes over time, the SLNs showed particles with sizes in the range of 68.5 - 99.2 nm for Dv10, and in the range of 165.7 - 215.0 nm for Dv50. On the other hand, Dv10 and Dv50 of the NLCs were among 80.2 - 115.4 nm and 219.1 - 291.7 nm, respectively. With the exception of the **$CP_3M_2T_3$** nanoformulation produced by hot HPH, that in the fourth month of assessment showed a sharp rise in Dv50 - 463.0 nm (more than twice the size in relation to the measurement made in the production day, $p < 0.05$, appendix – table B.11).

Although the little variation in the Dv10 and Dv50, the study of Dv90 over time (figure 4.4) showed significant differences between measurements made on days 0, 60 and 120 ($p < 0.05$, appendix – table B.12), with a larger variation for NLCs. The **CP_5T_2** formulation (SLN), produced by ultrasonication, was the only one without significant differences throughout the evaluation period of size stability. In the case of NLCs, the nanoformulation that proved most promising was the **$CP_3M_2T_2$**, with the less steep variation of the Dv90 over time.

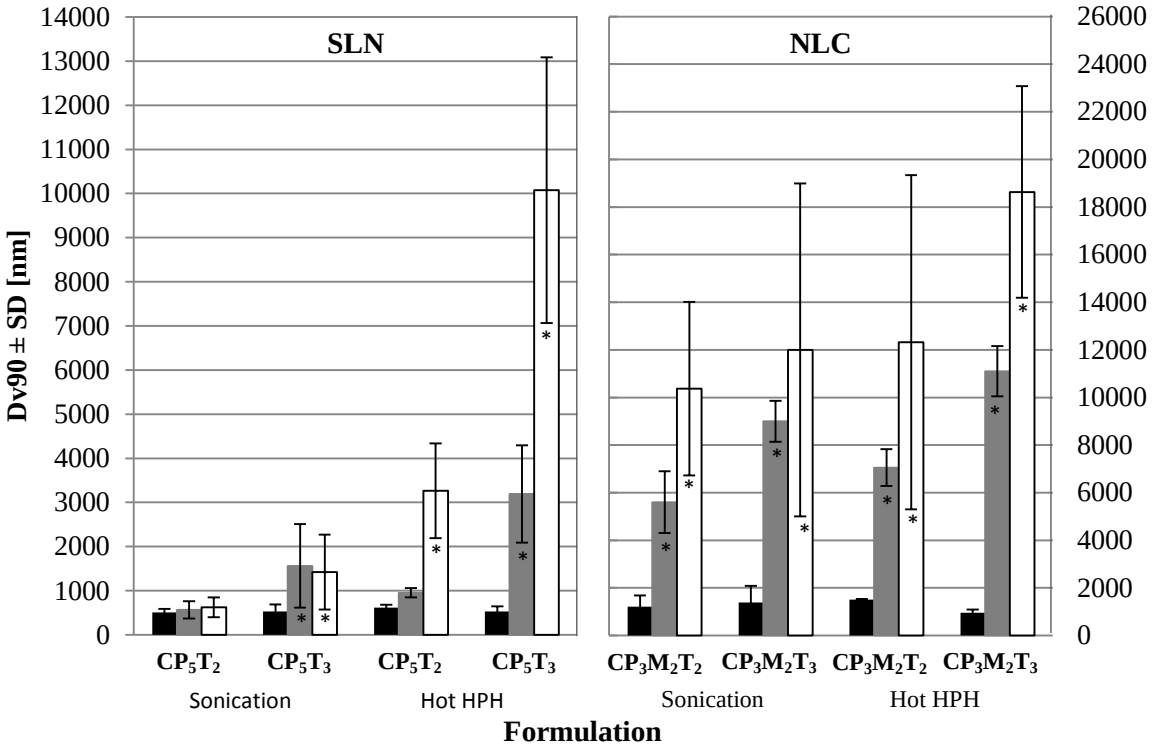

Figure 4.4 - Effect of time of storage (at 4°C) on particle size of empty SLNs and NLCs at different concentrations of lipid and surfactant, in ultrasonication and hot HPH. **Notes**: Dv90 on the production day (■), after 2 months (■), and 4 month (□). All data represent the mean ± standard deviation (n = 3). * Formulation data are statistically different ($p < 0.05$, appendix – table B.12) compared with the production day.

The evaluation of the stability by the DLS technique (figure 4.5) showed that there were not significant differences in the mean nanoformulations size of over time (0, 60 and 120 days) ($p > 0.05$, appendix – table B.13). The sizes range was between 167.1 nm and 215.5 nm for the eight formulations investigated. This size variation was comparable to the one that found in the LD technique, for Dv50, although the latter one presents higher values. This is due primarily to differences in each technique detection limit, wherein the DLS is not able to detect particles of

above 3 µm, while LD is [100]. The way this factor leads to differences of size between the two techniques is well evident in the case of NLCs. Some of these nanoformulations have Dv90s above 3 µm, 2 and 4 months after production. These larger populations will not be counted in the DLS technique contributing to the differences of results between the two techniques. In addition, as mentioned above, the way the data are collected has also a direct influence on different results obtained by both techniques. While the DLS records the average size of the entire population, the LD take into account that 10%, 50% and 90% of the population lies below of the size of particle obtained [100]. The DLS technique still allowed to evaluate the evolution of the polydispersity index (PI) over the four months (figure 4.5). All nanoformulations, except **$CP_3M_2T_3$** produced by hot HPH (PI = 0.217 ± 0.024 at day 120), showed PI below of 0.200 during the 4 month evaluation. These results come, once again, in confrontation with those observed in the LD technique. Although the LD do not provide the value of PI, from the "span" analysis (appendix – table A.13) it is evident the large sizes distribution existing in most nanoformulations in the 2nd and 4th month of evaluation. Of all nanoformulations studied, the **CP_5T_2** and **$CP_3M_2T_2$** produced by ultrasonication showed the smallest "span" for the SLNs and NLCs, respectively.

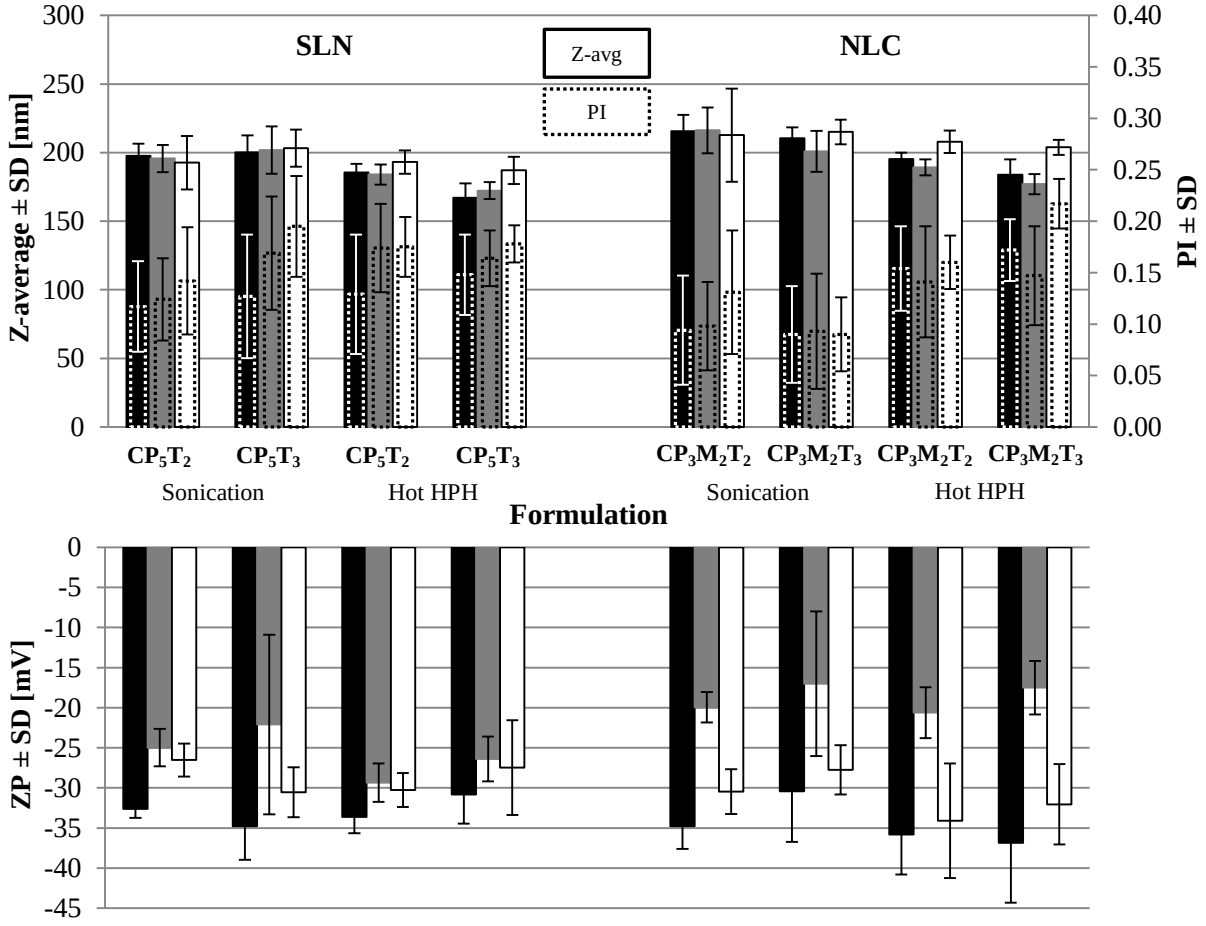

Figure 4.5 - Effect of time of storage (at 4°C) on particle size and zeta potential (ZP) of empty SLNs and NLCs at different concentrations of lipid and surfactant, in ultrasonication and hot HPH. **Notes**: Z-average, polydispersity index (PI) and zeta potential (ZP) on the production day (■), after 2 months (■), and 4 month (□). All data represent the mean ± standard deviation (n = 3).

Considering the determination of the zeta potential (results shown in figure 4.5) the values were always negative and around -30 mV. In the case of NLCs, a slight increase in the absolute value of the zeta potential in relation to the SLNs was noted. Furthermore, it was found that for all formulations, in the 2nd month of characterization, the absolute values of zeta potential were lower than those measured on the date of production and after 4 months. This phenomenon may result from electrode fault that was used in the first two months of characterization and which was replaced in the 4th month. Comparing the results on the production day and after four months, it was possible to verify that there are not apparent changes in the zeta potential values ($p > 0.05$, appendix – table B.14). Although the ZP has decreased slightly in absolute terms, the values remained around -30 mV. These data indicate that particle aggregation is unlikely to occur due to its high electrostatic repulsion [53, 102]. However, by the analysis that has been made to the Dv90 it was found that this is not entirely true. In some nanoformulations, the Dv90 in the 4th month of evaluation was 15 times higher than the one determined on the production day, suggesting a possible aggregation of particles over time. Although DLS and ELS techniques indicate a good stability for all studied nanoformulations, the LD technique shows the opposite for some of these colloidal dispersions.

In short, combining the results obtained in all the techniques performed, it appears that the most promising empty SLN was the **CP_5T_2** produced by ultrasonication. This nanoformulation seems to have a good stability of suspension, with Dv10, Dv50, Dv90 and Z-average with little variation over the four months of investigation. Furthermore, it has a low "span" and PI, and a zeta potential of around -30 mV during the study time. Regarding the NLC, taking into account the results obtained by the LD technique, no nanoformulation appears to be very stable, but the one with better behavior over the four months was the **$CP_3M_2T_2$**.

The values that gave rise to the graphs presented in figures 4.3, 4.4 and 4.5 are tabulated attached (appendix – table A.13 and A.15).

4.2. Optimization of the loaded nanoparticles

The eight most promising nanoformulations after characterized without drug were loaded with 0.1% and 0.05% of SQV. In the second stage of work, this group of loaded nanoparticles was evaluated by laser diffraction, dynamic light scattering and electrophoretic light scattering, in order to arrive at the best formulation.

4.2.1. Particle size measurements

The mean size (Dv10, Dv50 and Dv90) of the formulations under study, determined as LD, are present in table 4.3. For the formulations loaded with higher saquinavir concentration (0.1%), the addition of the drug seems to have interference with the mean size of the nanoparticles in the study. This influence was more evident in the Dv90 values compared to the values of this percentile in the drug-free nanoformulations (table 4.1). In the graphs shown in figure 4.6 it was found that for nanoformulations loaded with 0.1% saquinavir some peaks above 10 µm appeared, that were not evident at the saquinavir-free nanoformulations (figure 4.1 and 4.2). It is likely that these peaks correspond, in fact, to the unencapsulated drug that formed crystals.

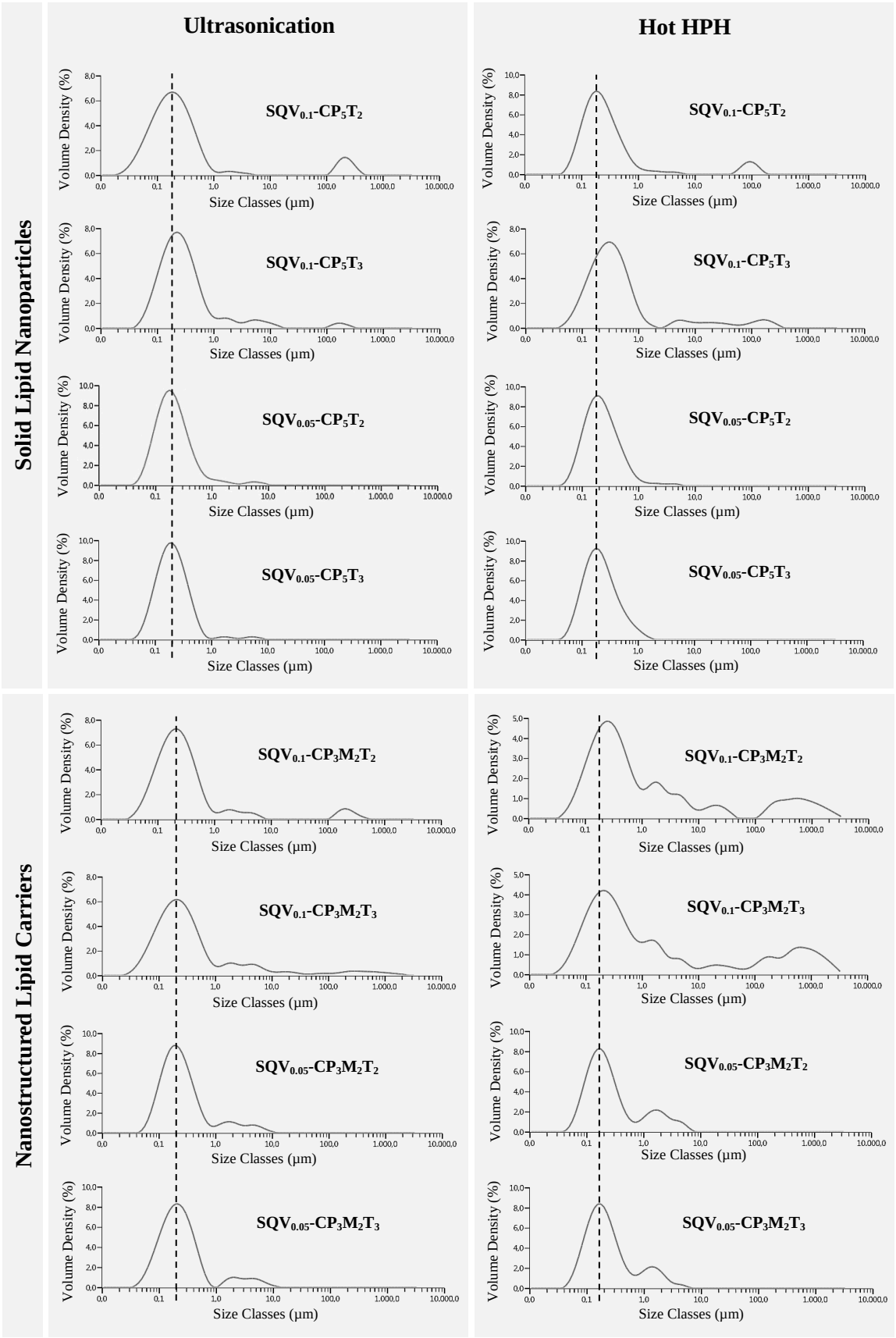

Figure 4.6 - Size Distribution (day 0) of drug-loaded SLNs and NLCs for the different proportions of lipid, surfactant and drug in both production methods (characterization technique: laser diffraction).

In order to overcome this problem, the amount of saquinavir to be encapsulated was reduced to half (0.05%). In the evaluation of the particle size, by LD, of these new nanoformulations, it was found that the peaks in the size range above 10 µm disappeared, reinforcing the idea that these peaks may correspond to saquinavir crystals. Comparing the results of the formulations loaded with 0.05% saquinavir and empty formulations with the same characteristics (manufacturing technique and proportions of ingredients) it was found that were no significant differences ($p > 0.05$, appendix – tables B.15-17), suggesting that incorporation of saquinavir does not influence the size of the nanoparticles.

Table 4.3– Mean Dv10, Dv50 and Dv90 of the drug-loaded nanoformulations tested on day 0.

Formulation			Mean DV10 ± SD [nm]	Mean Dv50 ± SD [nm]	Mean Dv90 ± SD [nm]	Mean Span ± SD
Ultrasonication	SLN	$SQV_{0.1}$-CP_5T_2	84.7 ± 17.8	234.7 ± 9.6	4066.3 ± 1729.5	16.910 ± 7.222
		$SQV_{0.1}$-CP_5T_3	98.7 ± 2.1	251.0 ± 2.6	1506.7 ± 175.6	5.609 ± 0.693
		$SQV_{0.05}$-CP_5T_2	90.0 ± 5.9	203.8 ± 15.0	497.7 ± 68.8	2.184 ± 0.328
		$SQV_{0.05}$-CP_5T_3	90.0 ± 10.9	191.5 ± 24.8	414.3 ± 67.1	1.685 ± 0.099
	NLC	$SQV_{0.1}$- $CP_3M_2T_2$	80.3 ± 9.4	223.3 ± 7.0	2200.0 ± 544.4	9.471 ± 2.260
		$SQV_{0.1}$- $CP_3M_2T_3$	79.3 ± 1.1	248.3 ± 10.1	7280.0 ± 2919.6	29.143 ± 12.495
		$SQV_{0.05}$- $CP_3M_2T_2$	89.9 ± 8.9	211.3 ± 14.8	1015.6 ± 405.8	4.205 ± 1.469
		$SQV_{0.05}$- $CP_3M_2T_3$	78.7 ± 9.6	209.8 ± 6.2	1562.5 ± 327.8	7.054 ± 1.548
Hot HPH	SLN	$SQV_{0.1}$-CP_5T_2	95.4 ± 2.5	215.3 ± 9.0	1293.3 ± 337.1	5.555 ± 1.515
		$SQV_{0.1}$-CP_5T_3	112.7 ± 3.1	322.0 ± 10.8	5586.7 ± 2498.6	16.854 ± 7.216
		$SQV_{0.05}$-CP_5T_2	88.7 ± 30.2	217.9 ± 8.6	609.9 ± 112.4	2.351 ± 0.532
		$SQV_{0.05}$-CP_5T_3	93.1 ± 1.3	203.3 ± 2.5	557.0 ± 14.7	2.280 ± 0.100
	NLC	$SQV_{0.1}$- $CP_3M_2T_2$	111.3 ± 0.6	464.3 ± 40.5	373000 ± 110855.8	722.380 ± 199.792
		$SQV_{0.1}$- $CP_3M_2T_3$	98.7 ± 11.6	596.3 ± 239.6	643000 ± 283867.9	1052.517 ± 254.718
		$SQV_{0.05}$- $CP_3M_2T_2$	82.1 ± 2.7	210.9 ± 20.0	2138.8 ± 189.2	9.815 ± 0.808
		$SQV_{0.05}$- $CP_3M_2T_3$	87.9 ± 1.1	201.0 ± 6.1	1370.0 ± 138.9	6.362 ± 0.508

*To calculate the mean and standard deviation (Dv10, Dv50 and Dv90) of the tabulated formulations were used three or more lots. The values of individual sizes of each batch are in appendix (tables A.6-9)

In nanoformulations loaded with 0.05% saquinavir, the particle size (Dv50) obtained by LD are in accordance with the results obtained by DLS ($p > 0.05$, appendix – table B.18) (table 4.4), with slightly smaller dimensions observed using the DLS technique. However, for nanoparticles with 0.1% drug the results obtained by LD do not match those obtained by DLS. Again, this happened because DLS technique has not the ability to detect particles above 3 µm [100].

Table 4.4 – Mean size (Z-average), polydispersity index and zeta potential of the most saquinavir-loaded nanoformulations, on day 0.

Formulation			Z-average ± SD [nm]	PI ± SD	ZP ± SD [mV]
Ultrasonication	SLN	$SQV_{0.1}$-CP_5T_2	212.2 ± 6.9	0.109 ± 0.027	-18.22 ± 1.93
		$SQV_{0.1}$-CP_5T_3	225.7 ± 22.2	0.207 ± 0.084	0.14 ± 8.79
		$SQV_{0.05}$-CP_5T_2	197.3 ± 7.6	0.114 ± 0.051	-24.05 ± 2.34
		$SQV_{0.05}$-CP_5T_3	195.3 ± 9.4	0.069 ± 0.056	-22.24 ± 6.16
	NLC	$SQV_{0.1}$- $CP_3M_2T_2$	227.4 ± 28.9	0.130 ± 0.035	-9.99 ± 1.93
		$SQV_{0.1}$- $CP_3M_2T_3$	186.6 ± 38.8	0.163 ± 0.070	-10.32 ± 3.51
		$SQV_{0.05}$- $CP_3M_2T_2$	201.3 ± 17.0	0.083 ± 0.035	-24.95 ± 3.10
		$SQV_{0.05}$- $CP_3M_2T_3$	198.3 ± 7.9	0.068 ± 0.056	-19.80 ± 2.44
Hot HPH	SLN	$SQV_{0.1}$-CP_5T_2	208.1 ± 9.6	0.136 ± 0.030	-19.81 ± 1.68
		$SQV_{0.1}$-CP_5T_3	199.0 ± 17.5	0.205 ± 0.039	-11.24 ± 2.85
		$SQV_{0.05}$-CP_5T_2	216.8 ± 8.1	0.142 ± 0.036	-20.87 ± 3.92
		$SQV_{0.05}$-CP_5T_3	203.2 ± 6.3	0.197 ± 0.017	-17.63 ± 1.52
	NLC	$SQV_{0.1}$- $CP_3M_2T_2$	191.7 ± 10.0	0.130 ± 0.046	-13.18 ± 2.67
		$SQV_{0.1}$- $CP_3M_2T_3$	185.0 ± 38.1	0.202 ± 0.046	-9.72 ± 4.68
		$SQV_{0.05}$- $CP_3M_2T_2$	184.3 ± 5.8	0.134 ± 0.041	-18.18 ± 2.38
		$SQV_{0.05}$- $CP_3M_2T_3$	159.4 ± 3.4	0.190 ± 0.039	-13.39 ± 1.64

*To calculate the mean and standard deviation (Z-average, PI, ZP) of the tabulated formulations were used three or more lots. The values of individual sizes of each batch are in appendix (tables A.10-12)

With regard to the polydispersity index, the majority of the dispersions were monodisperse, with PI less than 0.200. The unique formulations with PI above 0.200 were the ones with 0.1% SQV, 5% lipid and 3% surfactant, with the exception of the $SQV_{0.1}$-$CP_3M_2T_3$ formulation produced by ultrasonication in which the PI was 0.163 ± 0.070. There were no significant differences between these formulations and the corresponding empty nanoparticles ($p > 0.05$, appendix – table B.19).

4.2.2. Zeta potential measurements

The results obtained from the zeta potential measurements (table 4.4) showed that the suspensions under study were affected by the incorporation of the saquinavir drug. If for drug-free nanoparticles the zeta potential was around -30 mV (table 4.2), in the case of drug-loaded nanoparticles the ZP was always higher than -25 mV. These differences were even more pronounced in the colloidal dispersions with 0.1% saquinavir in their constitution ($p < 0.05$, appendix – table B.20). The $SQV_{0.05}$-CP_5T_2 and $SQV_{0.05}$-$CP_3M_2T_2$ formulations produced by ultrasonication were those with the best zeta potential, around -24 mV.

4.2.3. Stability

Due to the appearance of peaks in the size ranges above 10 µm (probably due to the formation of unencapsulated saquinavir crystals) and unappealing zeta potential presented in the nanoparticles loaded with 0.1% drug, only nanoformulations with 0.05% drug were evaluated

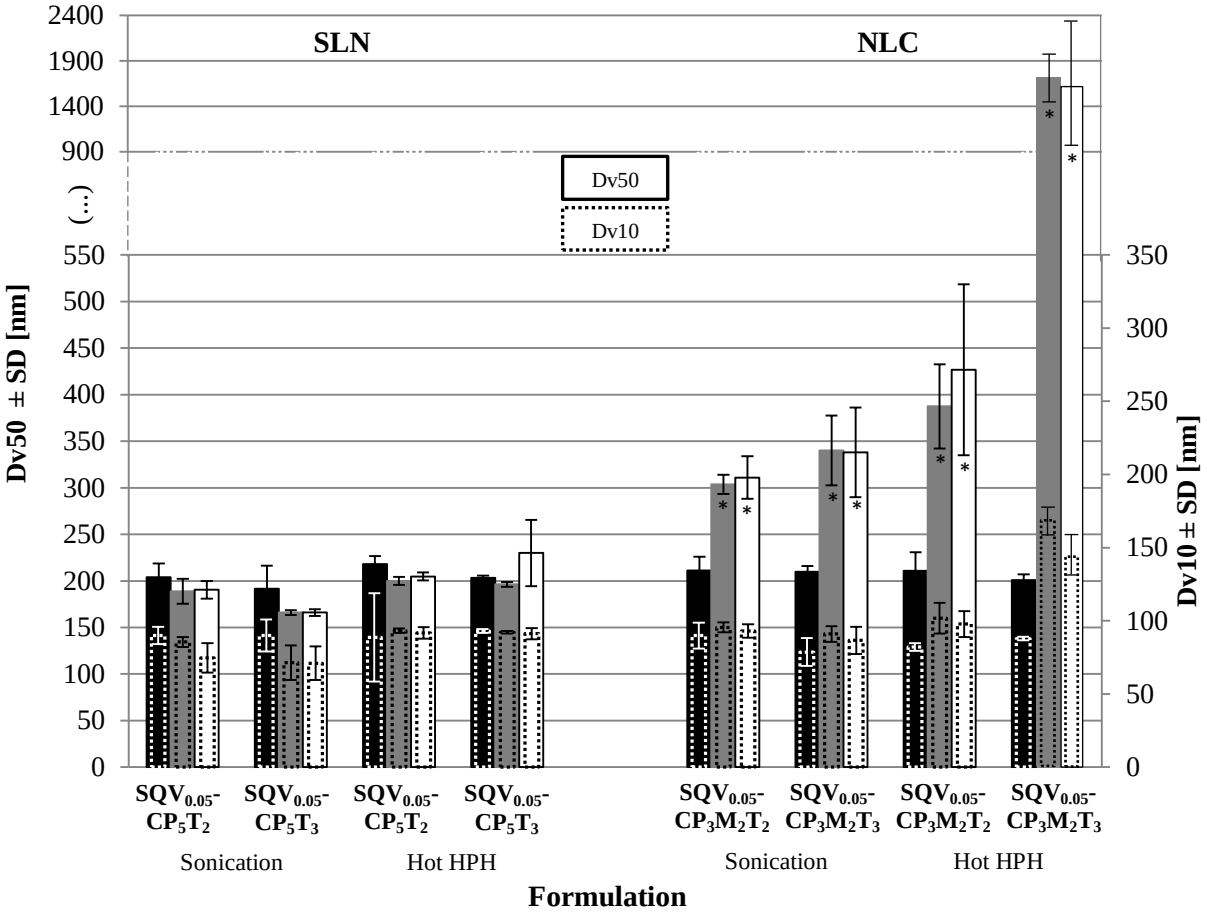

Figure 4.7 - Effect of time of storage (at 4°C) on particle size of loaded SLNs and NLCs at different concentrations of lipid and surfactant, in ultrasonication and hot HPH. **Notes**: Dv10 and Dv50 on the production day (■), after 45 days (■), and 90 days (□). All data represent the mean ± standard deviation ($n \geq 3$). * Formulation data are statistically different ($p < 0.05$, appendix – tables B.21 and B.22) compared with the production day.

over time. The nanoformulations during storage remained at 4 °C. The stability study was performed over 3 months: at production day, day 45 and day 90. The studied characteristics over this period were the mean size (by LD and DLS), the polydispersity index and zeta potential. The results are shown in figures 4.7, 4.8 and 4.9.

If on the production day, Dv10 and Dv50 values were similar between SLNs and NLCs, with the passage of time it did not happen (figure 4.7). Unlike the SLNs, which kept the Dv10 and Dv50 in the same range of values over 3 months of evaluation ($p > 0.05$, appendix – tables B.21 and B.22), the NLCs had a sharp growth of Dv50 ($p < 0.05$, appendix – tables B.21 and B.22) and slight differences in Dv10. The NLCs who managed to keep Dv10 and Dv50 values more stable and reduced, over the three months of evaluation, was the **$SQV_{0.05}$-$CP_3M_2T_2$** formulation, produced by ultrasonication. In the case of SLNs, the nanoformulations who presented the best behavior during the time of investigation were the **$SQV_{0.05}$-CP_5T_2** and **$SQV_{0.05}$-CP_5T_3** produced by ultrasonication, with Dv10 and Dv50 values, over the three months, in order 90 nm and 200 nm, respectively.

The Dv90 values of the SLNs, on the production day, were lower than those presented in the NLCs. These differences became even more apparent during the storage time. During this period, the SLNs maintained their Dv90 values almost constant, unlike the NLCs that after 45 days of storage showed an abrupt increase of this parameter, exceeding 15 μm after 90 days of storage.

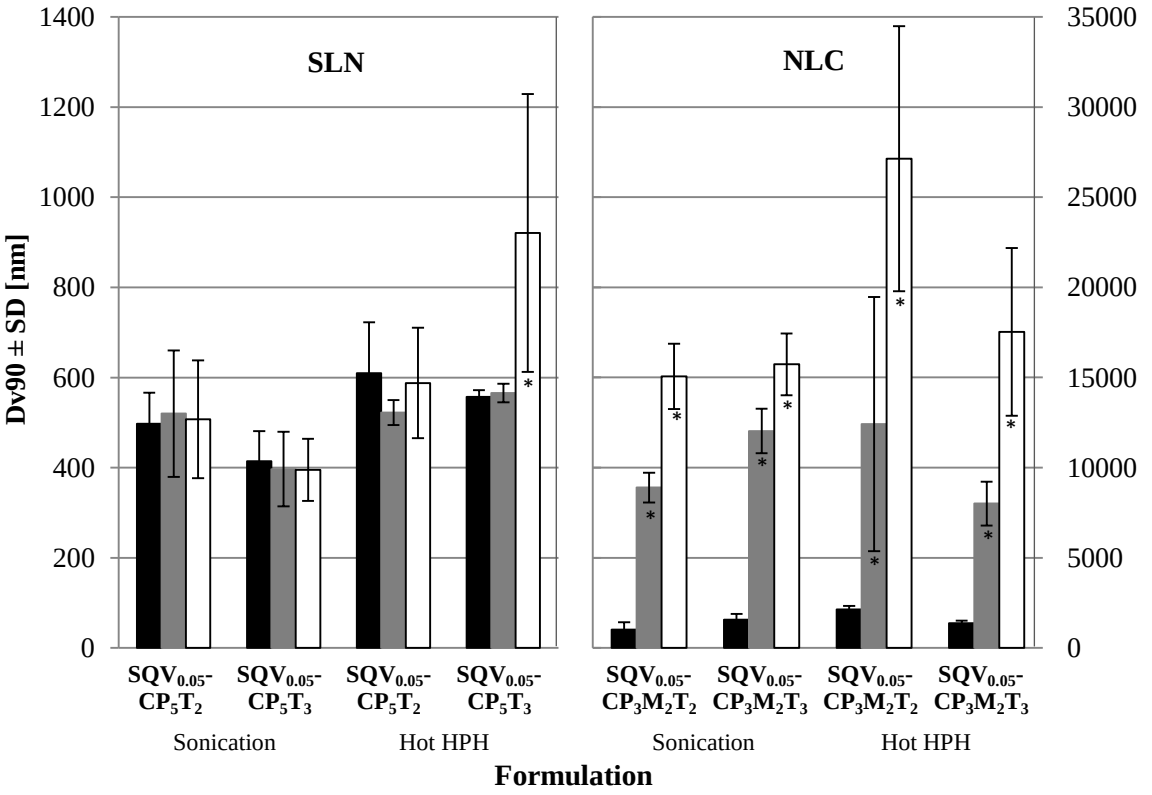

Figure 4.8 - Effect of time of storage (at 4°C) on particle size of loaded SLNs and NLCs at different concentrations of lipid and surfactant, in ultrasonication and hot HPH. **Notes**: Dv90 on the production day (■), after after 45 days (■), and 90 days (□). All data represent the mean ± standard deviation ($n \geq 3$). * Formulation data are statistically different ($p < 0.05$, appendix – table B.23) compared with the production day.

The SLNs with the best performance over the three months of study were the **$SQV_{0.05}$-CP_5T_2** and **$SQV_{0.05}$-CP_5T_3** produced by ultrasonication, with very small size variations over this period. In the case of NLCs, the evolution of the Dv90 was better in **$SQV_{0.05}$-$CP_3M_2T_2$** nanoformulation produced by ultrasonication. Despite the large increase in Dv90 values over study time, it was the NLCs that were more stable and had smaller size ranges. These results can be seen in figure 4.8.

The results obtained by DLS and ELS techniques are shown in figure 4.9. The mean size of the nanoparticles under study (Z-average), determined by DLS, was stable over the 3 months of research for both types of nanoparticles (SLNs and NLCs). The Z-average ranged between 159.2 nm and 218.9 nm.

In the case of SLNs, these results are consistent with the Dv50 values obtained by the LD technique ($p > 0.05$, appendix – table B.22). The same happens only with the NLCs in the production day. While using the DLS technique, NLCs shown good storage stability, using the LD technique this does not occur. For example, the Dv50 value in the **$SQV_{0.05}$-$CP_3M_2T_3$** formulation, produced by hot HPH, reached 1.7 μm on day 45, unlike the LD technique in

which the Z-average did not exceed 160 nm. Again, these differences were related with the fact of the LD technique did not cover upper size ranges 3 µm [100].

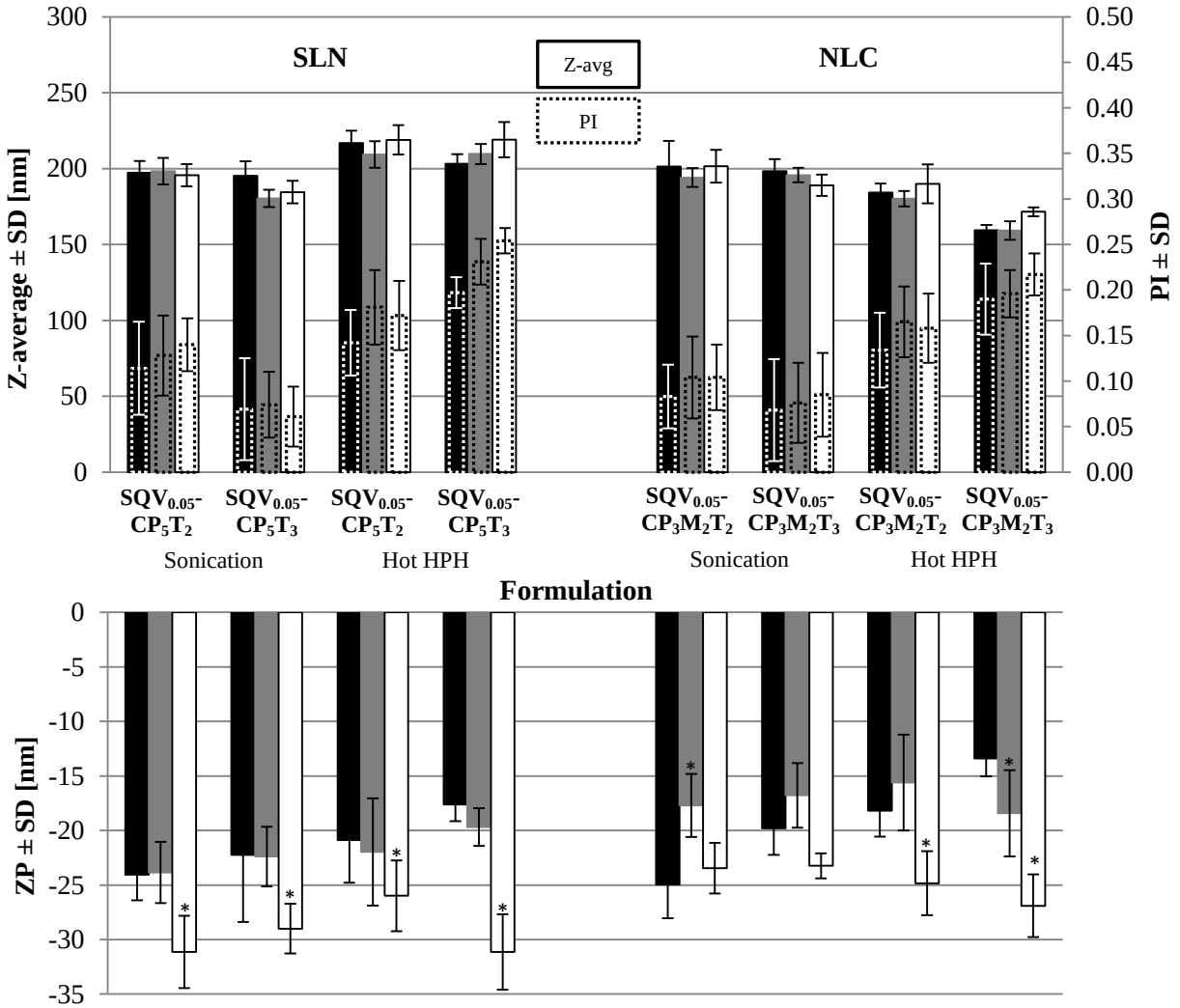

Figure 4.9 - Effect of time of storage (at 4°C) on particle size and zeta potential (ZP) of loaded SLNs and NLCs at different concentrations of lipid and surfactant, in ultrasonication and hot HPH. **Notes**: Z-average, polydispersity index (PI) and zeta potential (ZP) on the production day (■), after 45 days (■), and 90 days (□). All data represent the mean ± standard deviation ($n \geq 3$). * Formulation data are statistically different ($p < 0.05$, appendix – table B.22 and B.24) compared with the production day.

All nanoformulations had a polydispersity index lower than 0.200 over the 3 months, except for **$SQV_{0.05}$-CP_5T_3** and **$SQV_{0.05}$-$CP_3M_2T_3$**, both produced by hot HPH. Although the LD technique does not assess this parameter, it gives us the bandwidth of the size distribution ('span'). The 'span' of the SLNs (~2) was low compared with NLCs (~40) (appendix – table A.14). This may be an indication that the NLCs have a high sizes distribution, contrary to what the DLS technique makes believe.

Generally, the lipid nanoparticles under investigation revealed a more negative zeta potential at day 90 (-30 mV) than on the production day. The SLNs and NLCs with best zeta potential over the three months were **$SQV_{0.05}$-CP_5T_2** and **$SQV_{0.05}$-$CP_3M_2T_2$** (obtained by ultrasonication), respectively. The values that gave rise to the graphs presented in figures 4.7, 4.8 and 4.9 are tabulated attached (appendix – table A.14 and A.16).

During the stability assessment phase of lipid nanoparticles with and without drug, it was found that in all SLN with 3% surfactant two distinct phases appeared, as shown in figure 4.10. The rest of nanoformulations were visually characterized as having milky aspect.

Figure 4.10 – Nanoformulations presenting two phases.

After all the preliminary characterization tests have been carried out, a compromise situation (an appropriate size, a low PI and a good stability of the samples) was sought for choosing the SLNs and NLCs that will later be exposed to a deeper characterization.

Thus, taking into account all parameters evaluated, the nanoformulations that showed to have the best features were: CP_5T_2 (**SLN**), $CP_3M_2T_2$ (**NLC**), $SQV_{0.05}$-CP_5T_2 (**SQV-SLN**) and $SQV_{0.05}$-$CP_3M_2T_2$ (**SQV-NLC**). Henceforth, the SLN, NLC, SQV-SLN, SQV-NLC denominations will be used to classify the chosen nanoformulations. In this third stage of work the morphology, encapsulation efficiency and thermodynamic behavior of the selected nanoparticles will be determined.

4.3. Morphology determination

The cryo-SEM is a visual technique with which are obtained information on the mean particle size and morphology in suspension. The morphology of the LN with and without drug determined by cryo-SEM is shown in figure 4.11. The images demonstrated the almost spherical shape that SLN (A), SQV-SLN (B), NLC (C) and SQV-NLC (D) exhibit and its relatively homogeneous size distribution.

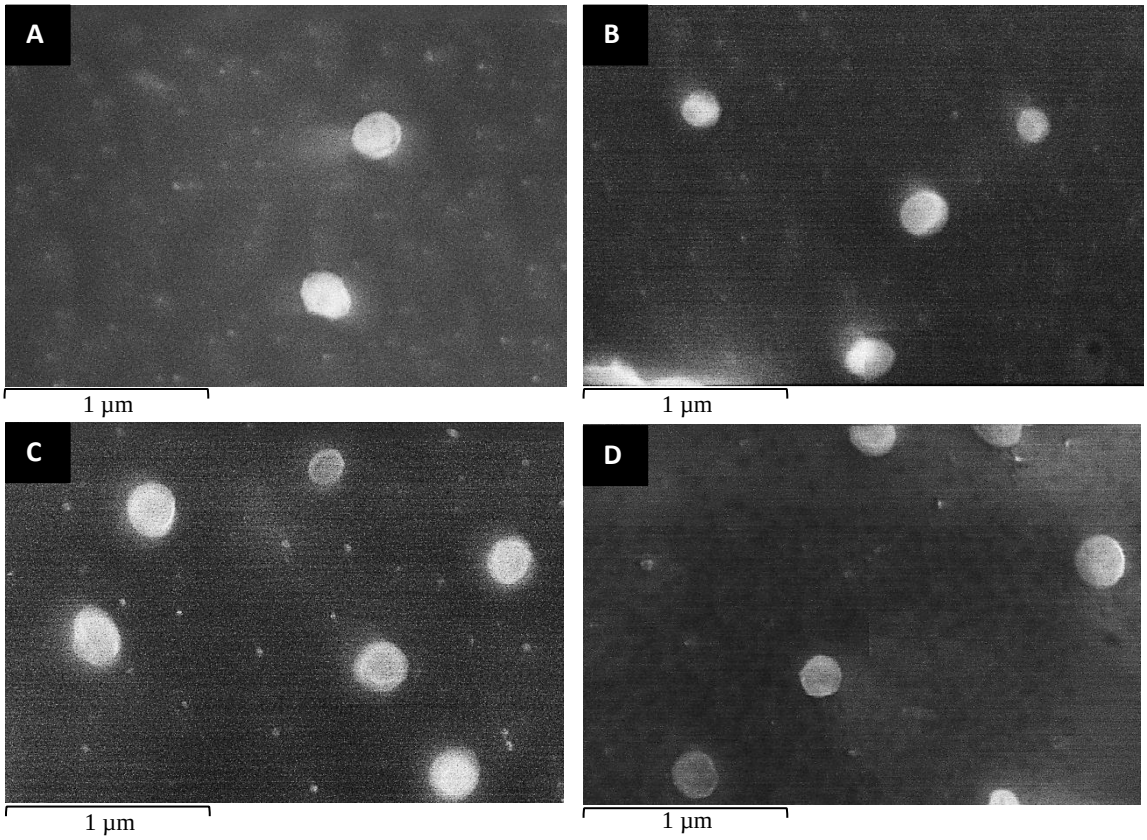

Figure 4.11 - Cryo-scanning electron microscopy images of (A) SLN, (B) SLN-SQV (C) NLC and (D) NLC-SQV at 40,000× magnification, 15kV and WD=15mm.

This result runs in favor to the polydispersity index values obtained by DLS technique, presented in tables 4.2 and 4.4. The average diameter was in the range of 150-250 nm and no particle coalescence apparent. This sizes range was consistent with the results obtained by DLS and LD techniques at day 0 (table 4.1, 4.2, 4.3 and 4.4). Slight differences are related with the fact of the techniques being based on different sample preparation processes and principles. The size determination by DLS and LD was carried out in the aqueous state, resulting in hydrated particles and diameters greater than the ones detected by the microscopic technique. In this case, the water was removed by sublimation, what could promote the shrinkage of the particles and therefore slightly smaller sizes. Finally, the incorporation of saquinavir did not appear to cause size and morphological alterations in the loaded LN.

4.4. Encapsulation efficiency

The development of the analytical method (HPLC) for the determination of SQV calibration curve was initiated by setting the wavelength to be used. After obtaining the SQV spectrum, it showed that the maximum absorption was obtained at wavelength 240 nm (figure 4.12), and therefore this was the chosen one for this analytical method.

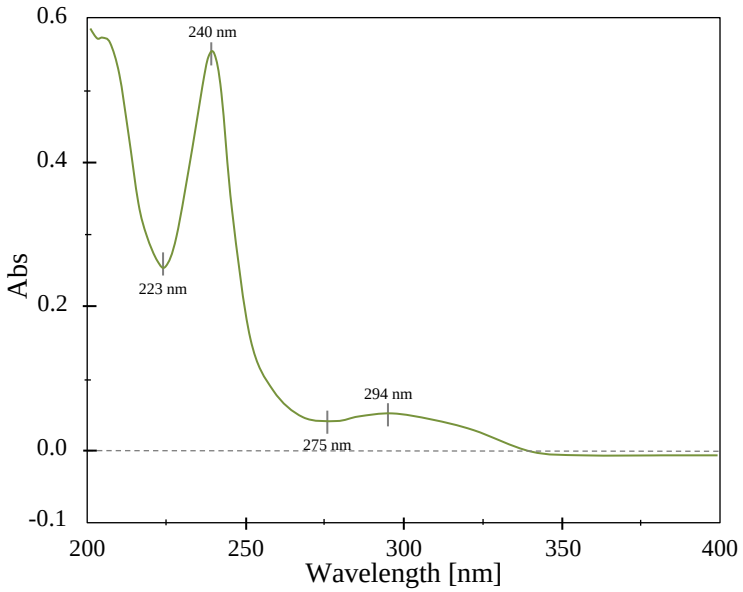

Figure 4.12 - SQV spectrum obtained by spectrophotometry.

Moreover, the most appropriate composition of the mobile phase was investigated by comparing the systems composed of ACN:KH_2PO_4 in different ratios (46:54, 50:50 and 55:45 v/v). The mobile phase composed of ACN: KH_2PO_4 (55:45 v/v) was shown to be the most suitable, presenting well resolved peak and 2.9 min retention time, as shown in figure 4.13. The other proportions have shown to be less suitable due to higher retention time. It is highlighted the importance of careful selection of the mobile phase composition, because ideally it is desired that the analytical run is the faster possible, using minimal amounts of organic solvent, with direct impact on reducing the cost of analysis [89].

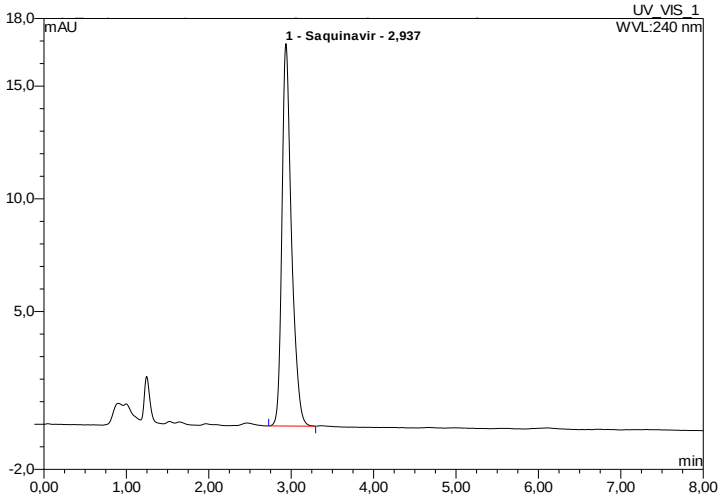

Figure 4.13 - Saquinavir chromatogram analyzed for HPLC using C18 column, mobile phase composed of ACN:KH_2PO_4 (55:45, v/v), 1.0 mL/min flow rate, at 240 nm.

Specificity

The specificity was considered the first analytical validation step, since it is important to ensure that the excipients of nanoformulations, such as cetyl palmitate, miglyol 812 and polysorbate 80, do not interfere with the quantification of SQV.

It was found that the UV spectrum of saquinavir kept the same profile throughout the peak (in the front, maximum and in the tail). In figure 4.14 there is an example of a "pure" peak [88].

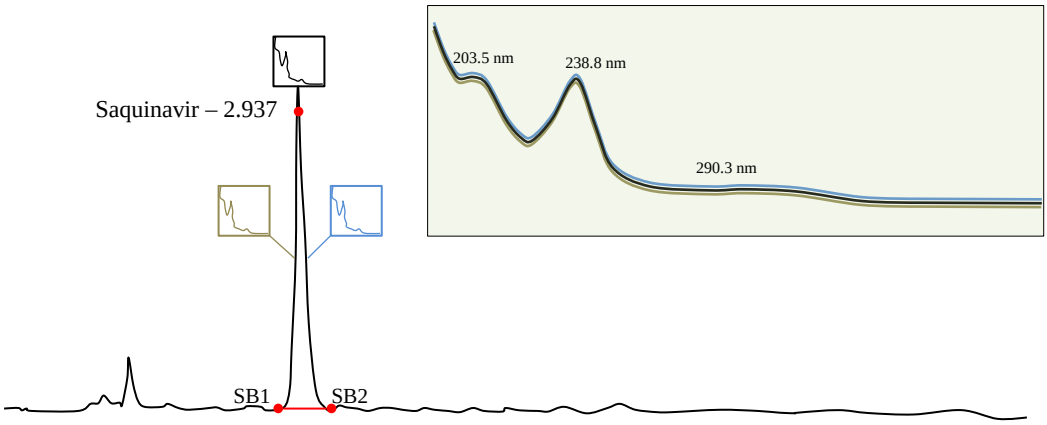

Figure 4.14 - Saquinavir spectrum at beginning (—), middle (—) and end (—) of the chromatographic peak obtained by HPLC.

After exposing the empty lipid nanoparticles at the same type of treatment of loaded nanoparticles - direct method (see section 4.4.2.) - it was found that none of the excipients (that may has stayed in the treated sample) eluted at SQV retention time, and that the main peak is well separated from other compounds present in the sample (figure 4.14) [85].

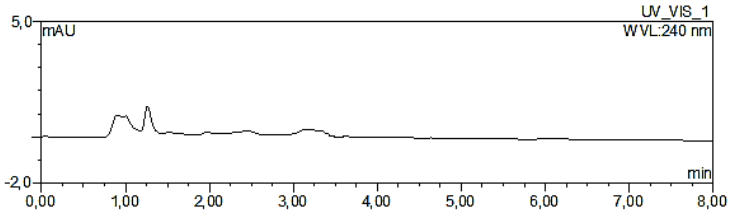

Figure 4.15 - Chromatogram of empty lipid nanoparticles after being exposed to the direct method.

These forms of assessing specificity have allowed to ensure that the response peak is exclusively saquinavir and therefore, the proposed method is specific to the studied drug [85].

Linearity

The calibration curve constructed by plotting the peak area of each standard as a function of the concentration of the substance to be analyzed is presented in figure 4.16.

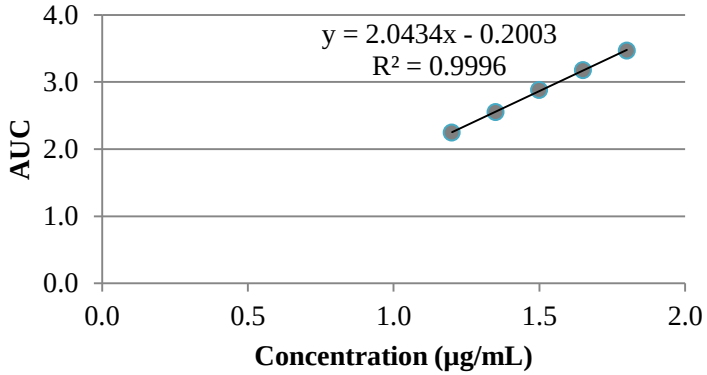

Figure 4.16 - Calibration curve used to interpolate SQV concentration values using HPLC method.

The developed method was linear in the range 1.20 to 1.80 µg/mL. After adjusting the data by linear regression using the least square method, the values of the areas obtained showed to be directly proportional to the concentration, in the assessed range, (area = 2.0434 *x* concentration [µg/mL] + 0.2003), R = 0.9998. The good linearity is also confirmed by the randomness of the points in the residual plot (figure 4.17) and low RSS (0.00036).

Furthermore, using the graph of the relative responses it was possible to verify whether points of the analytic curve are inserted in the linear range. It was concluded that the method is linear over the range, since the relative response never intersects the 95 and 105% line (figure 4.18).

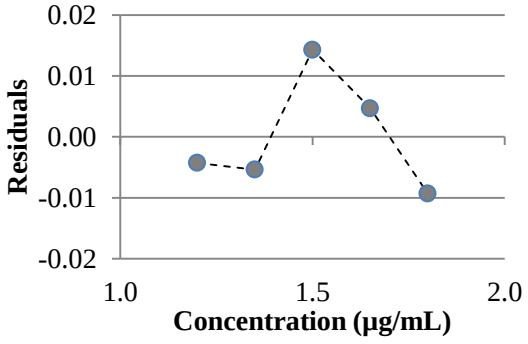

Figure 4.17 - Graph of residuals.

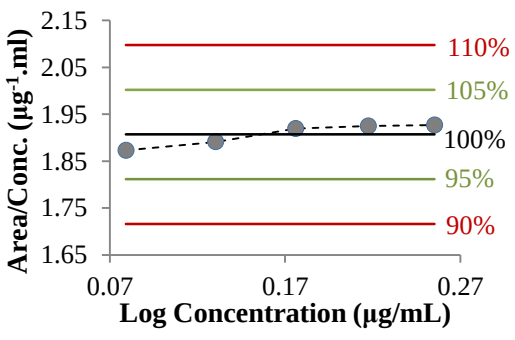

Figure 4.18 - Graph of relative responses.

Precision

For drug reliable analysis, the method should prove to be precise, that is, to present little dispersion among reading results of the same concentration [89].

The results in table 4.5 show that the method is precise for both determinations, repeatability, whose maximum CV was 2.93% for one of the concentrations tested, 1.50 µg/mL, and intermediate precision, where the maximum CV corresponded to 5.06% for lower concentration, 1.35 µg/mL.

Table 4.5 - Precision of the chromatographic method used in the analysis of SQV.

Repeatability			
Theoretical concentration [µg/mL]	1.35	1.50	1.65
n	3	3	3
CV (%)	0.26	2.93	0.94
Intermediate precision			
Theoretical concentration [µg/mL]	1.35	1.50	1.65
n	3	3	3
CV (%)	5.06	3.07	2.02

n: number of replicates, CV: coefficient of variation

Accuracy

For drug reliable analysis the method should also to be accurate. The accuracy is represented by the degree of agreement among individual results in the same assay, in relation to a reference value accepted as true [89]. Table 4.6 shows that the developed method is accurate, since the deviations from the nominal values remained between -1.93 and 0.59% for the standard solutions, and between -1.33 and 1.22% for the exposed nanoparticles to the "direct method", without the first filtration.

Table 4.6 - Accuracy of the chromatographic method used in the analysis of SQV.

Accuracy			
Theoretical concentration [µg/mL]	1.35	1.50	1.65
Concentration obtained [µg/mL]	1.3240	1.5121	1.6598
n	3	3	3
A (%)	-1.93	0.81	0.59
Overall accuracy			
Type of LN	**SQV-SLN**	**SQV-NLC**	
Theoretical concentration [µg/mL]	1.67	1.67	
Concentration obtained [µg/mL]	1.6904	1.6478	
n	3	3	
A (%)	1.22	-1.33	

n: number of replicates, A: accuracy, LN: lipid nanoparticles

4.4.2. Encapsulation efficiency

The lipid nanoparticles are known to be suitable systems for incorporating drugs that can prevent degradation [75]. The lipophilic nature of saquinavir (octanol/water partition coefficient, logP = 4.51) [24, 26, 27] suggests its preferential partition into the lipid matrix of the nanoparticles rather than to remain in the aqueous medium. The encapsulation

efficiency (EE) of SQV-SLN and SQV-NLC formulations on the production day are shown in table 4.7 (appendix – table A.17).

Table 4.7 - Encapsulation efficiency of lipid nanoparticles under study (SQV-SLN and SQV-NLC), on the production day.

Formulation	Encapsulation Efficiency ± SD [%]
SQV-SLN	92.37 ± 5.99
SQV-NLC	93.72 ± 3.17

The percentage of encapsulation in both types of nanoparticles was satisfactorily high, averaging more than 90% EE. The SQV-NLC showed slightly higher encapsulation efficiency to SQV-SLN, but no statistically significant variation in encapsulation efficiency between each formulation ($p > 0.05$, appendix – table B.25).

4.4.3. Stability

Figure 4.19 shows the results of saquinavir EE for 3 months (days 0, 30, 60 and 90). The percentages obtained for SQV-SLN and SQV-NLC, on the production day, showed that a large quantity of drug was incorporated. Over the 3 months of evaluation, the decrease in EE felt by SQV-SLN was slightly higher than that in the SQV-NLC, with no significant differences ($p > 0.05$, appendix – table B.25).

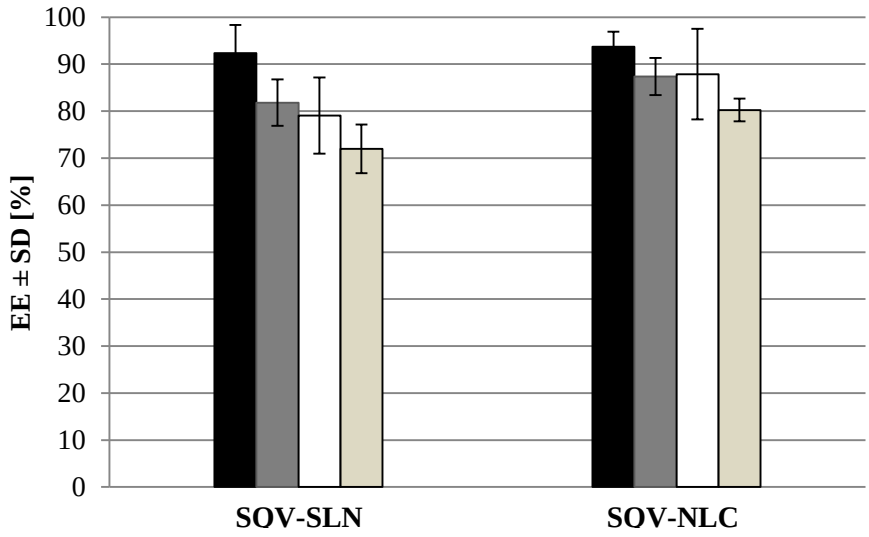

Figure 4.19 - Effect of time of storage (at 4°C) on encapsulation efficiency (EE) of SQV-SLN and SQV-NLC. **Notes**: EE on the production day (■), after 30 days (■), 60 days (□), and 90 days (■). All data represent the mean ± standard deviation (n = 6). No statistically significant differences were observed ($p > 0.05$).

The SQV-SLN in the first month of storage lost about 10% of its content, and at the end of the second month its EE decreases by around 3% compared to the last assessment. Because of the crystalline nature of the solid lipids, the polymorphism is a typical feature of SLN. During storage, the rearrangement of the crystal lattice may occur in favor of the thermodynamically more stable configurations, with expulsion of drug molecules [53, 54]. This problem is partially solved by the NLC, which due to the addition of a liquid lipid in its constitution avoid recrystallization. In this study, SQV-NLC had less pronounced losses that SQV-SLN. In the first month of storage there was a decrease of about 6% of EE, and there were no losses in the

second month of evaluation. In the third month of the stability study, the SQV-SLN and SQV-NLC formulations lost the same amount of active substance compared to the previous month, about 7%.

In short, both systems can be considered suitable for incorporating saquinavir, with more positive results for the NLC. The values that gave rise to the graphs presented in figure 4.19 are tabulated attached (appendix – table A.18).

4.5. Thermal behavior

In order to evaluate the thermal behavior of the formulations under study, samples SLN, NLC, SQV-SLN and SQV-NLC were submitted to the differential scanning calorimetry technique (DSC). DSC is a technique used to study polymorphic types, transition states and crystallization behaviors of lipid nanoparticles.

4.5.1. Bulk solid lipid analysis

Initially the bulk solid lipid used to prepare lipid nanoparticles – cetyl palmitate – was analyzed. The thermogram obtained after thermal analysis has been performed is shown in figure 4.20. It is possible to visualize two peaks with slightly different melting points. The existence of these two peaks can be related to purity of compound, appearing other substances interfering with the peak. Another explanation relates to the possible existence of two different thermodynamic configurations. The first peak may correspond to α polymorphic form (unstable) with 39.8 °C onset temperature; while the second peak may correspond to the β polymorphic form (stable) with 50.9 °C onset temperature.

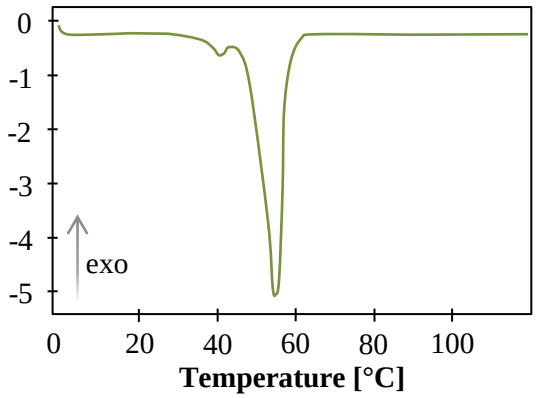

Figure 4.20 - Differential scanning calorimetry thermogram of the bulk cetyl palmitate.

4.5.2. Nanoparticles and bulk mixtures

The DSC thermograms for simple substances, bulk material, unloaded nanoparticles (SLN-placebo and NLC-placebo) and SQV-loaded nanoparticles (SQV-SLN and SQV-NLC) are depicted in figure 4.21, while the respective onset temperature values, enthalpy and recrystallization index (RI) are presented in table 4.8.

In the bulk material, the melting process occurred at an onset temperature of 49.9 °C in SLN and 45.0 °C in NLC. The unloaded nanoparticles showed a slightly lower onset temperature to corresponding bulk material: 49.0 °C in SLN-placebo and 44.0 °C in NLC-placebo. The decrease of onset temperature can be related to the presence of polysorbate 80 and the small diameter of the colloidal particles, in particular, their high surface area relative to volume [75, 103]. In the loaded nanoparticles, the onset temperature was slightly above the bulk material: 50.1 °C in SQV-SLN and 45.2 °C in SQV-NLC. This increase may be related to the presence of saquinavir, due to the its high onset temperature (241.1 °C). This and the fact that the thermogram of SQV-SLN and SQV-NLC formulations do not to show the peak corresponding

to saquinavir, reveals that the drug is well dissolved in the lipid matrix, reinforcing the good EE of these colloidal dispersions [103].

The melting enthalpy values were calculated from the area under the peaks, integrating the peak below the base line and dividing by the sample weight in each case [75]. Both unloaded nanoparticles (SLN-placebo and NLC-placebo) and loaded nanoparticles (SQV-SLN and SQV-NLC), had a lower melting enthalpy, in absolute value, to its bulk material. This means that with the formation of nanoparticles there was a decrease in crystallinity of lipid matrices in relation to their bulk counterparts and therefore the creation of defects on the network. Thus, due to the less orderly arrangement present in the lipid, less energy was required for the nanoparticles melting process.

The calculation of the degree of crystallinity or recrystallization index (RI) of SLN-placebo, NLC-placebo, SQV-SLN and NLC-SQV, has reinforced this idea. The enthalpy value of the bulk material was set at 100% crystallinity serving as a reference for calculating the degree of crystallinity of the lipid nanoparticles. As shown in table 4.8, the RI of SLN-placebo and NLC-placebo decreased 6.2% and 17.2%, respectively, compared with physical mixtures of its excipients. Moreover, the degree of crystallinity of SQV-SLN and SQV-NLC decreases 14.0% and 21.2%, respectively, relative to the bulk material, indicating that the addition of saquinavir to the lipid matrix increases its disorganization. With these results it stayed also evident that the lipid matrix of SLN is more organized than the NLC, due to the liquid lipid, confirming what is said in the bibliography [43].

In short, lipid nanoparticles, unloaded or loaded, presented a crystal organization lower than its reference.

Table 4.8 - Differential scanning calorimetry parameters of simple substances, unloaded and SQV-loaded solid lipid nanoparticles (SLNs) and nanostructured lipid carriers (NLCs), and physical mixture of their excipients: onset temperatures, melting enthalpies, and recrystallization index (RI).

			Onset [°C]	Enthalpy [J/g]	RI [%]
Polysorbate 80			-19.8	-	-
Miglyol 812			-13.1	-73.6	-
Cetyl Palmitate			50.9	-202.0	-
Saquinavir			241.1	-91.9	-
SLN	**Bulk material**		49.9	-126.5	100
	SLN-placebo		49.0	-118.6	93.8
	SQV-SLN		50.1	-108.0	86.0
NLC	**Bulk material**	**A**	-12.1	-19.3	-
		B	45.0	-83.1	100
	NLC-placebo	**A**	-8.6	-20.0	-
		B	44.0	-68.8	82.8
	SQV-NLC	**A**	-10.0	-20.1	-
		B	45.2	-65.0	78.8

* The individual values of each lot are attached (table A19).

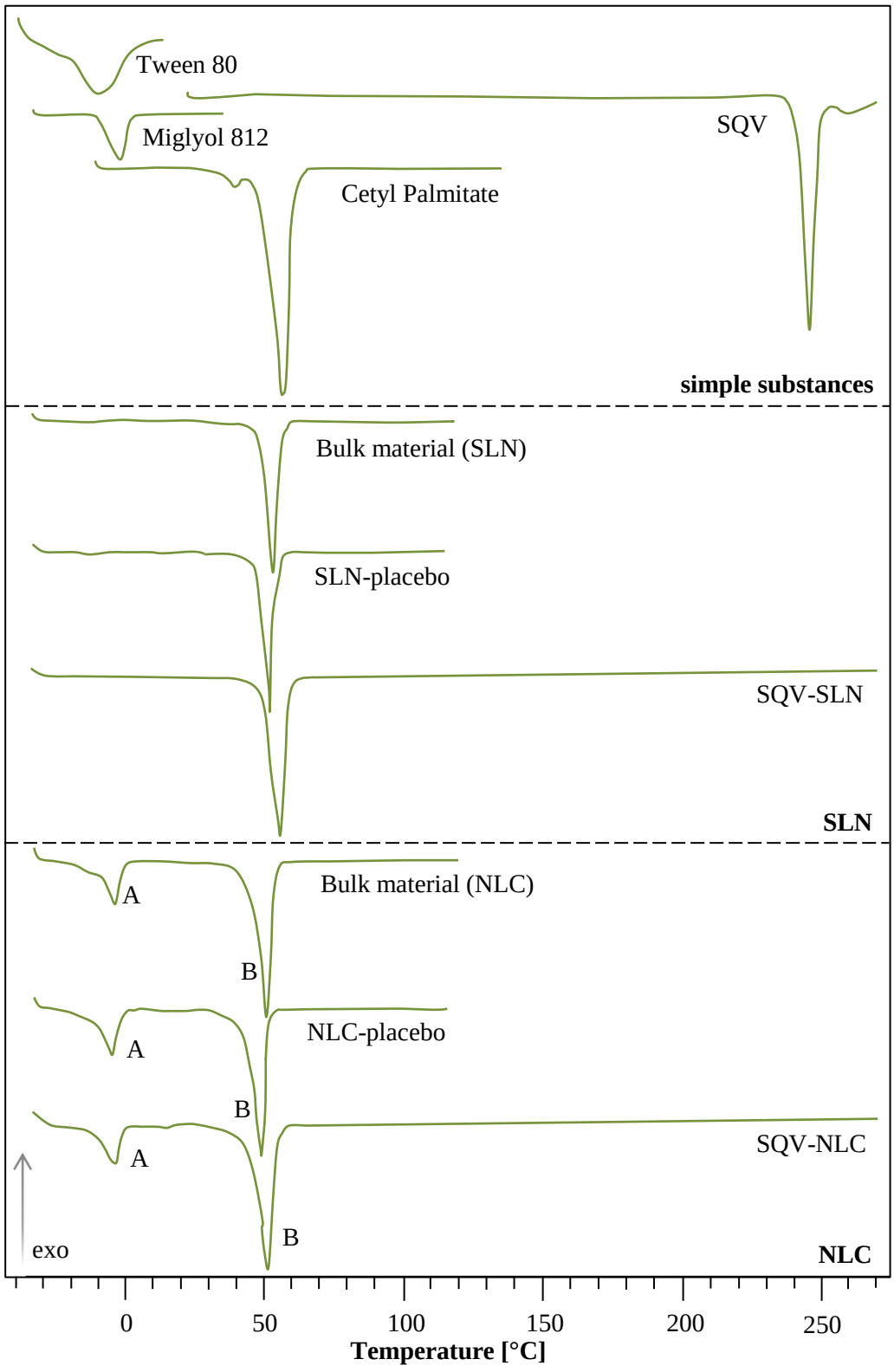

Figure 4.21 – DSC thermograms, on the production day, to simple substances, bulk material unloaded nanoparticles (SLN-placebo and NLC-placebo) and SQV-loaded nanoparticles (SQV-SLN and SQV-NLC).

4.5.3. Stability

The RI plays an important role in long-term stability of lipid nanoparticles. Polymorphic transitions of unstable configurations to more stable configurations, as occurs in the SLN, result in the expulsion of drug from the lipid matrix. On the other hand, less organized structures, as

the NLC, offer more space to accommodate the drug therein. In this study, the RI of SLN-placebo and SQV-SLN (93.8 and 86.0%, respectively) were higher than those in the NLC-placebo and SQV-NLC (82.8 and 78.8%, respectively), which indicates that the NLC may have better matrix stability (table 4.8). This happened because the liquid lipid, existing in NLC, provides a less ordered crystalline structure to the lipid matrix. The miglyol 812 behaves as an impurity in the solid lipid, reducing the RI of lipid nanoparticles, increasing EE and providing a greater capacity for the controlled release of the drug [103].

After production, it is necessary to ensure the solid state of cetyl palmitate present in the formulations. Supercooled melts are produced when the melting point of the peak corresponding to cetyl palmitate is below room temperature. In this study, the solid state of the SLN and NLC was confirmed to room (25 °C) and physiological (37 °C) temperature, since the onset temperature of the peak corresponding to the cetyl palmitate is above these temperatures in the two types of lipid nanoparticles (table 4.8 e figure 4.21). Still, the NLC had lower onset temperatures than SLN and, therefore, a higher probability of existence of these structures.

4.6. *In vitro* studies

4.6.1. Determination of cell viability by MTT

Before performing the viability analysis, different cell concentrations of U87-MG were tested in order to choose the most appropriate for the assay. The incubation time was not tested, settling at 2 hours of incubation after addition of the MTT solution as it was previously determined by other lab members. Through the analysis of the figure 4.22 it can be observed that the reaction is only within the linear range when 5000 cell and 10000 for this cell line are seeded. At higher cell numbers (20000 and 40000), the absorbance reaches a plateau and tends to remain almost constant.

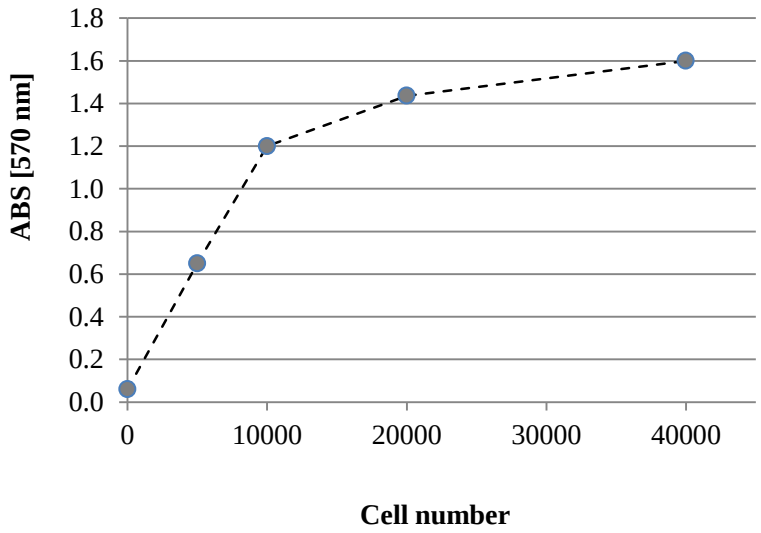

Figure 4.22- Graph of absorbance values obtained for each tested U-87 MG cell density.

In the figure 4.23, it was observed that from the concentration $2x10^5$ cell/mL, the cells begin to cluster resulting in cell death. This can justify the fact that starting from this cell density the absorbance values tend to be constant.

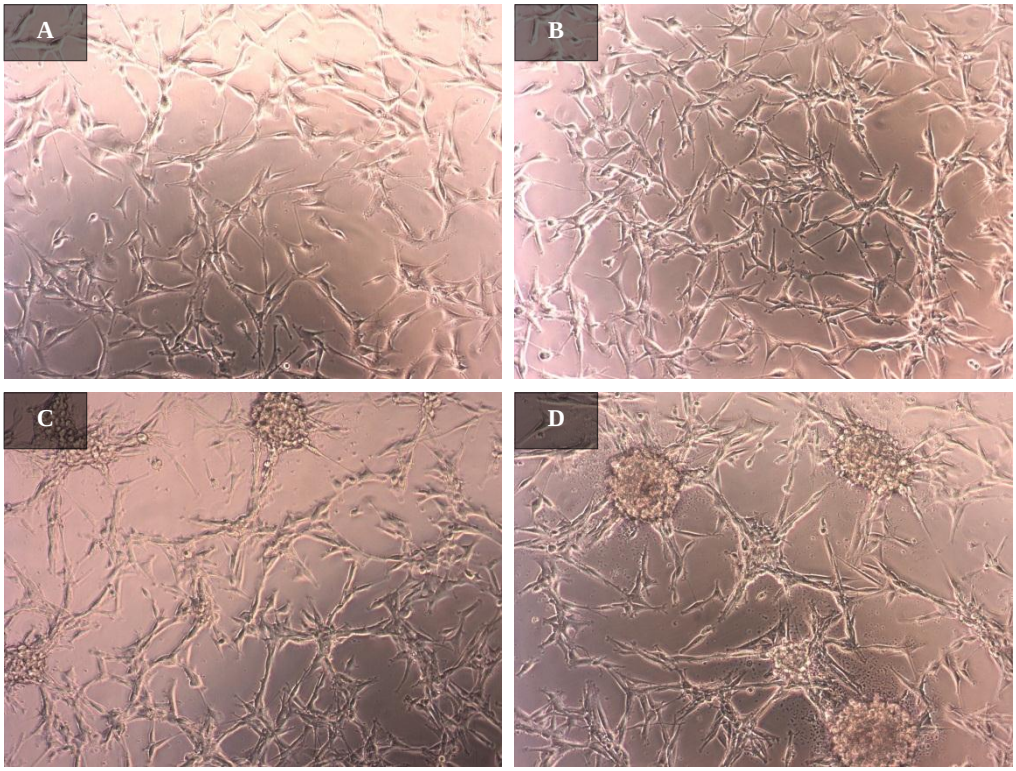

Figure 4.23- Observation under inverted microscope of U87-MG cell line seeded in 96 well plates at different cell densities, after 48 hours of incubation (100X magnification). A $5X10^4$, B $1X10^5$, C $2X10^5$ and D $4X10^5$ cell/mL.

Given all this, the chosen concentration was the $1x10^5$ cell/mL ($1x10^4$ cell/well).

Figure 4.24 shows the results of viability assays using free SQV, drug-free SLN and NLC, and SQV-loaded SLN and NLC.

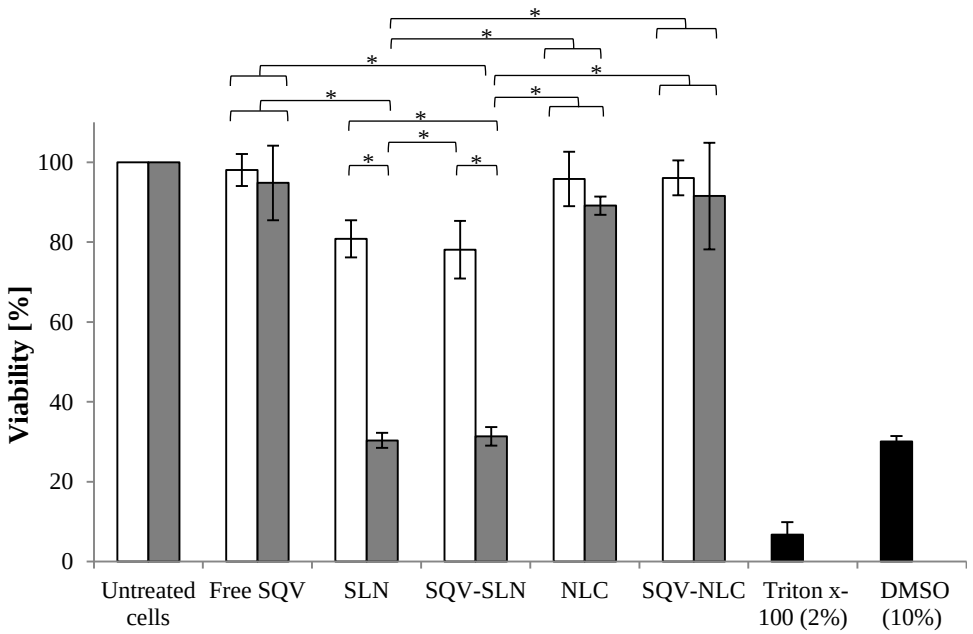

Figure 4.24– Cellular viability of U87-MG cell line using the MTT cell proliferation assay kit. The results are presented for two concentrations of drug: 2.5 µM (□) and 25 µM (■). Data are expressed as percentage of MTT reduction in formazan and represents the average of three independent assays. * data are statistically different ($p < 0.05$, appendix – table B.26).

The MTT analysis (figure 4.24) showed that the free drug presented low cytotoxicity to both concentrations tested, with a slightly lower viability to the highest concentration (25 µM). In NLC (loaded and unloaded), the viability was also high at both concentrations. On the other hand, when the cytotoxicity of SLN (loaded and unloaded) was assessed, it has been observed

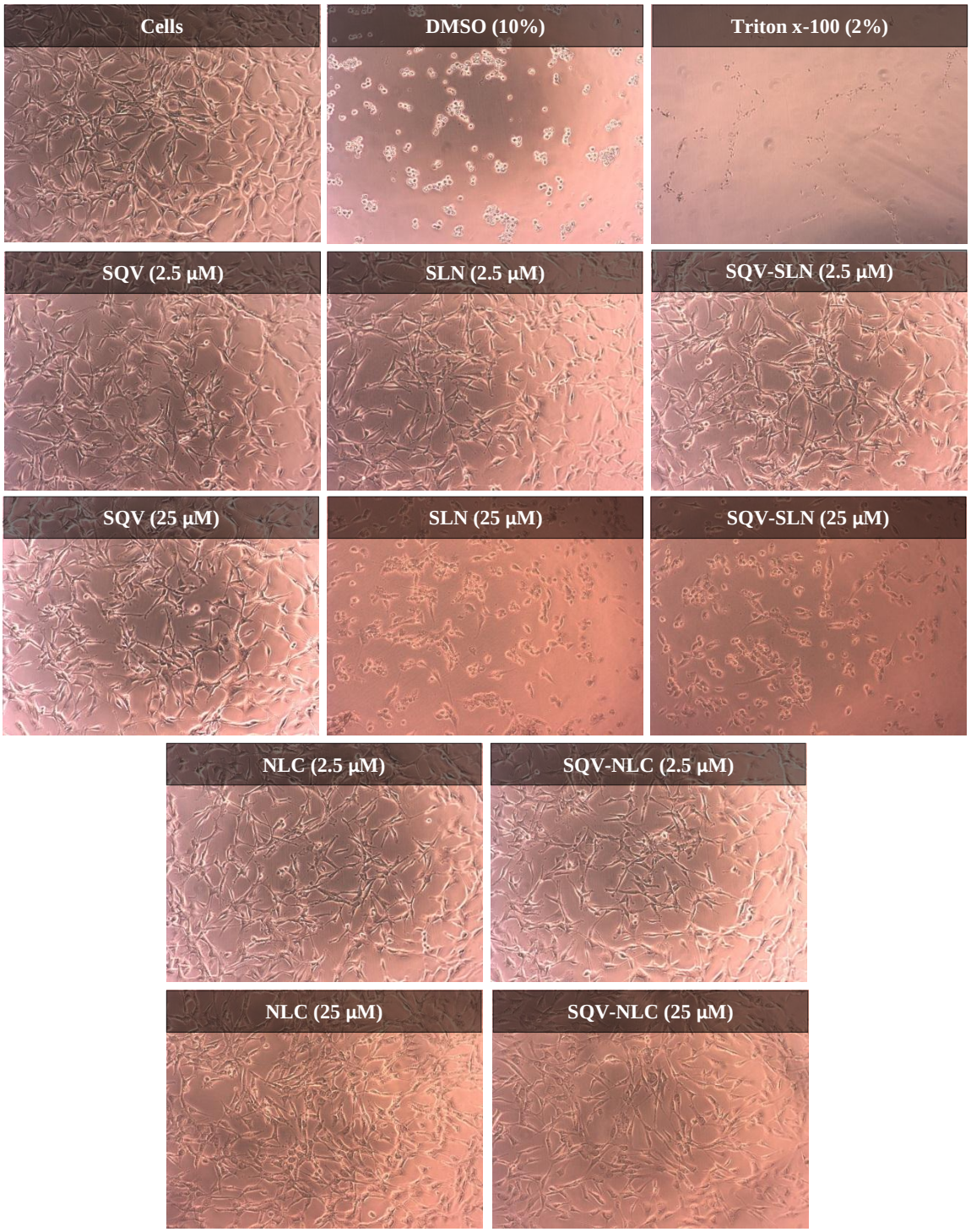

Figure 4.25- Observation under inverted microscope of U87-MG cell line in different conditions tested, the third day of the MTT assay (100X magnification).

that there was a large difference between the concentrations tested. In the case of the 25 µM concentration, the SLN showed significantly reduced cell viability (around 30%). On the opposite, at lower concentrations the viability reached 80%. This suggests that the excipients

used in the matrix of SLNs induce cell death. Both in SLN as in NLC, the incorporation of drug do not seems to interfere significantly in the cell viability. The microscopic images of the different conditions are shown in figure 4.25. As expected cells treated with Triton X-100 (2%) and DMSO (10%) (negative controls) exhibit low cell viability.

4.6.2. Determination of cell viability by propidium iodide exclusion

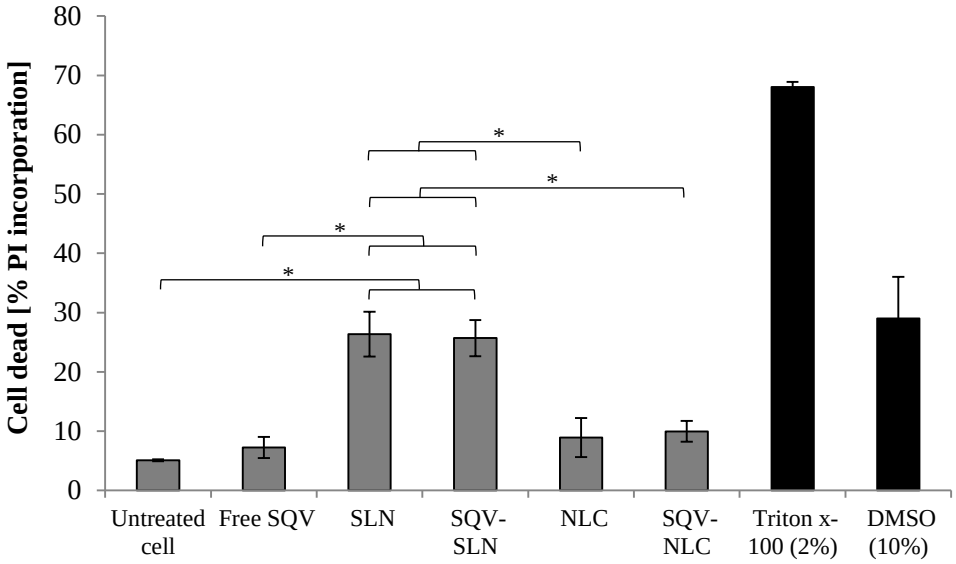

Figure 4.26– Cellular cytotoxicity of U87-MG cell line using the propidium iodide assay. The results are shown for a drug concentration 25 µM. Data are expressed as percentage of incorporation of propidium iodide by dead cells and represents the average of four independent assays. * Data are statistically different ($p < 0.05$, appendix – table B.27).

Examples of the histograms obtained by flow cytometry are shown in figure 4.27.

For PI staining assay, only the highest concentration of SQV (25 µM) was tested. The cytotoxicity of the tested conditions was determined by the percentage of PI incorporated by dead cells. Flow cytometry results are shown in figure 4.26 for the different conditions tested. The cells treated with SLN and SQV-SLN showed a high incorporation of PI, suggesting loss of plasma membrane integrity and cell death. On the other hand, the cells treated with free SQV, NLC and SQV-NLC showed a low incorporation of PI as compared to the untreated cells, confirming the low cytotoxicity also obtained by the MTT assay. The microscopic images of the different conditions are shown in figure 4.28. Also in this assay, the incorporation of drug by SLN and NLC not appear to interfere in cell viability.

The values that gave rise to the graphs presented in figures 4.24 and 4.26 are tabulated attached (appendix – table A.20 and A.21).

Several studies suggested a low cytotoxicity associated to SLNs as one of its major advantages. However, as in this work, start to emerge studies showing that these nanoparticles can greatly affect cell viability depending on their chemical properties (lipid nature, surfactant concentration and combination of its components) [104]. In addition, the cytotoxic potential of these nanoparticles is often associated with their physical characteristics (size, shape, colloidal stability, etc.). Each type of nanoparticles has its own distinct physicochemical characteristics, and thus the toxic effects exerted on the cells may also vary. The mechanism of action, which leads to cell death may also be different [105]. This may explain the difference toxicity

evidenced between SLN (with and without drug) and NLC (with and without drug). Both the MTT as in PI assay, SLN presented a high cellular cytotoxicity for the range of higher concentration (25 µM). In contrast the NLCs, in both assays, showed high cell viability (identical to untreated cells), presented as the most promising lipid nanoparticles in the *in vitro* assays.

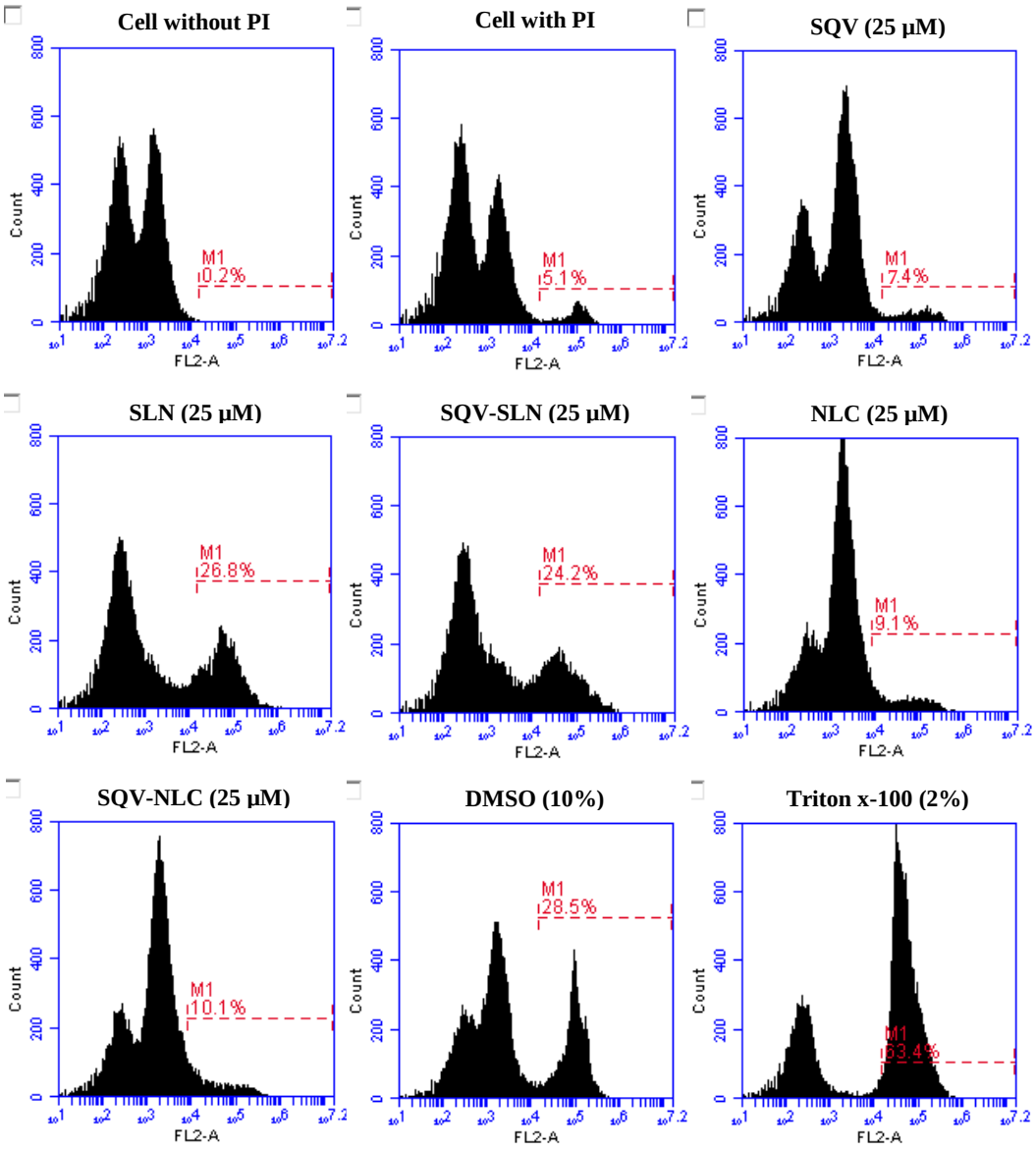

Figure 4.27– Histograms of the different conditions obtained by flow cytometry (BD ACCURI C6 *software*).

Nevertheless, complementary *in vitro* studies will be needed to confirm the obtained results. Other cytotoxicity tests to assess the cellular mechanisms, such as the neutral red dye test, the release assay of cytoplasmic enzymes such as lactate dehydrogenase (LDH), or the alamarBlue test, could be made. In addition to the drug concentrations tested (2.5 and 25 mM) other could be evaluated. Cell viability assays in other cell lines, such as hCMEC/d3 and human astrocytes, could be important to assess whether the SLN studied are also cytotoxic for other types of human cells that might be in contact with drugs used for the treatment of brain tumors. If eventually these SLN were found non toxic to these cell lines, on the opposite to what happened to U-87 MG cell line, the obtained results would be highly promising. The SLN would only be

toxic to (tumoral) glioma cells and harmless to the "healthy" human cells, which is what is intended. Moreover, other promising formulations studied in this work (with different proportions of cetyl palmitate and polysorbate 80) could be evaluated in *in vitro* assays, since the concentration of ingredients used to manufacture the SLNs may have interference in its toxicity.

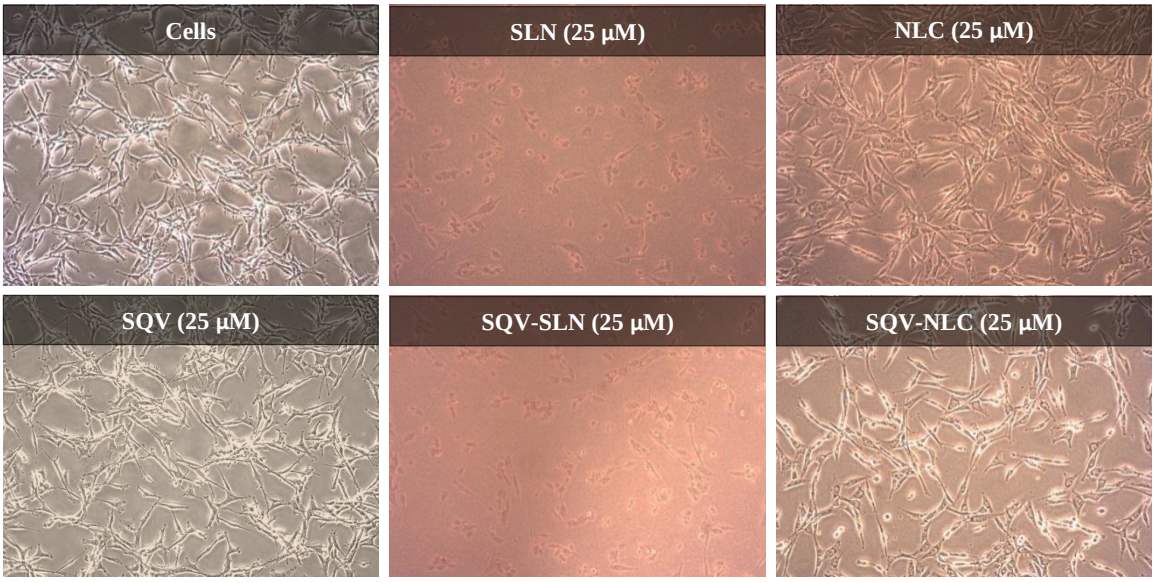

Figure 4.28 - Observation under inverted microscope of U87-MG cell line in different conditions tested, the third day of the PI assay (100X magnification).

In table 4.9 are present all the results obtained during this project to the four most promising formulations.

Table 4.9 - Table summary of the mean results obtained on the production day for the four most promising colloidal dispersions.

Parameters	Formulations			
	SLN	**SQV-SLN**	**NLC**	**SQV-NLC**
Mean Size ± SD [nm]	-	-	-	-
Dv50	205.5 ± 12.8	203.8 ± 15.0	230.8 ± 8.7	211.3 ± 14.8
Z-average	197.7 ± 8.8	197.3 ± 7.6	215.5 ± 12.0	201.3 ± 17.0
Mean Span ± SD	1.985 ± 0.238	2.184 ± 0.328	4.334 ± 1.561	4.205 ± 1.469
Mean PI ± SD	0.117 ± 0.044	0.114 ± 0.051	0.094 ± 0.053	0.083 ± 0.035
Mean ZP ± SD [mV]	-32.6 ± 1.1	-24.1 ± 2.3	-34.8 ± 2.8	-25.0 ± 3.1
Mean EE ± SD [%]	-	92.4 ± 5.99	-	93.7 ± 3.17
Mean RI [%]	93.8	86	82.8	78.8
Viability ± SD [%] (MTT)	-	-	-	-
2.5 µM	80.9 ± 4.64	78.1 ± 7.19	95.8 ± 6.82	96.1 ± 4.37
25 µM	30.4 ± 1.86	31.4 ± 2.34	89.1 ±2.29	91.5 ± 13.33
Cytotoxicity ± SD [%] (PI)	26.4 ± 3.04	25.7 ± 3.30	8.9 ± 1.74	10.0 ± 0.88

Chapter V - Conclusions

In recent decades, the sharp growth in studies related with the CNS has led to increased research into new drugs that aim to treat brain diseases. However, some of the existing drugs in the market have difficulties to cross the BBB and to reach the brain efficiently. The saquinavir drug is an example. Due to its lipophilic nature (octanol/water partition coefficient - log P of 4.51) [24, 26, 27] it is impermeable across the BBB [22, 26]. Furthermore, it is a substrate of P-gp, which also explains the reduced penetration into the brain [15, 21, 27, 29]. As a result, there is a need to develop strategies for improving the bioavailability of poorly water soluble drugs, such as SQV [22, 28]. Nanotechnology arises then as an important tool for improving the affinity of these drugs with BBB, allowing them to reach the brain. The SLN and NLC, in particular, have shown to be promising vehicles for the transport of lipophilic drugs to the brain [53, 59].

In this work, lipid nanoparticles were developed for carrying SQV through the BBB. The optimization of lipid nanoparticles (SQV-SLN and SQV-NLC) developed in this study allowed to assess that the optimal proportion of ingredients was: 5% lipid, 2% surfactant and 0.05% drug. The technique that was more promising was ultrasonication. The optimization process resulted in mean sizes of around 200 nm, zeta potential reasonably good (~ -25 mV) and high SQV encapsulation efficacy (over 90%). Lipid nanoparticles proved to be a good choice for the transport of SQV. Furthermore, the size obtained (~ 200 nm) is ideal for efficiently cross the BBB and invade tumor tissue (EPR effect) [9, 11]. This shows that optimization of these nanoparticles was successful.

In the stability study, it was found that SQV-SLN kept the same size range during the investigation time, showing good stability of the suspension. On the opposite, SQV-NLC had a marked increase in the particle size, when evaluated by the LD technique. During the stability study significant differences in results between LD and DLS characterization techniques were noticed. If on the production day of LN, the Dv50 and Z-average values obtained by LD and DLS, respectively, were often comparable, with the passage of time and the formation of aggregates this is no longer happened. The DLS technique ceased to be able to measure the populations with higher size ranges and therefore, the results began to distance themselves from those obtained by LD.

In the EE stability study, it was found that SQV-NLC presented better matrix stability than SQV-SLN. The SQV-NLC had less loss of drug over the 3 months of study, reinforcing the idea that the SQV-SLN undergoes recrystallization during storage. The results of the DSC technique followed those obtained by HPLC. The SQV-NLC had a more disorganized crystalline lattice

that SQV-SLN, allowing greater accommodation of the drug. In addition, through the thermograms of loaded lipid nanoparticles it was possible to verify that the drug was monodispersed in the lipid matrix.

In the *in vitro* studies, SLNs (loaded and unloaded) showed a higher cytotoxicity at the concentration of 25 µM. On the contrary, the NLCs showed a high cell viability in both techniques assessed (MTT and PI). The NLCs were the most promising formulations in these *in vitro* assays.

Interestingly, SQV in free form showed low cytotoxicity in both methods, suggesting that the use of lipid nanoparticles will only serve to target the drug through the BBB, to the tumor site and not to mask the cytotoxicity of the drug.

However, it will take more *in vitro* studies in order to corroborate the results obtained. Cell viability assays in other cell lines, such as hCMEC/d3 or human astrocytes could also be a good complement to this study.

Overall, the SLN and NLC had positive and negative aspects. If on one hand the SLN showed a good stability of the suspension while keeping the same size throughout the investigation period, the NLCs showed good stability of matrix with high encapsulation efficiency and fewer losses of the drug over time. Furthermore, cytotoxicity and viability studies also showed the most promising results for this type of lipid nanoparticles.

Chapter VI - Future work

In a future work, and in order to evaluate the advantages and effectiveness of the studied formulations, more *in vitro* tests could be done. Cell viability/cytotoxicity studies would be made in the hCMEC/D3 cell line (corresponding to immortalized human microvascular endothelial cells entodeliais) and in human astrocytes (HA), as happened in the U-87 MG cell line. Furthermore, to evaluate the flux of nanoparticles through the BBB, a two-dimensional BBB *in vitro* system seeded into Transwell membranes would be used. Permeation of BBB *in vitro* would be studied by adding of nanoparticles to the donor medium, followed by the recovery of samples from the basolateral compartment over time, determined by HPLC.

The functionalisation of the nanoparticles to a more effective targeting (active targeting) to the BBB would be another study to be performed. In these nanoparticles, *in vitro* tests would also be made.

Appendix

A) Additional results

Table A.1 - Dv10 values obtained in each lot produced (by ultrasonication and hot HPH) on day 0. These values were used to calculate means and standard deviations of Dv10 in the unloaded lipid nanoparticles.

Dv10 [nm] - Unloaded nanoparticles													
Lot number		SLN						NLC					
		$CP_{10}T_1$	$CP_{10}T_2$	$CP_{10}T_3$	CP_5T_1	CP_5T_2	CP_5T_3	$CP_7M_3T_1$	$CP_7M_3T_2$	$CP_7M_3T_3$	$CP_3M_2T_1$	$CP_3M_2T_2$	$CP_3M_2T_3$
Ultrasonication	1	358	169	225	148	102	107	356	158	207	152	107	83.6
	2	297	216	209	134	94.7	84.3	735	224	133	129	101	90.6
	3	272	229	120	146	91.8	80.2	461	261	132	242	110	90.2
	4	-	-	-	-	94.6	96.0	-	-	-	-	104	89.2
	5	-	-	-	-	98.8	97.9	-	-	-	-	104	91.2
	6	-	-	-	-	89.5	94.2	-	-	-	-	97	103
	7	-	-	-	-	90.8	102	-	-	-	-	104	99.2
	8	-	-	-	-	71.9	93.9	-	-	-	-	102	89
	9	-	-	-	-	87.7	94.6	-	-	-	-	81.7	97.6
	10	-	-	-	-	95.9	103	-	-	-	-	90.7	106
	11	-	-	-	-	93.5	85.9	-	-	-	-	101	102
	12	-	-	-	-	95.5	92.2	-	-	-	-	101	97.7
	13	-	-	-	-	91.8	82.0	-	-	-	-	95.4	90.3
	14	-	-	-	-	92.7	-	-	-	-	-	104	-
	15	-	-	-	-	-	-	-	-	-	-	105	-
	16	-	-	-	-	-	-	-	-	-	-	104	-
Hot HPH	1	137	131	122	134	102	110	140	116	116	125	105	101
	2	147	129	122	131	101	93.7	158	123	118	129	103	101
	3	139	122	128	122	101	106	163	120	119	121	103	102
	4	-	-	-	-	102	109	-	-	-	-	-	95.1
	5	-	-	-	-	98.4	83.4	-	-	-	-	-	95.4
	6	-	-	-	-	101	100	-	-	-	-	-	96.7
	7	-	-	-	-	89	85.3	-	-	-	-	-	94.3
	8	-	-	-	-	-	93.8	-	-	-	-	-	97.2
	9	-	-	-	-	-	90.7	-	-	-	-	-	95.9
	10	-	-	-	-	-	85.5	-	-	-	-	-	91.4
	11	-	-	-	-	-	84.5	-	-	-	-	-	92.3
	12	-	-	-	-	-	80.7	-	-	-	-	-	91.6
	13	-	-	-	-	-	79.5	-	-	-	-	-	-

Table A.2 – Dv50 values obtained in each lot produced (by ultrasonication and hot HPH) on day 0. These values were used to calculate means and standard deviations of Dv50 in the unloaded lipid nanoparticles.

Dv50 [nm] - Unloaded nanoparticles													
Lot number		SLN						NLC					
		$CP_{10}T_1$	$CP_{10}T_2$	$CP_{10}T_3$	CP_5T_1	CP_5T_2	CP_5T_3	$CP_7M_3T_1$	$CP_7M_3T_2$	$CP_7M_3T_3$	$CP_3M_2T_1$	$CP_3M_2T_2$	$CP_3M_2T_3$
Ultrasonication	1	742	401	573	327	231	249	869	387	740	354	241	175
	2	634	495	509	292	200	175	1480	738	327	296	221	197
	3	607	536	270	321	197	164	1190	942	315	725	246	197
	4	-	-	-	-	208	212	-	-	-	-	232	193
	5	-	-	-	-	220	218	-	-	-	-	241	204
	6	-	-	-	-	192	202	-	-	-	-	211	252
	7	-	-	-	-	196	238	-	-	-	-	233	233
	8	-	-	-	-	217	196	-	-	-	-	230	224
	9	-	-	-	-	183	214	-	-	-	-	231	233
	10	-	-	-	-	220	238	-	-	-	-	218	249
	11	-	-	-	-	201	182	-	-	-	-	236	241
	12	-	-	-	-	207	200	-	-	-	-	227	224
	13	-	-	-	-	202	170	-	-	-	-	230	226
	14	-	-	-	-	203	-	-	-	-	-	231	-
	15	-	-	-	-	-	-	-	-	-	-	232	-
	16	-	-	-	-	-	-	-	-	-	-	233	-
Hot HPH	1	313	305	276	326	227	248	336	267	266	301	246	226
	2	344	300	276	313	226	206	375	289	268	316	238	228
	3	315	286	293	285	224	245	408	284	275	291	243	234
	4	-	-	-	-	231	254	-	-	-	-	-	216
	5	-	-	-	-	219	256	-	-	-	-	-	216
	6	-	-	-	-	224	254	-	-	-	-	-	221
	7	-	-	-	-	196	182	-	-	-	-	-	213
	8	-	-	-	-	-	205	-	-	-	-	-	223
	9	-	-	-	-	-	197	-	-	-	-	-	218
	10	-	-	-	-	-	182	-	-	-	-	-	213
	11	-	-	-	-	-	183	-	-	-	-	-	218
	12	-	-	-	-	-	169	-	-	-	-	-	216
	13	-	-	-	-	-	165	-	-	-	-	-	-

Table A.3 – Dv90 values obtained in each lot produced (by ultrasonication and hot HPH) on day 0. These values were used to calculate means and standard deviations of Dv90 in the unloaded lipid nanoparticles.

Dv90 [nm] - Unloaded nanoparticles													
	Lot number	SLN						NLC					
		$CP_{10}T_1$	$CP_{10}T_2$	$CP_{10}T_3$	CP_5T_1	CP_5T_2	CP_5T_3	$CP_7M_3T_1$	$CP_7M_3T_2$	$CP_7M_3T_3$	$CP_3M_2T_1$	$CP_3M_2T_2$	$CP_3M_2T_3$
Ultrasonication	1	1710	1150	1760	740	630	786	2650	1820	3280	1400	1560	409
	2	1600	1420	1510	650	418	365	3960	2680	2490	1310	604	477
	3	1480	1550	626	765	447	335	3470	3130	1860	2730	975	710
	4	-	-	-	-	536	544	-	-	-	-	743	519
	5	-	-	-	-	571	565	-	-	-	-	1730	660
	6	-	-	-	-	436	450	-	-	-	-	588	2100
	7	-	-	-	-	405	758	-	-	-	-	1590	1870
	8	-	-	-	-	618	400	-	-	-	-	1150	1790
	9	-	-	-	-	467	668	-	-	-	-	1950	1900
	10	-	-	-	-	485	753	-	-	-	-	1340	2040
	11	-	-	-	-	564	410	-	-	-	-	1580	1970
	12	-	-	-	-	518	488	-	-	-	-	1040	1680
	13	-	-	-	-	558	362	-	-	-	-	1890	1950
	14	-	-	-	-	-	-	-	-	-	-	642	-
	15	-	-	-	-	-	-	-	-	-	-	747	-
	16	-	-	-	-	-	-	-	-	-	-	1210	-
Hot HPH	1	1090	1070	718	1300	613	643	1690	1450	1060	1810	1520	1070
	2	1340	1160	710	1210	642	591	1710	1690	907	2020	1460	855
	3	1100	961	752	1160	577	652	1980	1780	1170	1860	1530	830
	4	-	-	-	-	748	517	-	-	-	-	-	671
	5	-	-	-	-	585	681	-	-	-	-	-	784
	6	-	-	-	-	594	704	-	-	-	-	-	998
	7	-	-	-	-	568	443	-	-	-	-	-	1000
	8	-	-	-	-	-	512	-	-	-	-	-	1020
	9	-	-	-	-	-	482	-	-	-	-	-	1120
	10	-	-	-	-	-	423	-	-	-	-	-	982
	11	-	-	-	-	-	503	-	-	-	-	-	1150
	12	-	-	-	-	-	371	-	-	-	-	-	984
	13	-	-	-	-	-	362	-	-	-	-	-	-

Table A.4 – "Span" values obtained in each lot produced (by ultrasonication and hot HPH) on day 0. These values were used to calculate means and standard deviations of "span" in the unloaded lipid nanoparticles.

Span - Unloaded nanoparticles													
	Lot number	SLN						NLC					
		$CP_{10}T_1$	$CP_{10}T_2$	$CP_{10}T_3$	CP_5T_1	CP_5T_2	CP_5T_3	$CP_7M_3T_1$	$CP_7M_3T_2$	$CP_7M_3T_3$	$CP_3M_2T_1$	$CP_3M_2T_2$	$CP_3M_2T_3$
Ultrasonication	1	1.824	2.449	2.686	1.808	2.289	2.729	2.635	4.303	4.150	3.541	6.031	1.853
	2	2.055	2.424	2.548	1.768	1.619	1.606	2.185	3.333	7.204	3.982	2.280	1.959
	3	1.987	2.469	1.869	1.924	1.804	1.549	2.534	3.047	5.474	3.429	5.546	3.137
	4	-	-	-	-	2.124	2.110	-	-	-	-	3.513	2.230
	5	-	-	-	-	2.151	2.142	-	-	-	-	2.760	2.797
	6	-	-	-	-	1.764	1.761	-	-	-	-	5.662	7.929
	7	-	-	-	-	1.734	2.758	-	-	-	-	2.321	7.618
	8	-	-	-	-	2.362	1.563	-	-	-	-	6.373	7.594
	9	-	-	-	-	1.857	2.688	-	-	-	-	4.535	7.759
	10	-	-	-	-	1.881	2.738	-	-	-	-	5.762	7.775
	11	-	-	-	-	2.092	1.778	-	-	-	-	6.248	7.750
	12	-	-	-	-	2.148	1.976	-	-	-	-	4.120	7.029
	13	-	-	-	-	-	1.640	-	-	-	-	2.330	8.237
	14	-	-	-	-	-	-	-	-	-	-	2.769	-
	15	-	-	-	-	-	-	-	-	-	-	4.765	-
	16	-	-	-	-	-	-	-	-	-	-	-	-
Hot HPH	1	3.038	3.085	2.156	3.574	2.245	1.962	4.609	4.982	3.541	5.610	5.765	3.303
	2	3.462	3.415	2.128	3.428	2.389	1.940	4.130	5.404	2.942	5.969	5.699	2.720
	3	3.038	2.936	2.130	3.630	2.125	2.070	4.460	5.822	3.828	5.963	5.766	2.642
	4	-	-	-	-	2.800	2.059	-	-	-	-	-	2.529
	5	-	-	-	-	2.229	2.343	-	-	-	-	-	2.991
	6	-	-	-	-	2.201	2.345	-	-	-	-	-	3.824
	7	-	-	-	-	2.448	1.961	-	-	-	-	-	4.213
	8	-	-	-	-	-	2.046	-	-	-	-	-	4.254
	9	-	-	-	-	-	1.982	-	-	-	-	-	4.623
	10	-	-	-	-	-	1.854	-	-	-	-	-	4.172
	11	-	-	-	-	-	2.290	-	-	-	-	-	4.716
	12	-	-	-	-	-	1.719	-	-	-	-	-	4.076
	13	-	-	-	-	-	1.706	-	-	-	-	-	-

Table A.5 – Z-average, polydispersity index and zeta potential values obtained in each lot produced (by ultrasonication and hot HPH) on day 0. These values were used to calculate means and standard deviations in the unloaded lipid nanoparticles.

Unloaded nanoparticles													
Lot number		Z-average [nm]				Polydispersity Index				Zeta Potential [mV]			
		SLN		NLC		SLN		NLC		SLN		NLC	
		CP_5T_2	CP_5T_3	$CP_3M_2T_2$	$CP_3M_2T_3$	CP_5T_2	CP_5T_3	$CP_3M_2T_2$	$CP_3M_2T_3$	CP_5T_2	CP_5T_3	$CP_3M_2T_2$	$CP_3M_2T_3$
Ultrasonication	**1**	188.0	185.4	210.9	208.3	0.095	0.113	0.080	0.093	-32.26	-31.56	-36.20	-37.76
	2	198.8	199.7	205.5	221.0	0.119	0.183	0.074	0.060	-32.17	-33.30	-31.81	-38.69
	3	206.5	199.7	231.2	206.4	0.136	0.170	0.133	0.097	-33.39	-32.22	-36.33	-27.41
	4	-	218.1	-	212.6	-	0.045	-	0.101	-	-34.96	-	-27.66
	5	-	194.9	-	207.2	-	0.141	-	0.126	-	-42.21	-	-23.45
	6	-	199.2	-	202.9	-	0.158	-	0.072	-	-34.45	-	-27.68
Hot HPH	**1**	186.7	183.5	198.9	180.2	0.177	0.186	0.162	0.172	-32.41	-34.22	-36.87	-40.70
	2	182.2	181.0	195.3	187.8	0.113	0.152	0.150	0.144	-34.90	-33.22	-31.36	-41.92
	3	190.6	168.5	198.4	182.4	0.130	0.140	0.171	0.147	-32.38	-27.87	-31.63	-45.06
	4	181.6	180.4	189.3	176.0	0.090	0.159	0.134	0.169	-34.70	-29.61	-40.79	-21.60
	5	-	169.8	-	181.0	-	0.150	-	0.192	-	-28.44	-	-35.02
	6	-	154.9	-	176.7	-	0.193	-	0.178	-	-27.06	-	-29.40
	7	-	165.9	-	201.4	-	0.142	-	0.179	-	-31.76	-	-41.69
	8	-	161.5	-	185.6	-	0.131	-	0.237	-	-34.44	-	-37.70
	9	-	162.4	-	-	-	0.127	-	-	-	-30.78	-	-38.69

Table A.6 – Dv10 values obtained in each lot produced (by ultrasonication and hot HPH) on day 0. These values were used to calculate means and standard deviations of Dv10 in the SQV-loaded lipid nanoparticles.

Dv10 [nm] - SQV-loaded nanoparticles									
Lot number		**SLN**				**NLC**			
		$SQV_{0.1}$-CP_5T_2	**$SQV_{0.1}$-CP_5T_3**	**$SQV_{0.05}$-CP_5T_2**	**$SQV_{0.05}$-CP_5T_3**	**$SQV_{0.1}$-$CP_3M_2T_2$**	**$SQV_{0.1}$-$CP_3M_2T_3$**	**$SQV_{0.05}$-$CP_3M_2T_2$**	**$SQV_{0.05}$-$CP_3M_2T_3$**
Ultrasonication	**1**	97.5	96.3	91.9	80.5	69.6	79.5	74.4	85.1
	2	92.2	100	92.0	77.8	87	80.3	100.0	66.5
	3	64.3	99.8	97.4	84.2	84.4	78.2	92.5	74.3
	4	-	-	75.6	101	-	-	93.7	91.2
	5	-	-	88.1	104	-	-	102	76.3
	6	-	-	88.2	92.6	-	-	98.7	-
	7	-	-	90.3	-	-	-	92.4	-
	8	-	-	98.4	-	-	-	85.6	-
	9	-	-	98.1	-	-	-	76.4	-
	10	-	-	97.4	-	-	-	83.6	-
	11	-	-	95	-	-	-	85.3	-
	12	-	-	88.4	-	-	-	78.4	-
	13	-	-	89.9	-	-	-	90.8	-
	14	-	-	78.8	-	-	-	97.7	-
	15	-	-	85.1	-	-	-	97.6	-
	16	-	-	96.3	-	-	-	-	-
	17	-	-	87.5	-	-	-	-	-
	18	-	-	94.2	-	-	-	-	-
	19	-	-	92.4	-	-	-	-	-
	20	-	-	96.8	-	-	-	-	-
	21	-	-	91.9	-	-	-	-	-
	22	-	-	85.6	-	-	-	-	-
	23	-	-	90.6	-	-	-	-	-
Hot HPH	**1**	93	110	97.9	94.5	111	86.9	83.9	89.2
	2	95.2	112	100	92.9	112	110	84.5	87.1
	3	98	116	8.6	91.9	111	99.1	82.7	87.5
	4	-	-	101	-	-	-	83.5	-
	5	-	-	104	-	-	-	85.1	-
	6	-	-	101	-	-	-	78.2	-
	7	-	-	92.1	-	-	-	78.6	-
	8	-	-	96.4	-	-	-	80.3	-
	9	-	-	97.4	-	-	-	-	-

Table A.7 – Dv50 values obtained in each lot produced (by ultrasonication and hot HPH) on day 0. These values were used to calculate means and standard deviations of Dv50 in the SQV-loaded lipid nanoparticles.

Dv50 [nm] - SQV-loaded nanoparticles									
Lot number		**SLN**				**NLC**			
		$SQV_{0.1}$-CP_5T_2	**$SQV_{0.1}$-CP_5T_3**	**$SQV_{0.05}$-CP_5T_2**	**$SQV_{0.05}$-CP_5T_3**	**$SQV_{0.1}$-$CP_3M_2T_2$**	**$SQV_{0.1}$-$CP_3M_2T_3$**	**$SQV_{0.05}$-$CP_3M_2T_2$**	**$SQV_{0.05}$-$CP_3M_2T_3$**
Ultrasonication	**1**	233	249	202	169	216	247	224	211
	2	245	254	194	170	224	259	225	209
	3	226	250	218	172	230	239	198	200
	4	-	-	223	219	-	-	203	217
	5	-	-	187	222	-	-	226	212
	6	-	-	186	197	-	-	214	-
	7	-	-	193	-	-	-	222	-
	8	-	-	223	-	-	-	193	-
	9	-	-	228	-	-	-	200	-
	10	-	-	227	-	-	-	181	-
	11	-	-	214	-	-	-	202	-
	12	-	-	194	-	-	-	235	-
	13	-	-	196	-	-	-	222	-
	14	-	-	210	-	-	-	212	-
	15	-	-	183	-	-	-	213	-
	16	-	-	218	-	-	-	-	-
	17	-	-	186	-	-	-	-	-
	18	-	-	207	-	-	-	-	-
	19	-	-	198	-	-	-	-	-
	20	-	-	216	-	-	-	-	-
	21	-	-	205	-	-	-	-	-
	22	-	-	182	-	-	-	-	-
	23	-	-	198	-	-	-	-	-
Hot HPH	**1**	206	310	215	206	504	382	216	208
	2	216	325	223	203	466	855	241	197
	3	224	331	218	201	423	552	218	198
	4	-	-	223	-	-	-	215	-
	5	-	-	229	-	-	-	229	-
	6	-	-	221	-	-	-	186	-
	7	-	-	200	-	-	-	186	-
	8	-	-	210	-	-	-	196	-
	9	-	-	222	-	-	-	-	-

Table A.8 – Dv90 values obtained in each lot produced (by ultrasonication and hot HPH) on day 0. These values were used to calculate means and standard deviations of Dv90 in the SQV-loaded lipid nanoparticles.

Dv90 [nm] - SQV-loaded nanoparticles									
Lot number		**SLN**				**NLC**			
		$SQV_{0.1}$-CP_5T_2	**$SQV_{0.1}$-CP_5T_3**	**$SQV_{0.05}$-CP_5T_2**	**$SQV_{0.05}$-CP_5T_3**	**$SQV_{0.1}$-$CP_3M_2T_2$**	**$SQV_{0.1}$-$CP_3M_2T_3$**	**$SQV_{0.05}$-$CP_3M_2T_2$**	**$SQV_{0.05}$-$CP_3M_2T_3$**
Ultrasonication	**1**	5789	1340	532	359	2120	4270	1360.0	1550
	2	4080	1490	412	358	1700	7470	794.0	1330
	3	2330	1690	631	348	2780	10100	1240	1340
	4	-	-	483	494	-	-	525	2030
	5	-	-	465	482	-	-	694	-
	6	-	-	503	445	-	-	1400	-
	7	-	-	574	-	-	-	1390	-
	8	-	-	584	-	-	-	618	-
	9	-	-	434	-	-	-	1440	-
	10	-	-	412	-	-	-	1340	-
	11	-	-	548	-	-	-	1640	-
	12	-	-	442	-	-	-	512	-
	13	-	-	438	-	-	-	1100	-
	14	-	-	510	-	-	-	587	-
	15	-	-	-	-	-	-	594	-
Hot HPH	**1**	1020	3400	549	549	501000	328000	2260	1530
	2	1670	5050	606	548	308000	879000	2480	1280
	3	1190	8310	581	574	310000	722000	1980	1300
	4	-	-	558	-	-	-	2070	-
	5	-	-	561	-	-	-	2150	-
	6	-	-	542	-	-	-	2080	-
	7	-	-	643	-	-	-	1860	-
	8	-	-	552	-	-	-	2230	-
	9	-	-	897	-	-	-	-	-

Table A.9 – "Span" values obtained in each lot produced (by ultrasonication and hot HPH) on day 0. These values were used to calculate means and standard deviations of "span" in the SQV-loaded lipid nanoparticles.

Span - SQV-loaded nanoparticles									
Lot number		SLN				NLC			
		$SQV_{0.1}$-CP_5T_2	$SQV_{0.1}$-CP_5T_3	$SQV_{0.05}$-CP_5T_2	$SQV_{0.05}$-CP_5T_3	$SQV_{0.1}$-$CP_3M_2T_2$	$SQV_{0.1}$-$CP_3M_2T_3$	$SQV_{0.05}$-$CP_3M_2T_2$	$SQV_{0.05}$-$CP_3M_2T_3$
Ultrasonication	**1**	24.427	4.995	2.176	1.643	9.493	16.966	5.365	6.941
	2	16.277	5.472	1.649	1.648	7.201	28.532	5.303	6.268
	3	10.025	6.361	2.450	1.531	11.720	41.932	3.048	5.750
	4	-	-	2.117	1.793	-	-	4.737	9.258
	5	-	-	2.025	1.706	-	-	2.190	-
	6	-	-	2.139	1.787	-	-	2.964	-
	7	-	-	2.697	-	-	-	5.742	-
	8	-	-	2.556	-	-	-	5.318	-
	9	-	-	2.493	-	-	-	2.422	-
	10	-	-	2.521	-	-	-	5.970	-
	11	-	-	1.897	-	-	-	2.367	-
	12	-	-	2.642	-	-	-	5.034	-
	13	-	-	1.745	-	-	-	-	-
	14	-	-	2.190	-	-	-	-	-
	15	-	-	1.772	-	-	-	-	-
	16	-	-	1.937	-	-	-	-	-
	17	-	-	2.125	-	-	-	-	-
Hot HPH	**1**	4.500	10.613	2.102	2.205	952.890	802.247	10.241	6.948
	2	7.291	15.194	2.265	2.241	599.016	1043.844	9.976	6.040
	3	4.875	24.755	2.213	2.394	615.233	1311.461	8.746	6.099
	4	-	-	2.046	-	-	-	9.224	-
	5	-	-	1.994	-	-	-	9.022	-
	6	-	-	2.000	-	-	-	10.762	-
	7	-	-	2.745	-	-	-	9.594	-
	8	-	-	2.165	-	-	-	10.952	-
	9	-	-	3.631	-	-	-	-	-

Table A.10 – Z-average values obtained in each lot produced (by ultrasonication and hot HPH) on day 0. These values were used to calculate means and standard deviations of Z-average in the SQV-loaded lipid nanoparticles.

Z-average [nm] - SQV-loaded nanoparticles									
Lot number		**SLN**				**NLC**			
		$SQV_{0.1}$-CP_5T_2	**$SQV_{0.1}$-CP_5T_3**	**$SQV_{0.05}$-CP_5T_2**	**$SQV_{0.05}$-CP_5T_3**	**$SQV_{0.1}$-$CP_3M_2T_2$**	**$SQV_{0.1}$-$CP_3M_2T_3$**	**$SQV_{0.05}$-$CP_3M_2T_2$**	**$SQV_{0.05}$-$CP_3M_2T_3$**
Ultrasonication	**1**	203.9	210.4	206.1	191.3	266.9	161.2	203.2	196.0
	2	213.9	251.2	202.8	184.8	221.7	247.8	202.8	197.2
	3	218.5	215.4	198.0	198.0	202.5	170.2	193.9	192.5
	4	-	-	188.8	194.0	-	-	200.2	203.5
	5	-	-	196.1	199.9	-	-	203.5	197.9
	6	-	-	193.6	206.2	-	-	201.6	202.8
	7	-	-	193.4	-	-	-	182.1	-
	8	-	-	192.5	-	-	-	211.5	-
	9	-	-	204.2	-	-	-	211.7	-
Hot HPH	**1**	209.4	184.6	223.5	203.0	182.8	153.7	187.8	159.0
	2	201.9	206.5	225.2	199.1	185.5	164.3	186.3	160.6
	3	214.7	209.4	236.8	206.7	199.6	232.9	188.1	158.6
	4	-	-	218.4	-	-	-	183.9	-
	5	-	-	220.5	-	-	-	184.6	-
	6	-	-	207.8	-	-	-	186.8	-
	7	-	-	219.4	-	-	-	175.8	-
	8	-	-	208.2	-	-	-	178.4	-
	9	-	-	213.7	-	-	-	190.8	-

Table A.11 – Polydispersity index values obtained in each lot produced (by ultrasonication and hot HPH) on day 0. These values were used to calculate means and standard deviations of polydispersity index in the SQV-loaded lipid nanoparticles.

Polydispersity Index - SQV-loaded nanoparticles									
Lot number		**SLN**				**NLC**			
		$SQV_{0.1}$-CP_5T_2	**$SQV_{0.1}$-CP_5T_3**	**$SQV_{0.05}$-CP_5T_2**	**$SQV_{0.05}$-CP_5T_3**	**$SQV_{0.1}$-$CP_3M_2T_2$**	**$SQV_{0.1}$-$CP_3M_2T_3$**	**$SQV_{0.05}$-$CP_3M_2T_2$**	**$SQV_{0.05}$-$CP_3M_2T_3$**
Ultrasonication	**1**	0.128	0.157	0.100	0.054	0.134	0.138	0.100	0.102
	2	0.099	0.191	0.120	0.056	0.161	0.251	0.087	0.059
	3	0.103	0.270	0.209	0.028	0.109	0.131	0.069	0.100
	4	-	-	0.088	0.111	-	-	0.046	0.052
	5	-	-	0.073	0.116	-	-	0.068	0.079
	6	-	-	0.086	0.058	-	-	0.120	0.017
	7	-	-	0.130	-	-	-	0.107	-
	8	-	-	0.107	-	-	-	0.090	-
	9	-	-	0.136	-	-	-	0.059	-
Hot HPH	**1**	0.140	0.201	0.114	0.205	0.162	0.186	0.176	0.213
	2	0.131	0.249	0.127	0.195	0.124	0.155	0.163	0.169
	3	0.139	0.167	0.186	0.192	0.139	0.254	0.138	0.188
	4	-	-	0.159	-	-	-	0.108	-
	5	-	-	0.123	-	-	-	0.119	-
	6	-	-	0.142	-	-	-	0.123	-
	7	-	-	0.148	-	-	-	0.152	-
	8	-	-	0.116	-	-	-	0.145	-
	9	-	-	0.155	-	-	-	0.081	-

Table A.12 – Zeta potential values obtained in each lot produced (by ultrasonication and hot HPH) on day 0. These values were used to calculate means and standard deviations of zeta potential in the SQV-loaded lipid nanoparticles.

Zeta Potential [mV] - SQV-loaded nanoparticles									
Lot number		**SLN**				**NLC**			
		$SQV_{0.1}$-CP_5T_2	**$SQV_{0.1}$-CP_5T_3**	**$SQV_{0.05}$-CP_5T_2**	**$SQV_{0.05}$-CP_5T_3**	**$SQV_{0.1}$-$CP_3M_2T_2$**	**$SQV_{0.1}$-$CP_3M_2T_3$**	**$SQV_{0.05}$-$CP_3M_2T_2$**	**$SQV_{0.05}$-$CP_3M_2T_3$**
Ultrasonication	**1**	-19.98	1.41	-22.82	-32.57	-9.61	-11.92	-25.96	-23.27
	2	-18.36	9.59	-24.76	-21.17	-8.11	-6.34	-26.14	-18.26
	3	-16.34	-10.57	-28.51	-23.66	-11.12	-12.71	-28.03	-17.50
	4	-	-	-21.92	-22.39	-	-	-21.09	-20.06
	5	-	-	-23.56	-22.57	-	-	-24.00	-21.09
	6	-	-	-22.42	-22.34	-	-	-25.00	-19.68
	7	-	-	-23.21	-	-	-	-20.83	-
	8	-	-	-23.66	-	-	-	-28.80	-
	9	-	-	-22.72	-	-	-	-21.22	-
Hot HPH	**1**	-21.19	-13.88	-26.39	-18.42	-14.50	-10.64	-16.03	-13.50
	2	-19.48	-8.28	-23.17	-16.60	-15.32	-16.48	-15.00	-12.92
	3	-18.75	-12.79	-20.61	-17.46	-9.72	-5.88	-18.44	-13.78
	4	-	-	-22.73	-	-	-	-20.20	-
	5	-	-	-19.63	-	-	-	-15.28	-
	6	-	-	-21.46	-	-	-	-16.40	-
	7	-	-	-22.24	-	-	-	-23.80	-
	8	-	-	-21.28	-	-	-	-22.60	-
	9	-	-	-15.93	-	-	-	-20.42	-

able A.13 – Mean and standard deviation (SD) of DV10, DV50, Dv90 and "span" over 4 months of research to unloaded nanoparticles.

			Formulation	Day 0	Day 60	Day 120
Mean Dv10 ± SD [nm]	SLN	S	CP_5T_2	92.2 ± 6.9	82.5 ± 0.8	77.7 ± 8.9
			CP_5T_3	93.3 ± 8.3	80.1 ± 6.0	82.4 ± 0.7
		H	CP_5T_2	99.2 ± 4.7	82.8 ± 2.8	71.4 ± 11.0
			CP_5T_3	92.5 ± 10.7	79.8 ± 1.5	68.5 ± 4.2
	NLC	S	$CP_3M_2T_2$	100.7 ± 6.9	107.8 ± 12.0	89.1 ± 29.7
			$CP_3M_2T_3$	94.6 ± 6.7	86.7 ± 10.1	80.2 ± 10.5
		H	$CP_3M_2T_2$	103.7 ± 1.2	105.3 ± 0.6	90.3 ± 2.2
			$CP_3M_2T_3$	96.2 ± 3.6	99.1 ± 0.8	115.4 ± 19.1
Mean Dv50 ± SD [nm]	SLN	S	CP_5T_2	205.5 ± 12.8	171.3 ± 4.0	192.0 ± 11.1
			CP_5T_3	204.5 ± 27.2	210.7 ± 26.3	210.7 ± 24.2
		H	CP_5T_2	221.0 ± 11.6	179.0 ± 14.8	200.0 ± 14.0
			CP_5T_3	211.2 ± 35.2	165.7 ± 8.1	215.0 ± 21.2
	NLC	S	$CP_3M_2T_2$	230.8 ± 8.7	238.5 ± 26.2	222.5 ± 19.1
			$CP_3M_2T_3$	219.1 ± 23.8	284.3 ± 44.1	282.0 ± 1.4
		H	$CP_3M_2T_2$	242.3 ± 4.0	272.3 ± 9.3	291.7 ± 17.2
			$CP_3M_2T_3$	220.2 ± 6.5	251.3 ± 7.6	463.0 ± 123.2
Mean Dv90 ± SD [nm]	SLN	S	CP_5T_2	511.8 ± 74.8	566.3 ± 194.9	624.7 ± 221.5
			CP_5T_3	529.5 ± 163.5	1563.0 ± 947.6	1422.7 ± 847.9
		H	CP_5T_2	618.1 ± 62.4	954.5 ± 106.8	3267.0 ± 1074.2
			CP_5T_3	529.5 ± 115.6	3189.7 ± 1101.9	10075.0 ± 3010.6
	NLC	S	$CP_3M_2T_2$	1208.7 ± 468.9	5600.0 ± 1298.4	10376.7 ± 3644.3
			$CP_3M_2T_3$	1390.4 ± 698.9	9000.0 ± 859.8	12003.0 ± 6993.4
		H	$CP_3M_2T_2$	1503.3 ± 37.9	7053.3 ± 770.3	12320.0 ± 7024.2
			$CP_3M_2T_3$	955.3 ± 142.6	11100.0 ± 1053.6	18633.3 ± 4445.6
Mean Span ± SD	SLN	S	CP_5T_2	1.985 ± 0.238	2.805 ± 1.065	2.807 ± 1.025
			CP_5T_3	2.080 ± 0.488	6.720 ± 3.980	6.092 ± 3.561
		H	CP_5T_2	2.348 ± 0.228	4.870 ± 2.822	15.145 ± 10.552
			CP_5T_3	2.021 ± 0.208	17.943 ± 23.947	44.609 ± 29.891
	NLC	S	$CP_3M_2T_2$	4.334 ± 1.561	23.028 ± 11.345	34.218 ± 26.488
			$CP_3M_2T_3$	5.667 ± 2.723	31.352 ± 15.600	42.626 ± 20.951
		H	$CP_3M_2T_2$	5.743 ± 0.038	25.516 ± 10.657	41.111 ± 21.795
			$CP_3M_2T_3$	3.672 ± 0.794	43.744 ± 5.435	43.415 ± 19.362

Table A.14 – Mean and standard deviation (SD) of Dv10, Dv50, Dv90 and "span" over 3 months of research to SQV-loaded nanoparticles.

			Formulation	Day 0	Day 45	Day 90
Mean Dv10 ± SD [nm]	SLN	S	$SQV_{0.05}$-CP_5T_2	90.0 ± 5.9	85.5 ± 3.4	74.7 ± 10.0
			$SQV_{0.05}$-CP_5T_3	90.0 ± 10.9	71.4 ± 11.9	71.0 ± 11.5
		H	$SQV_{0.05}$-CP_5T_2	88.7 ± 30.2	93.2 ± 1.5	91.7 ± 3.9
			$SQV_{0.05}$-CP_5T_3	93.1 ± 1.3	92.1 ± 0.9	91.2 ± 3.9
	NLC	S	$SQV_{0.05}$- $CP_3M_2T_2$	89.9 ± 8.9	95.5 ± 3.4	93.1 ± 4.6
			$SQV_{0.05}$- $CP_3M_2T_3$	78.7 ± 9.6	91.0 ± 5.4	86.6 ± 9.2
		H	$SQV_{0.05}$- $CP_3M_2T_2$	82.1 ± 2.7	101.8 ± 10.4	97.8 ± 8.9
			$SQV_{0.05}$- $CP_3M_2T_3$	87.9 ± 1.1	166.3 ± 7.2	143.7 ± 15.3
Mean Dv50 ± SD [nm]	SLN	S	$SQV_{0.05}$-CP_5T_2	203.8 ± 15.0	188.8 ± 13.4	190.4 ± 9.5
			$SQV_{0.05}$-CP_5T_3	191.5 ± 24.8	166.0 ± 2.6	166.0 ± 3.6
		H	$SQV_{0.05}$-CP_5T_2	217.9 ± 8.6	200.0 ± 4.4	204.8 ± 4.4
			$SQV_{0.05}$-CP_5T_3	203.3 ± 2.5	196.3 ± 2.5	230.0 ± 35.5
	NLC	S	$SQV_{0.05}$- $CP_3M_2T_2$	211.3 ± 14.8	303.7 ± 10.3	311.0 ± 22.9
			$SQV_{0.05}$- $CP_3M_2T_3$	209.8 ± 6.2	340.0 ± 37.5	338.0 ± 48.1
		H	$SQV_{0.05}$- $CP_3M_2T_2$	210.9 ± 20.0	387.4 ± 45.2	426.8 ± 91.8
			$SQV_{0.05}$- $CP_3M_2T_3$	201.0 ± 6.1	1710.0 ± 233.9	1653.3 ± 703.2
Mean Dv90 ± SD [nm]	SLN	S	$SQV_{0.05}$-CP_5T_2	497.7 ± 68.8	519.8 ± 140.6	507.3 ± 130.6
			$SQV_{0.05}$-CP_5T_3	414.3 ± 67.1	396.7 ± 82.8	395.3 ± 69.0
		H	$SQV_{0.05}$-CP_5T_2	609.9 ± 112.4	522.4 ± 27.8	587.8 ± 122.7
			$SQV_{0.05}$-CP_5T_3	557.0 ± 14.7	565.7 ± 20.4	921.0 ± 308.3
	NLC	S	$SQV_{0.05}$- $CP_3M_2T_2$	1015.6 ± 405.8	8893.3 ± 831.9	15066.7 ± 1809.6
			$SQV_{0.05}$- $CP_3M_2T_3$	1562.5 327.8	12033.3 ± 1242.3	15733.3 ± 1715.6
		H	$SQV_{0.05}$- $CP_3M_2T_2$	2138.8 ± 189.2	12422 ± 7049.6	27133.3 ± 7351.9
			$SQV_{0.05}$- $CP_3M_2T_3$	1370.0 ± 138.9	8003.3 ± 1216.6	17533.3 ± 4650.1
Mean Span ± SD	SLN	S	$SQV_{0.05}$-CP_5T_2	2.184 ± 0.328	2.278 ± 0.597	2.297 ± 0.711
			$SQV_{0.05}$-CP_5T_3	1.685 ± 0.099	1.956 ± 0.557	1.951 ± 0.477
		H	$SQV_{0.05}$-CP_5T_2	2.351 ± 0.532	2.147 ± 0.108	2.407 ± 0.479
			$SQV_{0.05}$-CP_5T_3	2.280 ± 0.100	2.417 ± 0.119	3.509 ± 0.863
	NLC	S	$SQV_{0.05}$- $CP_3M_2T_2$	4.205 ± 1.469	29.034 ± 2.653	48.071 ± 4.404
			$SQV_{0.05}$- $CP_3M_2T_3$	7.054 ± 1.548	35.151 ± 3.079	46.706 ± 6.909
		H	$SQV_{0.05}$- $CP_3M_2T_2$	9.815 ± 0.808	32.599 ± 20.817	63.829 ± 15.667
			$SQV_{0.05}$- $CP_3M_2T_3$	6.362 ± 0.508	4.550 ± 0.068	10.941 ± 1.594

Table A.15 – Mean and standard deviation (SD) of Z-average, polydispersity index and zeta potential over 4 months of research to unloaded nanoparticles.

			Formulation	Day 0	Day 60	Day 120
Mean Z-average ± SD [nm]	SLN	S	CP_5T_2	197.7 ± 8.8	195.7 ± 9.9	192.7 ± 19.5
			CP_5T_3	200.1 ± 12.5	201.8 ± 17.2	203.2 ± 13.5
		H	CP_5T_2	185.6 ± 6.2	184.0 ± 7.3	193.1 ± 8.5
			CP_5T_3	167.1 ± 10.4	172.3 ± 6.2	187.1 ± 9.9
	NLC	S	$CP_3M_2T_2$	215.5 ± 12.0	216.2 ± 16.7	212.7 ± 33.9
			$CP_3M_2T_3$	210.5 ± 8.0	200.9 ± 14.9	215.1 ± 9.0
		H	$CP_3M_2T_2$	195.3 ± 4.7	189.2 ± 5.8	207.9 ± 8.2
			$CP_3M_2T_3$	183.8 ± 11.3	177.0 ± 7.3	203.9 ± 5.5
Mean PI ± SD	SLN	S	CP_5T_2	0.117 ± 0.044	0.124 ± 0.040	0.142 ± 0.052
			CP_5T_3	0.127 ± 0.060	0.169 ± 0.055	0.195 ± 0.049
		H	CP_5T_2	0.129 ± 0.058	0.174 ± 0.043	0.175 ± 0.029
			CP_5T_3	0.148 ± 0.039	0.164 ± 0.027	0.178 ± 0.018
	NLC	S	$CP_3M_2T_2$	0.094 ± 0.053	0.098 ± 0.043	0.131 ± 0.06
			$CP_3M_2T_3$	0.090 ± 0.047	0.093 ± 0.056	0.090 ± 0.036
		H	$CP_3M_2T_2$	0.154 ± 0.041	0.141 ± 0.054	0.160 ± 0.026
			$CP_3M_2T_3$	0.172 ± 0.030	0.147 ± 0.048	0.217 ± 0.024
Mean ZP ± SD [mV]	SLN	S	CP_5T_2	-32.61 ± 1.13	-24.98 ± 2.33	-26.52 ± 2.05
			CP_5T_3	-34.78 ± 4.17	-22.10 ± 11.18	-30.55 ± 3.11
		H	CP_5T_2	-33.60 ± 2.03	-29.33 ± 2.40	-30.26 ± 2.10
			CP_5T_3	-30.82 ± 3.62	-26.39 ± 2.78	-27.47 ± 5.92
	NLC	S	$CP_3M_2T_2$	-34.78 ± 2.83	-19.95 ± 1.89	-30.46 ± 2.78
			$CP_3M_2T_3$	-30.44 ± 6.28	-17.02 ± 9.02	-27.75 ± 3.09
		H	$CP_3M_2T_2$	-35.79 ± 5.00	-20.61 ± 3.17	-34.08 ± 7.14
			$CP_3M_2T_3$	-36.86 ± 7.44	-17.51 ± 3.35	-32.04 ± 5.01

Table A.16 – Mean and standard deviation (SD) of Z-average, polydispersity index and zeta potential over 3 months of research to SQV-loaded nanoparticles.

			Formulation	Day 0	Day 45	Day 90
Mean Z-average ± SD [nm]	SLN	S	$SQV_{0.05}$-CP_5T_2	197.3 ± 7.6	198.3 ± 8.7	195.6 ± 7.3
			$SQV_{0.05}$-CP_5T_3	195.3 ± 9.4	180.3 ± 5.7	184.5 ± 7.5
		H	$SQV_{0.05}$-CP_5T_2	216.8 ± 8.1	209.3 ± 8.8	218.9 ± 11.6
			$SQV_{0.05}$-CP_5T_3	203.2 ± 6.3	209.6 ± 6.6	219.0 ± 11.6
	NLC	S	$SQV_{0.05}$- $CP_3M_2T_2$	201.3 ± 17.0	194.1 ± 6.3	201.5 ± 10.8
			$SQV_{0.05}$- $CP_3M_2T_3$	198.3 ± 7.9	195.7 ± 4.8	189.0 ± 7.0
		H	$SQV_{0.05}$- $CP_3M_2T_2$	184.3 ± 5.8	180.2 ± 5.1	189.9 ± 12.9
			$SQV_{0.05}$- $CP_3M_2T_3$	159.4 ± 3.4	159.2 ± 6.1	171.5 ± 3.0
Mean PI ± SD [nm]	SLN	S	$SQV_{0.05}$-CP_5T_2	0.114 ± 0.051	0.128 ± 0.044	0.140 ± 0.029
			$SQV_{0.05}$-CP_5T_3	0.069 ± 0.056	0.074 ± 0.036	0.061 ± 0.033
		H	$SQV_{0.05}$-CP_5T_2	0.142 ± 0.036	0.181 ± 0.041	0.172 ± 0.038
			$SQV_{0.05}$-CP_5T_3	0.197 ± 0.017	0.231 ± 0.025	0.254 ± 0.014
	NLC	S	$SQV_{0.05}$- $CP_3M_2T_2$	0.083 ± 0.035	0.104 ± 0.045	0.104 ± 0.036
			$SQV_{0.05}$- $CP_3M_2T_3$	0.068 ± 0.056	0.076 ± 0.044	0.085 ± 0.046
		H	$SQV_{0.05}$- $CP_3M_2T_2$	0.134 ± 0.041	0.165 ± 0.039	0.158 ± 0.038
			$SQV_{0.05}$- $CP_3M_2T_3$	0.190 ± 0.039	0.196 ± 0.026	0.217 ± 0.023
Mean ZP ± SD [nm]	SLN	S	$SQV_{0.05}$-CP_5T_2	-24.05 ± 2.34	-23.85 ± 2.80	-31.14 ± 3.31
			$SQV_{0.05}$-CP_5T_3	-22.24 ± 6.16	-22.39 ± 2.73	-29.00 ± 2.28
		H	$SQV_{0.05}$-CP_5T_2	-20.87 ± 3.92	-21.96 ± 4.92	-25.99 ± 3.25
			$SQV_{0.05}$-CP_5T_3	-17.63 ± 1.52	-19.68 ± 1.72	-31.13 ± 3.45
	NLC	S	$SQV_{0.05}$- $CP_3M_2T_2$	-24.95 ± 3.10	-17.70 ± 2.90	-23.46 v 2.33
			$SQV_{0.05}$- $CP_3M_2T_3$	-19.80 ± 2.44	-16.78 ± 2.95	-23.24 ± 1.15
		H	$SQV_{0.05}$- $CP_3M_2T_2$	-18.18 ± 2.38	-15.60 ± 4.39	-24.83 ± 2.92
			$SQV_{0.05}$- $CP_3M_2T_3$	-13.39 ± 1.64	-18.42 ± 3.95	-26.9 ± 2.87

Table A.17 – Encapsulation efficiency (EE) values obtained in each lot produced on day 0. These values were used to calculate means and standard deviations of EE in the SQV-loaded lipid nanoparticles.

Lot number	Encapsulation Efficiency [%]	
	SQV- SLN	SQV-NLC
1	98.3	96.8
2	95.3	95.8
3	89.9	94.4
4	81.5	93.8
5	95.7	87.7
6	93.6	93.8

Table A.18 – Mean and standard deviation (SD) of encapsulation efficiency over 3 months of research to SQV-loaded nanoparticles.

Formulation	Mean Encapsulation Efficiency ± SD [%]			
	Day 0	Day 30	Day 60	Day 90
SQV-SLN	92.4 ± 6.0	81.8 ± 5.0	79.1 ± 8.1	71.9 ± 5.2
SQV-NLC	93.7 ± 3.2	87.4 ± 4.0	87.9 ± 9.6	80.2 ± 2.4

Table A.19 – Onset temperature and enthalpy values obtained in each lot produced, on day 0. These values were used to calculate means of onset temperature and enthalpy in the lipid nanoparticles.

Lot number	Onset temperature [°C]				Enthalpy [J/g]			
	SLN	SQV-SLN	NLC	SQV-NLC	SLN	SQV-SLN	NLC	SQV-NLC
1	49.9	49.4	45.4	45.2	-126.6	-138.7	-72.57	-67.12
2	49.9	50.2	44.7	45.1	-116.9	-91.82	-69.84	-63.08
3	49.8	50.1	45.2	45.4	-114.4	-103.3	-66.01	-67.60
4	49.8	50.6	44.8	45.1	-116.3	-89.59	-67.18	-62.27
5	-	50.1	45.0	-	-	-116.5	-68.55	-

Calibration curve A

RSS = 0.0251046

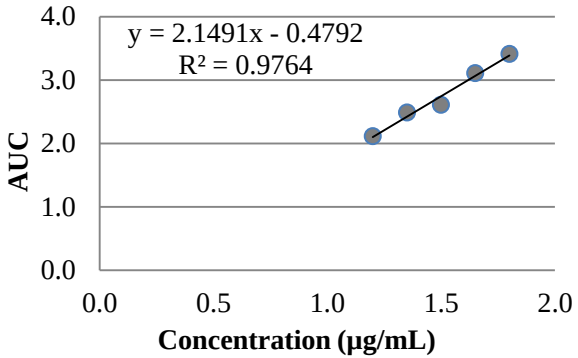

Figure A.1 - Graph of calibration curve

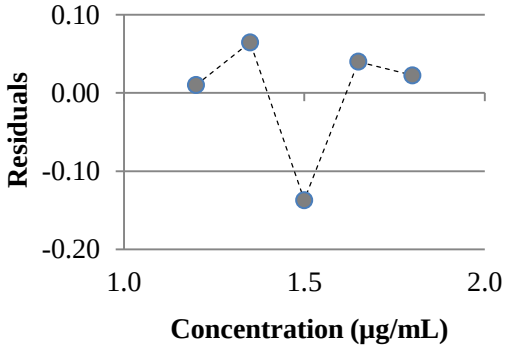

Figure A.2 - Graph of residuals.

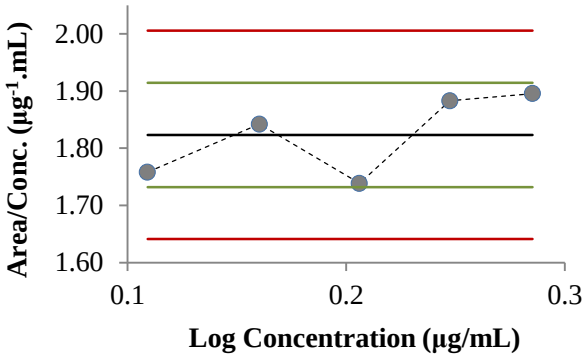

Figure A.3 - Graph of relative responses.

Calibration curve B

RSS = 0.0021625

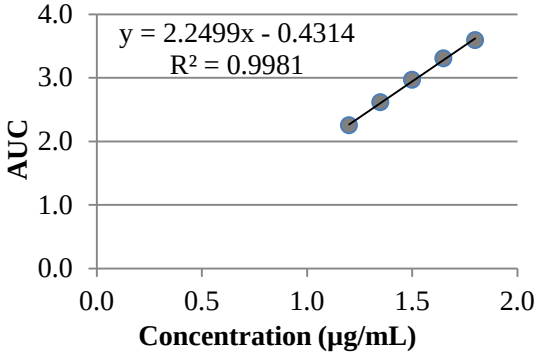

Figure A.4 - Graph of calibration curve.

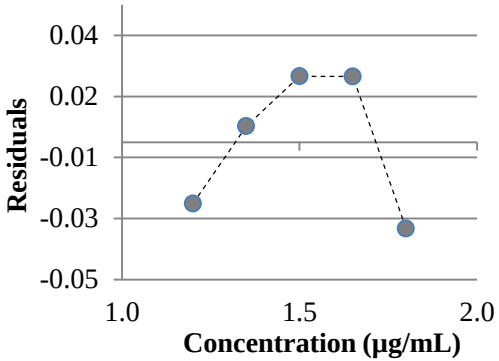

Figure A.5 - Graph of residuals.

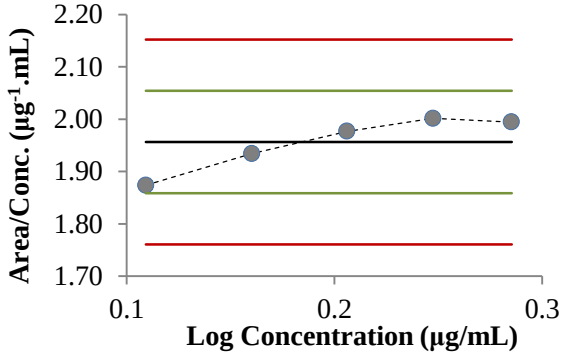

Figure A.6 - Graph of relative responses.

Calibration curve C

RSS = 0.0028046

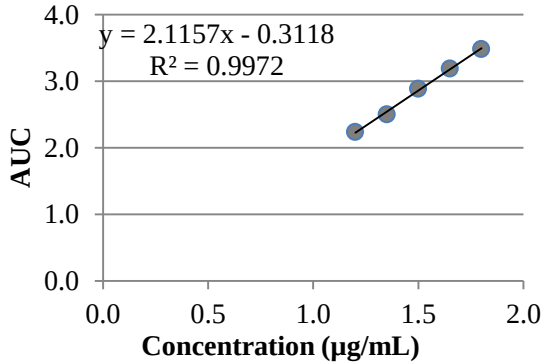

Figure A.7 - Graph of calibration curve.

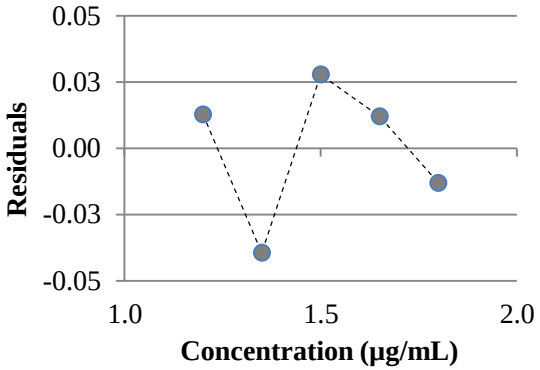

Figure A.8 - Graph of residuals.

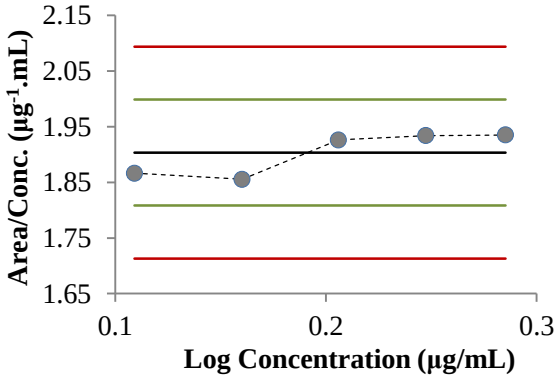

Figure A.9 - Graph of relative responses.

Calibration curve D

RSS = 0.0021093

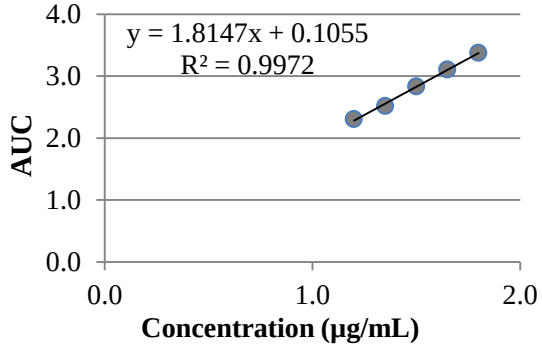

Figure A.10 - Graph of calibration curve.

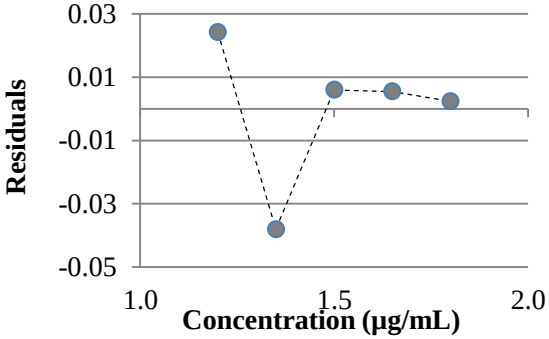

Figure A.11 - Graph of residuals.

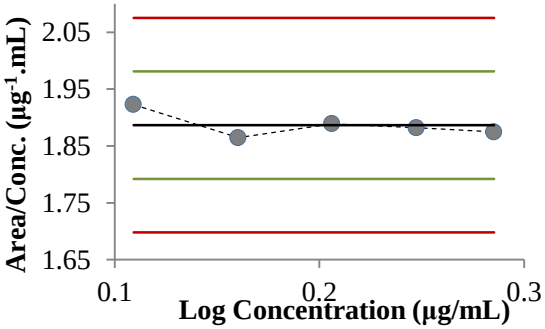

Figure A.12 - Graph of relative responses.

Calibration curve E

RSS = 0.0009692

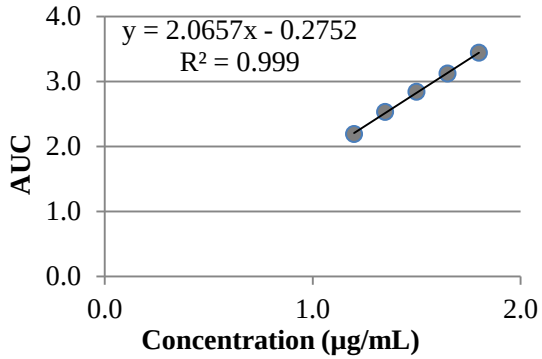

Figure A.13 - Graph of calibration curve.

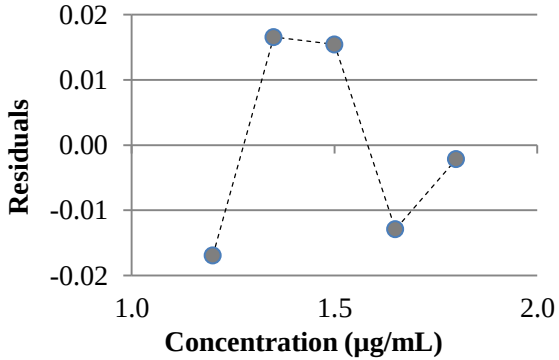

Figure A.14 - Graph of residuals.

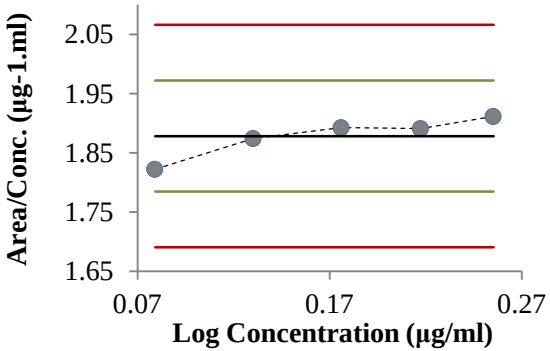

Figure A.15 - Graph of relative responses.

Calibration curves that resulted in the calibration curve shown in the results were: **B**, **C** and **E**.

Table A.20 - Mean and standard deviation (SD) of viability of different conditions (SQV, SLN, SQV-SLN, NLC, SQV-NLC) in the MTT assay.

Formulation	Viability ± SD [%]	
	2.5 µM	25 µM
SQV	98.1 ± 3.99	94.9 ± 9.34
SLN	80.9 ± 4.64	30.4 ± 1.86
SQV-SLN	78.1 ± 7.19	31.4 ± 2.34
NLC	95.8 ± 6.82	89.1 ±2.29
SQV-NLC	96.1 ± 4.37	91.5 ± 13.33
Triton x-100	6.7 ± 3.15	
DMSO	30.1 ± 1.41	

Table A.21 - Mean and standard deviation (SD) of cytotoxicity of different conditions (SQV, SLN, SQV-SLN, NLC, SQV-NLC) in the PI assay.

Formulation	Cytotoxicity ± SD [%]
Untreated cell	5.1 ± 1.77
SQV	7.3 ± 3.78
SLN	26.4 ± 3.04
SQV-SLN	25.7 ± 3.30
NLC	8.9 ± 1.74
SQV-NLC	10.0 ± 0.88
Triton	68.0 ± 6.97
DMSO	29.0 ± 9.14

B) Statistical analysis

Table B.1 – Statistical analysis of the Dv50 of the empty lipid nanoparticles with 5% lipid, in ultrasonication (□) and hot HPH (■).

Formulation		N	Subset for alpha = 0.05				
			1	2	3	4	5
Dv50 [nm]	CP_5T_3	13	204.5				
	CP_5T_2	14	205.5				
	CP_5T_3	13	211.2				
	$CP_3M_2T_3$	13	219.1				
	$CP_3M_2T_3$	12	220.2				
	CP_5T_2	7	221.0	221.0			
	$CP_3M_2T_2$	16	230.8	230.8	230.8		
	$CP_3M_2T_2$	3	242.3	242.3	242.3	242.3	
	$CP_3M_2T_1$	3		302.7	302.7	302.7	
	CP_5T_1	3			308.0	308.0	
	CP_5T_1	3				313.3	
	$CP_3M_2T_1$	3					458.3
	Sig.		**.923**	**.053**	**.087**	**.160**	**1.000**

Table B.2 – Statistical analysis of the Dv50 of the empty lipid nanoparticles with 10% lipid, in ultrasonication (□) and hot HPH (■).

Formulation		N	Subset for alpha = 0.05			
			1	2	3	4
Dv50 [nm]	$CP_7M_3T_3$	3	269.7			
	$CP_7M_3T_2$	3	280.0			
	$CP_{10}T_3$	3	281.7			
	$CP_{10}T_2$	3	297.0			
	$CP_{10}T_1$	3	324.0	324.0		
	$CP_7M_3T_1$	3		373.0		
	$CP_{10}T_3$	3		450.7		
	$CP_7M_3T_3$	3		460.7		
	$CP_{10}T_2$	3		477.3		
	$CP_{10}T_1$	3			661.0	
	$CP_7M_3T_2$	3			689.0	
	$CP_7M_3T_1$	3				1179.7
	Sig.		**.867**	**0.068**	**1.000**	**1.000**

Table B.3 – Statistical analysis of the Dv90 of the empty lipid nanoparticles with 5% lipid, in ultrasonication (□) and hot HPH (■).

Formulation		N	Subset for alpha = 0.05			
			1	2	3	4
Dv90 [nm]	CP_5T_2	13	511.8			
	CP_5T_3	13	529.5			
	CP_5T_3	13	529.5			
	CP_5T_2	7	618.1			
	CP_5T_1	3	718.3	718.3		
	$CP_3M_2T_3$	12	955.3	955.3	955.3	
	$CP_3M_2T_2$	16	1208.7	1208.7	1208.7	1208.7
	CP_5T_1	3	1223.3	1223.3	1223.3	1223.3
	$CP_3M_2T_3$	13		1390.4	1390.4	1390.4
	$CP_3M_2T_2$	3			1503.3	1503.3
	$CP_3M_2T_1$	3				1813.3
	$CP_3M_2T_1$	3				1896.7
	Sig.		**.062**	**.100**	**.340**	**.083**

Table B.4 – Statistical analysis of the Dv90 of the empty lipid nanoparticles with 10% lipid, in ultrasonication (□) and hot HPH (■).

Formulation		N	Subset for alpha = 0.05				
			1	2	3	4	5
Dv90 [nm]	$CP_{10}T_3$	3	726.7				
	$CP_7M_3T_3$	3		1045.7			
	$CP_{10}T_2$	3		1063.7			
	$CP_{10}T_1$	3		1176.7			
	$CP_{10}T_3$	3			1298.9		
	$CP_{10}T_2$	3			1373.3		
	$CP_{10}T_1$	3			1596.7		
	$CP_7M_3T_2$	3			1640.0		
	$CP_7M_3T_1$	3			1793.3		
	$CP_7M_3T_2$	3				2543.3	
	$CP_7M_3T_3$	3				2543.3	
	$CP_7M_3T_1$	3					3360.0
	Sig.		**1.000**	**.789**	**.093**	**1.000**	**1.000**

Table B.5 – Statistical analysis of the Dv50 between empty SLN (■) and NLC ( ) in the hot HPH.

Formulation		N	Subset for alpha = 0.05					
			1	2	3	4	5	6
Dv50 [nm] - Hot HPH	CP_5T_3	13	211.2					
	$CP_3M_2T_3$	12	220.2	220.2				
	CP_5T_2	7	221.0	221.0				
	$CP_3M_2T_2$	3	242.3	242.3	242.3			
	$CP_7M_3T_3$	3		269.7	269.7	269.7		
	$CP_7M_3T_2$	3			280.0	280.0	280.0	
	$CP_{10}T_3$	3			281.7	281.7	281.7	
	$CP_{10}T_2$	3				297.0	297.0	
	$CP_3M_2T_1$	3				302.7	302.7	
	CP_5T_1	3				308.0	308.0	
	$CP_{10}T_1$	3					324.0	324.0
	$CP_7M_3T_1$	3						373.0
	Sig.		**.709**	**.103**	**.369**	**.407**	**.218**	**.111**

Table B.6 – Statistical analysis of the Dv50 between empty SLN (■) and NLC ( ) in the ultrasonication.

Formulation		N	Subset for alpha = 0.05						
			1	2	3	4	5	6	7
Dv50 [nm] - Ultrasonication	CP_5T_3	13	204.5						
	CP_5T_2	14	205.5						
	$CP_3M_2T_3$	13	219.1	219.1					
	$CP_3M_2T_2$	16	230.8	230.8	230.8				
	CP_5T_1	3	313.3	313.3	313.3	313.3			
	$CP_{10}T_3$	3		450.7	450.7	450.7	450.7		
	$CP_3M_2T_1$	3			458.3	458.3	458.3	458.3	
	$CP_7M_3T_3$	3			460.7	460.7	460.7	460.7	
	$CP_{10}T_2$	3				477.3	477.3	477.3	
	$CP_{10}T_1$	3					661.0	661.0	
	$CP_7M_3T_2$	3						689.0	
	$CP_7M_3T_1$	3							1179.7
	Sig.		**.912**	**.055**	**.059**	**.439**	**.119**	**.057**	**1.000**

Table B.7 – Statistical analysis between Dv50 (■) and Z-average ( ) in empty lipid nanoparticles in the ultrasonication.

Formulation		N	Subset for alpha = 0.05	
			1	2
Size [nm] - Ultrasonication	**CP_5T_2**	3	197.8	
	CP_5T_3	6	199.5	
	CP_5T_3	13	204.5	204.5
	CP_5T_2	14	205.5	205.5
	$CP_3M_2T_3$	6	209.7	209.7
	$CP_3M_2T_2$	3	215.9	215.9
	$CP_3M_2T_3$	13	219.1	219.1
	$CP_3M_2T_2$	16		230.8
	Sig.		**.397**	**.156**

Table B.8 – Statistical analysis between Dv50 (■) and Z-average ( ) in empty lipid nanoparticles in the hot HPH.

Formulation		N	Subset for alpha = 0.05			
			1	2	3	4
Size [nm] - Hot HPH	**CP_5T_3**	9	169.8			
	$CP_3M_2T_3$	8	183.9	183.9		
	CP_5T_2	4	185.3	185.3		
	$CP_3M_2T_2$	4	195.5	195.5	195.5	
	CP_5T_3	13		211.2	211.2	211.2
	$CP_3M_2T_3$	12			220.2	220.2
	CP_5T_2	7			221.0	221.0
	$CP_3M_2T_2$	3				242.3
	Sig.		**.267**	**.201**	**.275**	**.095**

Table B.9 – Statistical analysis of the zeta potential of the empty lipid nanoparticles in ultrasonication ( ) and hot HPH (■).

Formulation		N	Subset for alpha = 0.05
			1
Zeta Potential [mV]	**$CP_3M_2T_3$**	9	-36.86
	$CP_3M_2T_2$	4	-35.16
	CP_5T_3	6	-34.78
	$CP_3M_2T_2$	3	-34.78
	CP_5T_2	4	-33.60
	CP_5T_2	3	-32.61
	CP_5T_3	9	-30.82
	$CP_3M_2T_3$	6	-30.44
	Sig.		**.479**

Table B.10 – Statistical analysis of the Dv10 of the empty lipid nanoparticles, in the ultrasonication ( ) and hot HPH ( ), over 4 months of evaluation.

Formulation		N	Subset for alpha = 0.05						
			1	2	3	4	5	6	7
Dv10 [nm]	**Day 120 - CP_5T_3**	3	68.5						
	Day 120 - CP_5T_2	3	71.4	71.4					
	Day 120 - CP_5T_2	3	77.7	77.7					
	Day 60 - CP_5T_3	3	79.8	79.8	79.8				
	Day 60 - CP_5T_3	3	80.1	80.1	80.1				
	Day 120 - $CP_3M_2T_3$	3	80.2	80.2	80.2				
	Day 120 - CP_5T_3	3	82.4	82.4	82.4	82.4			
	Day 60 - CP_5T_2	3	82.5	82.5	82.5	82.5	82.5		
	Day 60 - CP_5T_2	3	82.8	82.8	82.8	82.8	82.8		
	Day 60 - $CP_3M_2T_3$	3	86.7	86.7	86.7	86.7	86.7	86.7	
	Day 120 - $CP_3M_2T_2$	3	89.1	89.1	89.1	89.1	89.1	89.1	
	Day 120 - $CP_3M_2T_2$	3	90.3	90.3	90.3	90.3	90.3	90.3	
	Day 0 - CP_5T_2	14	92.7	92.7	92.7	92.7	92.7	92.7	92.7
	Day 0 - CP_5T_3	13	92.8	92.8	92.8	92.8	92.8	92.8	92.8
	Day 0 - CP_5T_3	13	93.3	93.3	93.3	93.3	93.3	93.3	93.3
	Day 0 - $CP_3M_2T_3$	13		94.6	94.6	94.6	94.6	94.6	94.6
	Day 0 - $CP_3M_2T_3$	12		96.1	96.1	96.1	96.1	96.1	96.1
	Day 60 - $CP_3M_2T_3$	3		99.1	99.1	99.1	99.1	99.1	99.1
	Day 0 - CP_5T_2	7		99.1	99.1	99.1	99.1	99.1	99.1
	Day 0 - $CP_3M_2T_2$	16			100.8	100.8	100.8	100.8	100.8
	Day 0 - $CP_3M_2T_2$	3				103.7	103.7	103.7	103.7
	Day 60 - $CP_3M_2T_2$	3					105.3	105.3	105.3
	Day 60 - $CP_3M_2T_2$	3						107.8	107.8
	Day 120 - $CP_3M_2T_3$	3							115.4
	Sig.		**.083**	**.101**	**.121**	**.107**	**.053**	**.117**	**.057**

Table B.11 – Statistical analysis of the Dv50 of the empty lipid nanoparticles, in the ultrasonication ( ) and hot HPH ( ), over 4 months of evaluation.

	Formulation	N	Subset for alpha = 0.05							
			1	2	3	4	5	6	7	8
Dv50 [nm]	**Day 60 - CP_5T_3**	3	165.7							
	Day 60 - CP_5T_2	3	171.3	171.3						
	Day 60 - CP_5T_2	3	179.0	179.0	179.0					
	Day 120 - CP_5T_2	3	192.0	192.0	192.0	192.0				
	Day 120 - CP_5T_2	3	200.0	200.0	200.0	200.0				
	Day 0 - CP_5T_3	13	204.5	204.5	204.5	204.5	204.5			
	Day 0 - CP_5T_2	14	205.5	205.5	205.5	205.5	205.5			
	Day 60 - CP_5T_3	3	210.7	210.7	210.7	210.7	210.7			
	Day 120 - CP_5T_3	3	210.7	210.7	210.7	210.7	210.7			
	Day 0 - CP_5T_3	13	211.2	211.2	211.2	211.2	211.2			
	Day 120 - CP_5T_3	3	215.0	215.0	215.0	215.0	215.0	215.0		
	Day 0 - $CP_3M_2T_3$	13	219.1	219.1	219.1	219.1	219.1	219.1		
	Day 0 - $CP_3M_2T_3$	12	220.2	220.2	220.2	220.2	220.2	220.2		
	Day 0 - CP_5T_2	7	221.0	221.0	221.0	221.0	221.0	221.0		
	Day 120 - $CP_3M_2T_2$	3	222.5	222.5	222.5	222.5	222.5	222.5	222.5	
	Day 0 - $CP_3M_2T_2$	16	230.8	230.8	230.8	230.8	230.8	230.8	230.8	
	Day 60 - $CP_3M_2T_2$	3		238.5	238.5	238.5	238.5	238.5	238.5	
	Day 0 - $CP_3M_2T_2$	3			242.3	242.3	242.3	242.3	242.3	
	Day 60 - $CP_3M_2T_3$	3				251.3	251.3	251.3	251.3	
	Day 60 - $CP_3M_2T_2$	3					272.3	272.3	272.3	
	Day 120 - $CP_3M_2T_3$	3						282.0	282.0	
	Day 60 - $CP_3M_2T_3$	3						284.3	284.3	
	Day 120 - $CP_3M_2T_2$	3							291.7	
	Day 120 - $CP_3M_2T_3$	3								463.0
	Sig.		**.107**	**.080**	**.137**	**.228**	**.072**	**.057**	**.059**	**1.000**

Table B.12 – Statistical analysis of the Dv90 of the empty lipid nanoparticles, in the ultrasonication ( ) and hot HPH ( ), over 4 months of evaluation.

	Formulation	N	Subset for alpha = 0.05							
			1	2	3	4	5	6	7	8
D90 [nm]	**Day 0 - CP_5T_2**	13	511.8							
	Day 0 - CP_5T_3	13	529.5							
	Day 0 - CP_5T_3	13	529.5							
	Day 60 - CP_5T_2	3	566.3							
	Day 0 - CP_5T_2	7	618.1							
	Day 120 - CP_5T_2	3	624.7							
	Day 60 -CP_5T_2	3	954.5							
	Day 0 - $CP_3M_2T_3$	12	955.3							
	Day 0 - $CP_3M_2T_2$	16	1208.7							
	Day 0 - $CP_3M_2T_3$	13	1390.4							
	Day 120 - CP_5T_3	3		1422.7						
	Day 0 - $CP_3M_2T_2$	3		1503.3						
	Day 60 -CP_5T_3	3		1563.0						
	Day 60 -CP_5T_3	3			3189.7					
	Day 120 - CP_5T_2	3			3267.0					
	Day 60 -$CP_3M_2T_2$	3				5600.0				
	Day 60 -$CP_3M_2T_2$	3				7053.3				
	Day 60 -$CP_3M_2T_3$	3					9000.0			
	Day 120 - CP_5T_3	3					10075.0	10075.0		
	Day 120 - $CP_3M_2T_2$	3					10376.7	10376.7		
	Day 60 -$CP_3M_2T_3$	3						11100.0	11100.0	
	Day 120 - $CP_3M_2T_3$	3							12003.0	
	Day 120 - $CP_3M_2T_2$	3							12320.0	
	Day 120 - $CP_3M_2T_3$	3								18633.0
	Sig.		**.890**	**1.000**	**1.000**	**.118**	**.184**	**.733**	**.395**	**1.000**

Table B.13 – Statistical analysis of the Z-average of the empty lipid nanoparticles, in the ultrasonication ( ) and hot HPH ( ), over 4 months of evaluation.

	Formulation	N	Subset for alpha = 0.05	
			1	2
Z-average [nm]	**Day 0 - CP_5T_3**	9	169.8	
	Day 60 - CP_5T_2	3	172.0	172.0
	Day 60 - CP_5T_3	3	172.3	172.3
	Day 60 - $CP_3M_2T_3$	3	177.0	177.0
	Day 0 - $CP_3M_2T_3$	8	183.9	183.9
	Day 60 - CP_5T_2	3	184.0	184.0
	Day 60 - CP_5T_3	3	184.6	184.6
	Day 0 - CP_5T_2	4	185.3	185.3
	Day 120 - CP_5T_3	3	187.1	187.1
	Day 60 - $CP_3M_2T_2$	3	189.2	189.2
	Day 120 - CP_5T_2	3	192.7	192.7
	Day 120 - CP_5T_2	3	193.1	193.1
	Day 0 - $CP_3M_2T_2$	4	195.5	195.5
	Day 0 - CP_5T_2	3	197.8	197.8
	Day 0 - CP_5T_3	6	199.5	199.5
	Day 60 - $CP_3M_2T_3$	3	200.9	200.9
	Day 120 - CP_5T_3	3	203.2	203.2
	Day 120 - $CP_3M_2T_3$	3	203.9	203.9
	Day 120 - $CP_3M_2T_2$	3	207.9	207.9
	Day 0 - $CP_3M_2T_3$	6	209.7	209.7
	Day 120 - $CP_3M_2T_2$	3	212.7	212.7
	Day 120 - $CP_3M_2T_3$	3		215.1
	Day 0 - $CP_3M_2T_2$	3		215.9
	Day 60 - $CP_3M_2T_2$	3		216.2
	Sig.		**.075**	**.054**

Table B.14 – Statistical analysis of the Zeta Potential of the empty lipid nanoparticles, in the ultrasonication ( ) and hot HPH ( ), over 4 months of evaluation.

	Formulation	N	Subset for alpha = 0.05						
			1	2	3	4	5	6	7
Zeta Potential [mV]	**Day 0 - $CP_3M_2T_3$**	9	-36.86						
	Day 0 - $CP_3M_2T_2$	4	-35.16	-35.16					
	Day 0 - CP_5T_3	6	-34.78	-34.78					
	Day 0 - $CP_3M_2T_2$	3	-34.78	-34.78					
	Day 60 - $CP_3M_2T_2$	3	-34.06	-34.06	-34.06				
	Day 0 - CP_5T_2	4	-33.60	-33.60	-33.60				
	Day 0 - CP_5T_2	3	-32.61	-32.61	-32.61	-32.61			
	Day 60 - $CP_3M_2T_3$	6	-32.00	-32.00	-32.00	-32.00			
	Day 0 - CP_5T_3	9	-30.82	-30.82	-30.82	-30.82			
	Day 60 - CP_5T_3	6	-30.53	-30.53	-30.53	-30.53			
	Day 0 - $CP_3M_2T_3$	6	-30.44	-30.44	-30.44	-30.44			
	Day 60 - $CP_3M_2T_2$	3	-30.41	-30.41	-30.41	-30.41			
	Day 60 - CP_5T_2	3	-30.22	-30.22	-30.22	-30.22			
	Day 120 - CP_5T_2	3	-29.29	-29.29	-29.29	-29.29	-29.29		
	Day 60 - $CP_3M_2T_3$	6		-27.78	-27.78	-27.78	-27.78	-27.78	
	Day 60 - CP_5T_3	6		-27.39	-27.39	-27.39	-27.39	-27.39	
	Day 60 - CP_5T_2	3			-26.61	-26.61	-26.61	-26.61	
	Day 120 - CP_5T_3	3			-26.38	-26.38	-26.38	-26.38	
	Day 120 - CP_5T_2	3				-24.89	-24.89	-24.89	-24.89
	Day 120 - CP_5T_3	3					-22.06	-22.06	-22.06
	Day 120 - $CP_3M_2T_2$	3						-20.57	-20.57
	Day 120 - $CP_3M_2T_2$	3						-20.06	-20.06
	Day 120 - $CP_3M_2T_3$	3							-17.56
	Day 120 - $CP_3M_2T_3$	3							-17.06
	Sig.		**.100**	**.077**	**.088**	**.083**	**.154**	**.083**	**.071**

Table B.15 – Statistical analysis of the Dv10 between unloaded and loaded nanoparticles in ultrasonication (□) and hot HPH (■).

	Formulation	N	Subset for alpha = 0.05	
			1	2
Dv10 [nm]	$SQV_{0.05}$- $CP_3M_2T_3$	5	78.7	
	$SQV_{0.05}$- $CP_3M_2T_2$	8	82.1	82.1
	$SQV_{0.05}$- $CP_3M_2T_3$	3	87.9	87.9
	$SQV_{0.05}$-CP_5T_2	9	88.7	88.7
	$SQV_{0.05}$- $CP_3M_2T_2$	15	89.9	89.9
	$SQV_{0.05}$-CP_5T_3	6	90.0	90.0
	$SQV_{0.05}$-CP_5T_2	23	90.9	90.9
	CP_5T_2	14	92.7	92.7
	CP_5T_3	13	92.8	92.8
	$SQV_{0.05}$-CP_5T_3	3	93.1	93.1
	CP_5T_3	13	93.3	93.3
	$CP_3M_2T_3$	13	94.6	94.6
	$CP_3M_2T_3$	12	96.1	96.1
	CP_5T_2	7		99.1
	$CP_3M_2T_2$	16		100.8
	$CP_3M_2T_2$	3		103.7
	Sig.		**.094**	**.113**

Table B.16 – Statistical analysis of the Dv50 between unloaded and loaded nanoparticles in ultrasonication (□) and hot HPH (■).

	Formulation	N	Subset for alpha = 0.05		
			1	2	3
Dv50 [nm]	$SQV_{0.05}$-CP_5T_3	6	191.5		
	$SQV_{0.05}$- $CP_3M_2T_3$	3	201.0	201.0	
	$SQV_{0.05}$-CP_5T_3	3	203.3	203.3	
	$SQV_{0.05}$-CP_5T_2	23	203.8	203.8	
	CP_5T_3	13	204.5	204.5	
	CP_5T_2	14	205.5	205.5	
	$SQV_{0.05}$- $CP_3M_2T_3$	5	209.8	209.8	209.8
	$SQV_{0.05}$- $CP_3M_2T_2$	8	210.9	210.9	210.9
	CP_5T_3	13	211.2	211.2	211.2
	$SQV_{0.05}$- $CP_3M_2T_2$	15	211.3	211.3	211.3
	$SQV_{0.05}$-CP_5T_2	9	217.9	217.9	217.9
	$CP_3M_2T_3$	13	219.1	219.1	219.1
	$CP_3M_2T_3$	12	220.2	220.2	220.2
	CP_5T_2	7	221.0	221.0	221.0
	$CP_3M_2T_2$	16		230.8	230.8
	$CP_3M_2T_2$	3			242.3
	Sig.		**.186**	**.173**	**.085**

Table B.17 – Statistical analysis of the Dv90 between unloaded and loaded nanoparticles in ultrasonication ( ) and hot HPH ( ).

	Formulation	N	Subset for alpha = 0.05
			1
Dv90 [nm]	**$SQV_{0.05}$-CP_5T_3**	6	414.3
	$SQV_{0.05}$-CP_5T_2	14	497.7
	CP_5T_2	13	511.8
	CP_5T_3	13	529.5
	CP_5T_3	13	529.5
	$SQV_{0.05}$-CP_5T_3	3	557.0
	$SQV_{0.05}$-CP_5T_2	9	609.9
	CP_5T_2	7	618.1
	$CP_3M_2T_3$	12	955.3
	$CP_3M_2T_2$	16	1208.7
	$SQV_{0.05}$- $CP_3M_2T_3$	3	1370.0
	$CP_3M_2T_3$	13	1390.4
	$CP_3M_2T_2$	3	1503.3
	$SQV_{0.05}$- $CP_3M_2T_3$	4	1562.5
	$SQV_{0.05}$- $CP_3M_2T_2$	8	2138.8
	$SQV_{0.05}$- $CP_3M_2T_2$	15	2308.0
	Sig.		**.228**

Table B.18 – Statistical analysis between Dv50 and Z-average in lipid nanoparticles with 0.05% drug in the ultrasonication ( ) and hot HPH ( ).

	Formulation	N	Subset for alpha = 0.05		
			1	2	3
Size [nm]	**DLS - $SQV_{0.05}$- $CP_3M_2T_3$**	3	159.4		
	DLS - $SQV_{0.05}$- $CP_3M_2T_2$	9	184.7		
	LD - $SQV_{0.05}$-CP_5T_3	6	191.5	191.5	
	DLS - $SQV_{0.05}$-CP_5T_3	6	195.7	195.7	195.7
	DLS - $SQV_{0.05}$-CP_5T_2	9	197.3	197.3	197.3
	DLS - $SQV_{0.05}$- $CP_3M_2T_3$	6	198.3	198.3	198.3
	LD - $SQV_{0.05}$- $CP_3M_2T_3$	3	201.0	201.0	201.0
	DLS - $SQV_{0.05}$- $CP_3M_2T_2$	9	201.2	201.2	201.2
	DLS - $SQV_{0.05}$-CP_5T_3	3	202.9	202.9	202.9
	LD - $SQV_{0.05}$-CP_5T_3	3	203.3	203.3	203.3
	LD - $SQV_{0.05}$-CP_5T_2	23	203.8	203.8	203.8
	LD - $SQV_{0.05}$- $CP_3M_2T_2$	7	206.6	206.6	206.6
	LD - $SQV_{0.05}$- $CP_3M_2T_3$	5	209.8	209.8	209.8
	LD - $SQV_{0.05}$- $CP_3M_2T_2$	15		211.3	211.3
	LD - $SQV_{0.05}$-CP_5T_2	9			217.9
	DLS - $SQV_{0.05}$-CP_5T_2	9			219.3
	Sig.		**.051**	**.302**	**.090**

Table B.19 – Statistical analysis of the polydispersity index between unloaded and loaded nanoparticles in the ultrasonication (□) and hot HPH (■).

Formulation		N	Subset for alpha = 0.05						
			1	2	3	4	5	6	7
Polydispersity Index	**$SQV_{0.05}$- $CP_3M_2T_3$**	6	.068						
	$SQV_{0.05}$-CP_5T_3	6	.071	.071					
	$SQV_{0.05}$- $CP_3M_2T_2$	9	.083	.083					
	$CP_3M_2T_3$	6	.092	.092	.092				
	$CP_3M_2T_2$	3	.096	.096	.096	.096			
	$SQV_{0.1}$-CP_5T_2	3	.110	.110	.110	.110	.110		
	$SQV_{0.05}$-CP_5T_2	9	.117	.117	.117	.117	.117	.117	
	CP_5T_2	3	.117	.117	.117	.117	.117	.117	
	CP_5T_2	4	.128	.128	.128	.128	.128	.128	.128
	$SQV_{0.05}$- $CP_3M_2T_2$	9	.134	.134	.134	.134	.134	.134	.134
	$SQV_{0.1}$- $CP_3M_2T_2$	3	.135	.135	.135	.135	.135	.135	.135
	CP_5T_3	6	.135	.135	.135	.135	.135	.135	.135
	$SQV_{0.1}$-CP_5T_2	3	.137	.137	.137	.137	.137	.137	.137
	$SQV_{0.05}$-CP_5T_2	9	.141	.141	.141	.141	.141	.141	.141
	$SQV_{0.1}$- $CP_3M_2T_2$	3	.142	.142	.142	.142	.142	.142	.142
	CP_5T_3	9		.153	.153	.153	.153	.153	.153
	$CP_3M_2T_2$	4		.154	.154	.154	.154	.154	.154
	$SQV_{0.1}$- $CP_3M_2T_3$	3			.173	.173	.173	.173	.173
	$CP_3M_2T_3$	8				.177	.177	.177	.177
	$SQV_{0.05}$- $CP_3M_2T_3$	3					.190	.190	.190
	$SQV_{0.05}$-CP_5T_3	3						.197	.197
	$SQV_{0.1}$- $CP_3M_2T_3$	3						.198	.198
	$SQV_{0.1}$-CP_5T_3	3							.206
	$SQV_{0.1}$-CP_5T_3	3							.206
	Sig.		**.185**	**.056**	**.072**	**.074**	**.090**	**.072**	**.107**

Table B.20 – Statistical analysis of the zeta potential between unloaded and loaded nanoparticles in the ultrasonication ( ) and hot HPH ( ).

	Formulation	N	Subset for alpha = 0.05									
			1	2	3	4	5	6	7	8	9	10
Zeta Potential [mV]	**$CP_3M_2T_3$**	9	-36.86									
	$CP_3M_2T_2$	4	-35.16									
	CP_5T_3	6	-34.78	-34.78								
	$CP_3M_2T_2$	3	-34.78	-34.78								
	CP_5T_2	4	-33.60	-33.60	-33.60							
	CP_5T_2	3	-32.61	-32.61	-32.61							
	CP_5T_3	9	-30.82	-30.82	-30.82	-30.82						
	$CP_3M_2T_3$	6	-30.44	-30.44	-30.44	-30.44						
	$SQV_{0.05}$- $CP_3M_2T_2$	9		-24.56	-24.56	-24.56	-24.56					
	$SQV_{0.05}$-CP_5T_3	6			-24.12	-24.12	-24.12					
	$SQV_{0.05}$-CP_5T_2	9			-23.73	-23.73	-23.73	-23.73				
	$SQV_{0.05}$-CP_5T_2	9				-21.49	-21.49	-21.49	-21.49			
	$SQV_{0.05}$- $CP_3M_2T_3$	6					-19.98	-19.98	-19.98	-19.98		
	$SQV_{0.1}$-CP_5T_2	3					-19.81	-19.81	-19.81	-19.81	-19.81	
	$SQV_{0.05}$- $CP_3M_2T_2$	9					-18.69	-18.69	-18.69	-18.69	-18.69	
	$SQV_{0.1}$-CP_5T_2	3					-18.23	-18.23	-18.23	-18.23	-18.23	
	$SQV_{0.05}$-CP_5T_3	3					-17.49	-17.49	-17.49	-17.49	-17.49	
	$SQV_{0.05}$- $CP_3M_2T_3$	3						-13.40	-13.40	-13.40	-13.40	
	$SQV_{0.1}$- $CP_3M_2T_2$	3							-13.18	-13.18	-13.18	
	$SQV_{0.1}$-CP_5T_3	3							-11.65	-11.65	-11.65	
	$SQV_{0.1}$- $CP_3M_2T_3$	3								-11.00	-11.00	
	$SQV_{0.1}$- $CP_3M_2T_3$	3								-10.32	-10.32	
	$SQV_{0.1}$- $CP_3M_2T_2$	3									-9.61	-9.61
	$SQV_{0.1}$-CP_5T_3	3										0.14
	Sig.		**.791**	**.057**	**.082**	**.136**	**.630**	**.051**	**.084**	**.101**	**.059**	**.091**

Table B.21 – Statistical analysisof the Dv10 of the loaded lipid nanoparticles in the ultrasonication ( ) and hot HPH ( ), over the 3 month evaluation.

Formulation		N	Subset for alpha = 0.05	
			1	2
Dv10 [nm]	**Day 90 - $SQV_{0.05}$-CP_5T_3**	3	71.0	
	Day 45 - $SQV_{0.05}$-CP_5T_3	3	71.3	
	Day 0 - $SQV_{0.05}$- $CP_3M_2T_3$	5	78.7	
	Day 90 - $SQV_{0.05}$-CP_5T_2	6	81.5	
	Day 0 - $SQV_{0.05}$- $CP_3M_2T_2$	8	82.1	
	Day 90 - $SQV_{0.05}$- $CP_3M_2T_3$	3	86.7	
	Day 0 - $SQV_{0.05}$- $CP_3M_2T_3$	3	87.9	
	Day 45 - $SQV_{0.05}$-CP_5T_2	6	88.7	
	Day 0 - $SQV_{0.05}$-CP_5T_2	9	88.7	
	Day 0 - $SQV_{0.05}$- $CP_3M_2T_2$	15	89.9	
	Day 0 - $SQV_{0.05}$-CP_5T_3	6	90.0	
	Day 0 - $SQV_{0.05}$-CP_5T_2	23	90.9	
	Day 45 - $SQV_{0.05}$- $CP_3M_2T_3$	3	91.0	
	Day 90 - $SQV_{0.05}$-CP_5T_3	3	91.3	
	Day 90 - $SQV_{0.05}$-CP_5T_2	6	91.7	
	Day 45 - $SQV_{0.05}$-CP_5T_3	3	92.0	
	Day 45 - $SQV_{0.05}$-CP_5T_2	5	93.0	
	Day 0 - $SQV_{0.05}$-CP_5T_3	3	93.1	
	Day 90 - $SQV_{0.05}$- $CP_3M_2T_2$	6	93.2	
	Day 45 - $SQV_{0.05}$- $CP_3M_2T_2$	3	94.0	
	Day 45 - $SQV_{0.05}$- $CP_3M_2T_2$	6	95.7	
	Day 90 - $SQV_{0.05}$- $CP_3M_2T_2$	6	97.8	
	Day 90 - $SQV_{0.05}$- $CP_3M_2T_3$	3		143.7
	Day 45 - $SQV_{0.05}$- $CP_3M_2T_3$	3		166.3
	Sig.		**.083**	**.313**

Table B.22 – Statistical analysis between **Dv50** and **Z-average** in loaded nanoparticles, in the ultrasonication (□) and hot HPH (■), over the 3 month evaluation.

	Formulation	N	Subset for alpha = 0.05							
			1	2	3	4	5	6	7	8
Size [nm]	**Day 45 - $SQV_{0.05}$- $CP_3M_2T_3$**	3	159.2							
	Day 0 - $SQV_{0.05}$- $CP_3M_2T_3$	3	159.4							
	Day 45 - $SQV_{0.05}$-CP_5T_3	3	166.0							
	Day 90 - $SQV_{0.05}$-CP_5T_3	3	166.0							
	Day 90 - $SQV_{0.05}$- $CP_3M_2T_3$	3	171.5							
	Day 45 - $SQV_{0.05}$- $CP_3M_2T_2$	6	180.2							
	Day 45 - $SQV_{0.05}$-CP_5T_3	3	180.3							
	Day 90 - $SQV_{0.05}$-CP_5T_3	3	184.5	184.5						
	Day 0 - $SQV_{0.05}$- $CP_3M_2T_2$	6	184.7	184.7						
	Day 45 - $SQV_{0.05}$-CP_5T_2	6	188.8	188.8						
	Day 90 - $SQV_{0.05}$- $CP_3M_2T_3$	3	189.0	189.0						
	Day 90 - $SQV_{0.05}$- $CP_3M_2T_2$	6	189.9	189.9						
	Day 90 - $SQV_{0.05}$-CP_5T_2	6	190.4	190.4						
	Day 0 - $SQV_{0.05}$-CP_5T_3	3	191.5	191.5						
	Day 45 - $SQV_{0.05}$- $CP_3M_2T_2$	6	194.1	194.1						
	Day 90 - $SQV_{0.05}$-CP_5T_2	6	195.6	195.6						
	Day 45 - $SQV_{0.05}$- $CP_3M_2T_3$	3	195.7	195.7						
	Day 0 - $SQV_{0.05}$-CP_5T_3	3	195.7	195.7						
	Day 45 - $SQV_{0.05}$-CP_5T_3	3	196.3	196.3						
	Day 0 - $SQV_{0.05}$-CP_5T_2	6	197.3	197.3						
	Day 0 - $SQV_{0.05}$- $CP_3M_2T_3$	3	198.3	198.3						
	Day 45 - $SQV_{0.05}$-CP_5T_2	6	198.3	198.3						
	Day 45 - $SQV_{0.05}$-CP_5T_2	6	200.0	200.0						
	Day 0 - $SQV_{0.05}$- $CP_3M_2T_3$	3	201.0	201.0						
	Day 0 - $SQV_{0.05}$- $CP_3M_2T_2$	6	201.2	201.2						
	Day 90 - $SQV_{0.05}$- $CP_3M_2T_2$	6	201.5	201.5						
	Day 0 - $SQV_{0.05}$-CP_5T_3	3	202.9	202.9						
	Day 0 - $SQV_{0.05}$-CP_5T_3	3	203.3	203.3						
	Day 0 - $SQV_{0.05}$-CP_5T_2	6	203.8	203.8						
	Day 90 - $SQV_{0.05}$-CP_5T_2	6	204.8	204.8						
	Day 45 - $SQV_{0.05}$-CP_5T_2	6	209.3	209.3						
	Day 45 - $SQV_{0.05}$-CP_5T_3	3	209.6	209.6						
	Day 0 - $SQV_{0.05}$- $CP_3M_2T_3$	3	209.8	209.8						
	Day 0 - $SQV_{0.05}$- $CP_3M_2T_2$	6	210.9	210.9						
	Day 0 - $SQV_{0.05}$- $CP_3M_2T_2$	6	211.3	211.3						
	Day 0 - $SQV_{0.05}$-CP_5T_2	6	217.9	217.9	217.9					
	Day 90 - $SQV_{0.05}$-CP_5T_2	6	218.9	218.9	218.9	218.9				
	Day 90 - $SQV_{0.05}$-CP_5T_3	3	219.0	219.0	219.0	219.0				
	Day 0 - $SQV_{0.05}$-CP_5T_2	6	219.3	219.3	219.3	219.3				
	Day 90 - $SQV_{0.05}$-CP_5T_3	3	230.0	230.0	230.0	230.0	230.0			
	Day 45 - $SQV_{0.05}$- $CP_3M_2T_2$	6			303.7	303.7	303.7	303.7		
	Day 90 - $SQV_{0.05}$- $CP_3M_2T_2$	6			311.0	311.0	311.0	311.0	311.0	
	Day 90 - $SQV_{0.05}$- $CP_3M_2T_3$	3				338.0	338.0	338.0	338.0	
	Day 45 - $SQV_{0.05}$- $CP_3M_2T_3$	3					340.0	340.0	340.0	
	Day 45 - $SQV_{0.05}$- $CP_3M_2T_2$	6						387.4	387.4	
	Day 90 - $SQV_{0.05}$- $CP_3M_2T_2$	6							426.8	
	Day 90 - $SQV_{0.05}$- $CP_3M_2T_3$	3								1653.3
	Day 45 - $SQV_{0.05}$- $CP_3M_2T_3$	3								1710.0
	Sig.		**.971**	**.058**	**.056**	**.052**	**.149**	**.783**	**.083**	**1.000**

Table B.23 – Statistical analysis of the Dv90 of the loaded lipid nanoparticles, in the ultrasonication ( ) and hot HPH ( ), over the 3 month evaluation.

	Formulation	N	Subset for alpha = 0.05					
			1	2	3	4	5	6
Dv90 [nm]	**Day 90 - $SQV_{0.05}$-CP_5T_3**	3	395.3					
	Day 45 - $SQV_{0.05}$-CP_5T_3	3	396.7					
	Day 0 - $SQV_{0.05}$-CP_5T_3	6	414.3					
	Day 0 - $SQV_{0.05}$-CP_5T_2	14	497.7					
	Day 90 - $SQV_{0.05}$-CP_5T_2	3	507.3					
	Day 45 - $SQV_{0.05}$-CP_5T_2	5	519.8					
	Day 45 - $SQV_{0.05}$-CP_5T_2	5	522.4					
	Day 0 - $SQV_{0.05}$-CP_5T_3	3	557.0					
	Day 45 - $SQV_{0.05}$-CP_5T_3	3	565.7					
	Day 90 - $SQV_{0.05}$-CP_5T_2	6	587.8					
	Day 0 - $SQV_{0.05}$-CP_5T_2	9	609.9					
	Day 90 - $SQV_{0.05}$-CP_5T_3	3		921.0				
	Day 0 - $SQV_{0.05}$- $CP_3M_2T_3$	3		1370.0				
	Day 0 - $SQV_{0.05}$- $CP_3M_2T_3$	4		1562.5				
	Day 0 - $SQV_{0.05}$- $CP_3M_2T_2$	8		2138.8				
	Day 0 - $SQV_{0.05}$- $CP_3M_2T_2$	15		2308.0				
	Day 45 - $SQV_{0.05}$- $CP_3M_2T_3$	3			8003.3			
	Day 45 - $SQV_{0.05}$- $CP_3M_2T_2$	6			8893.3			
	Day 45 - $SQV_{0.05}$- $CP_3M_2T_3$	3			12033.3	12033.3	12033.3	
	Day 45 - $SQV_{0.05}$- $CP_3M_2T_2$	5			12422.0	12422.0	12422.0	
	Day 90 - $SQV_{0.05}$- $CP_3M_2T_2$	6				15066.7	15066.7	
	Day 90 - $SQV_{0.05}$- $CP_3M_2T_3$	3					15733.3	
	Day 90 - $SQV_{0.05}$- $CP_3M_2T_3$	3					17533.3	
	Day 90 - $SQV_{0.05}$- $CP_3M_2T_2$	6						27133.3
	Sig.		**1.000**	**.169**	**.732**	**.435**	**.309**	**1.000**

Table B.24 – Statistical analysis of the Zeta Potential of the loaded lipid nanoparticles, in the ultrasonication ( ) and hot HPH ( ), over the 3 month evaluation.

	Formulation	N	Subset for alpha = 0.05												
			1	2	3	4	5	6	7	8	9	10	11	12	13
Zeta Potential [mV]	**Day 90 - $SQV_{0.05}$-CP_5T_2**	6	-31.14												
	Day 90 - $SQV_{0.05}$-CP_5T_3	3	-31.13												
	Day 90 - $SQV_{0.05}$-CP_5T_3	3	-29.00	-29.00											
	Day 90 - $SQV_{0.05}$- $CP_3M_2T_3$	3	-26.90	-26.90	-26.90										
	Day 90 - $SQV_{0.05}$-CP_5T_2	6		-25.99	-25.99	-25.99									
	Day 90 - $SQV_{0.05}$- $CP_3M_2T_2$	6		-24.83	-24.83	-24.83	-24.83								
	Day 0 - $SQV_{0.05}$- $CP_3M_2T_2$	6		-24.56	-24.56	-24.56	-24.56	-24.56							
	Day 0 - $SQV_{0.05}$-CP_5T_3	3		-24.12	-24.12	-24.12	-24.12	-24.12							
	Day 45 - $SQV_{0.05}$-CP_5T_2	6			-23.85	-23.85	-23.85	-23.85							
	Day 0 - $SQV_{0.05}$-CP_5T_2	6			-23.73	-23.73	-23.73	-23.73							
	Day 90 - $SQV_{0.05}$- $CP_3M_2T_2$	6			-23.46	-23.46	-23.46	-23.46	-23.46						
	Day 90 - $SQV_{0.05}$- $CP_3M_2T_3$	3			-23.24	-23.24	-23.24	-23.24	-23.24	-23.24					
	Day 45 - $SQV_{0.05}$-CP_5T_3	3			-22.39	-22.39	-22.39	-22.39	-22.39	-22.39	-22.39				
	Day 45 - $SQV_{0.05}$-CP_5T_2	6			-21.96	-21.96	-21.96	-21.96	-21.96	-21.96	-21.96	-21.96			
	Day 0 - $SQV_{0.05}$-CP_5T_2	6				-21.49	-21.49	-21.49	-21.49	-21.49	-21.49	-21.49	-21.49		
	Day 0 - $SQV_{0.05}$- $CP_3M_2T_3$	3					-19.98	-19.98	-19.98	-19.98	-19.98	-19.98	-19.98	-19.98	
	Day 45 - $SQV_{0.05}$-CP_5T_3	3						-19.68	-19.68	-19.68	-19.68	-19.68	-19.68	-19.68	
	Day 0 - $SQV_{0.05}$- $CP_3M_2T_2$	6							-18.69	-18.69	-18.69	-18.69	-18.69	-18.69	
	Day 45 - $SQV_{0.05}$- $CP_3M_2T_3$	3								-18.42	-18.42	-18.42	-18.42	-18.42	
	Day 0 - $SQV_{0.05}$-CP_5T_3	3									-17.49	-17.49	-17.49	-17.49	-17.49
	Day 45 - $SQV_{0.05}$- $CP_3M_2T_2$	6										-17.17	-17.17	-17.17	-17.17
	Day 45 - $SQV_{0.05}$- $CP_3M_2T_3$	3											-16.78	-16.78	-16.78
	Day 45 - $SQV_{0.05}$- $CP_3M_2T_2$	6												-15.60	-15.60
	Day 0 - $SQV_{0.05}$- $CP_3M_2T_3$	3													-13.40
	Sig.		**.221**	**.058**	**.050**	**.135**	**.062**	**.058**	**.075**	**.066**	**.057**	**.071**	**.085**	**.172**	**.280**

Table B.25 – Statistical analysis of the encapsulation efficiency, in the ultrasonication ( ) and hot HPH ( ), over the 3 month evaluation.

Formulation		N	Subset for alpha = 0.05
			1
Encapsulation Efficiency [%]	**Day 90 - SQV-SLN**	6	72.0
	Day 60 - SQV-SLN	6	79.1
	Day 90 - SQV-NLC	6	80.2
	Day 30 - SQV-SLN	6	81.8
	Day 30 - SQV-NLC	6	87.4
	Day 60 - SQV-NLC	6	87.9
	Day 0 - SQV-SLN	6	92.4
	Day 0 - SQV-NLC	6	93.7
	Sig.		**.180**

Table B.26 - Statistical analysis of cell viability under different conditions studied in the MTT assay.

Formulation		N	Subset for alpha = 0.05			
			1	2	3	4
Viability [%]	**Triton x-100 (2%)**	3	6.7			
	DMSO (10%)	3		30.1		
	SLN (25 µM)	3		30.4		
	SQV-SLN (25 µM)	3		31.4		
	SQV-SLN (2.5 µM)	3			78.1	
	SLN (2.5 µM)	3			80.9	80.9
	NLC (25 µM)	3			89.1	89.1
	SQV-NLC (25 µM)	3			91.5	91.5
	SQV (25 µM)	3			94.9	94.9
	NLC (2.5 µM)	3			95.8	95.8
	SQV-NLC (2.5 µM)	3				96.1
	SQV (2.5 µM)	3				98.1
	Sig.		**1.000**	**1.000**	**.055**	**.068**

Table B.27 - Statistical analysis of cellular cytotoxicity under different conditions studied in the PI assay.

Formulation		N	Subset for alpha = 0.05		
			1	2	3
Cytotoxicity [%]	**Untreated cell**	4	5.1		
	SQV	4	7.3		
	NLC	4	8.9		
	SQV-NLC	4	10.0		
	SQV-SLN	4		25.7	
	SLN	4		26.4	
	DMSO (10%)	4		29.0	
	Triton x-100 (2%)	4			68.0
	Sig.		**.246**	**.710**	**1.000**

References

1. Louis, D.N., et al., *The 2007 WHO Classification of Tumours of the Central Nervous System.* Acta Neuropathologica, 2007. **114**(2): p. 97-109.
2. Woodworth, G.F., et al., *Emerging insights into barriers to effective brain tumor therapeutics.* Front Oncol, 2014. **4**: p. 126.
3. Juratli, T.A., G. Schackert, and D. Krex, *Current status of local therapy in malignant gliomas--a clinical review of three selected approaches.* Pharmacol Ther, 2013. **139**(3): p. 341-58.
4. Kreuter, J., *Application of nanoparticles for the delivery of drugs to the brain.* International Congress Series, 2005. **1277**: p. 85-94.
5. Reardon, D.A., et al., *Recent advances in the treatment of malignant astrocytoma.* J Clin Oncol, 2006. **24**(8): p. 1253-65.
6. Popescu, I.D., et al., *Potential serum biomarkers for glioblastoma diagnostic assessed by proteomic approaches.* Proteome Sci, 2014. **12**(1): p. 47.
7. Woo, S.R., et al., *KML001, a telomere-targeting drug, sensitizes glioblastoma cells to temozolomide chemotherapy and radiotherapy through DNA damage and apoptosis.* 2014. **2014**: p. 747415.
8. Costa, A.S.A., et al. *Factores de prognóstico, sobrevivênvia global e sobrevivênvia livre de progressão do glioblastoma multiforme*. 2011 01-11-2015]; Available from: http://www.sponcologia.pt/wp-content/uploads/2012/03/T079.pdf.
9. Aslan, B., et al., *NANOTECHNOLOGY IN CANCER THERAPY.* Journal of drug targeting, 2013. **21**(10): p. 904-913.
10. Jain, K.K., *Use of nanoparticles for drug delivery in glioblastoma multiforme.* Expert Rev Neurother, 2007. **7**(4): p. 363-72.
11. Egusquiaguirre, S.P., et al., *Nanoparticle delivery systems for cancer therapy: advances in clinical and preclinical research.* Clin Transl Oncol, 2012. **14**(2): p. 83-93.
12. Chow, W.A., C. Jiang, and M. Guan, *Anti-HIV drugs for cancer therapeutics: back to the future?* Lancet Oncol, 2009. **10**(1): p. 61-71.
13. Monini, P., et al., *Antitumour effects of antiretroviral therapy.* Nat Rev Cancer, 2004. **4**(11): p. 861-75.
14. Gupta, A.K., et al., *HIV protease inhibitors block Akt signaling and radiosensitize tumor cells both in vitro and in vivo.* Cancer Res, 2005. **65**(18): p. 8256-65.
15. Pajonk, F., et al., *The human immunodeficiency virus (HIV)-1 protease inhibitor saquinavir inhibits proteasome function and causes apoptosis and radiosensitization in non-HIV-associated human cancer cells.* Cancer Res, 2002. **62**(18): p. 5230-5.
16. Donia, M., et al., *In vitro and in vivo anticancer action of Saquinavir-NO, a novel nitric oxide-derivative of the protease inhibitor saquinavir, on hormone resistant prostate cancer cells.* Cell Cycle, 2011. **10**(3): p. 492-9.
17. Ghosh, S., M. Basu, and S.S. Roy, *ETS-1 protein regulates vascular endothelial growth factor-induced matrix metalloproteinase-9 and matrix metalloproteinase-13 expression*

in human ovarian carcinoma cell line SKOV-3. J Biol Chem, 2012. **287**(18): p. 15001-15.
18. Timeus, F., et al., *In vitro anti-neuroblastoma activity of saquinavir and its association with imatinib.* Oncol Rep, 2012. **27**(3): p. 734-40.
19. Beloqui, A., et al., *Mechanism of transport of saquinavir-loaded nanostructured lipid carriers across the intestinal barrier.* J Control Release, 2013. **166**(2): p. 115-23.
20. Amidon, G.L., et al., *A theoretical basis for a biopharmaceutic drug classification: the correlation of in vitro drug product dissolution and in vivo bioavailability.* Pharm Res, 1995. **12**(3): p. 413-20.
21. Kuo, Y.C. and C.Y. Chung, *Solid lipid nanoparticles comprising internal Compritol 888 ATO, tripalmitin and cacao butter for encapsulating and releasing stavudine, delavirdine and saquinavir.* Colloids Surf B Biointerfaces, 2011. **88**(2): p. 682-90.
22. Mahajan, S.D., et al., *Enhancing the delivery of anti retroviral drug "Saquinavir" across the blood brain barrier using nanoparticles.* Curr HIV Res, 2010. **8**(5): p. 396-404.
23. Kumar, V.P. and Y. Sunandamma, *New RP - HPLC Method Development and validation for Analysis of Protease Inhibitor Saquinavir.* International Journal of Research in Pharmaceutical and Biomedical Sciences, 2011. **2**: p. 301-303.
24. Kuo, Y.C. and H.H. Chen, *Entrapment and release of saquinavir using novel cationic solid lipid nanoparticles.* Int J Pharm, 2009. **365**(1-2): p. 206-13.
25. *Saquinavir mesylate*. [cited 2014 19-11-2014]; Available from: http://www.glentham.com/en/products/product/GP7183/.
26. Kuo, Y.C. and C.Y. Kuo, *Electromagnetic interference in the permeability of saquinavir across the blood-brain barrier using nanoparticulate carriers.* Int J Pharm, 2008. **351**(1-2): p. 271-81.
27. Griffin, B.T. and C.M. O'Driscoll, *A comparison of intestinal lymphatic transport and systemic bioavailability of saquinavir from three lipid-based formulations in the anaesthetised rat model.* J Pharm Pharmacol, 2006. **58**(7): p. 917-25.
28. Pathak, S.M., et al., *Development and validation of a reversed-phase liquid chromatographic method with fluorescence detection for the study of Saquinavir pharmacokinetics in rat plasma.* Analytica Chimica Acta, 2007. **594**(2): p. 248-256.
29. Bachmeier, C.J., et al., *Quantitative Assessment of HIV-1 Protease Inhibitor Interactions with Drug Efflux Transporters in the BloodYBrain Barrier.* Pharmaceutical Research, 2005. **22**: p. 1259-1267.
30. Kuo, Y.C. and F.L. Su, *Transport of stavudine, delavirdine, and saquinavir across the blood-brain barrier by polybutylcyanoacrylate, methylmethacrylate-sulfopropylmethacrylate, and solid lipid nanoparticles.* Int J Pharm, 2007. **340**(1-2): p. 143-52.
31. Gomes, M.J., J. Neves, and B. Sarmento, *Nanoparticle-based drug delivery to improve the efficacy of antiretroviral therapy in the central nervous system.* Int J Nanomedicine, 2014. **9**: p. 1757-69.
32. Strazielle, N. and J.F. Ghersi-Egea, *Factors affecting delivery of antiviral drugs to the brain.* Rev Med Virol, 2005. **15**(2): p. 105-33.
33. Kreuter, J., *Nanoparticulate systems for brain delivery of drugs.* Adv Drug Deliv Rev, 2001. **47**(1): p. 65-81.
34. Abbott, N.J., L. Ronnback, and E. Hansson, *Astrocyte-endothelial interactions at the blood-brain barrier.* Nat Rev Neurosci, 2006. **7**(1): p. 41-53.
35. Deeken, J.F. and W. Loscher, *The blood-brain barrier and cancer: transporters, treatment, and Trojan horses.* Clin Cancer Res, 2007. **13**(6): p. 1663-74.
36. Roy, U., et al., *Specific Increase in MDR1 Mediated Drug-Efflux in Human Brain Endothelial Cells following Co-Exposure to HIV-1 and Saquinavir.* PLoS ONE, 2013. **8**(10): p. e75374.

37. Mallipeddi, R. and L.C. Rohan, *Progress in antiretroviral drug delivery using nanotechnology.* Int J Nanomedicine, 2010. **5**: p. 533-47.
38. Beloqui, A., et al., *Dextran-protamine coated nanostructured lipid carriers as mucus-penetrating nanoparticles for lipophilic drugs.* Int J Pharm, 2014. **468**(1-2): p. 105-11.
39. Sharma, A., N. Jain, and R. Sareen, *Nanocarriers for Diagnosis and Targeting of Breast Cancer*. BioMed Research International, 2013. **2013**: p. 960821.
40. Wang, Y., P. Brown, and Y. Xia, *Nanomedicine: Swarming towards the target.* Nat Mater, 2011. **10**(7): p. 482-483.
41. Bazak, R., et al., *Passive targeting of nanoparticles to cancer: A comprehensive review of the literature*. Mol Clin Oncol, 2014. **2**(6): p. 904-908.
42. Biswas, S. and V.P. Torchilin, *Nanopreparations for organelle-specific delivery in cancer*. Advanced Drug Delivery Reviews, 2014. **66**: p. 26-41.
43. Souto, E.B. and C.M. Lopes, *Novas formas farmacêuticas para administração de fármacos*. 2011: Universidade Fernando Pessoa.
44. Lee, G., et al., *Preparation and Characterization of Bis-ethylhexyloxyphenolmethoxyphenyltriazine (BEMT) Loaded Solid Lipid Nano-particles (SLN).* J. Ind. Eng. Chem, 2007. **13**: p. 1180-1187.
45. Kaur, T. and R. Slavcev, *Solid Lipid Nanoparticles: Tuneable Anti-Cancer Gene/Drug Delivery Systems*, in *Novel Gene Therapy Approaches*, M. Wei and D. Good, Editors. 2013, InTech. p. 53-73.
46. Weiss, J., et al., *Solid Lipid Nanoparticles as Delivery Systems for Bioactive Food Components.* Food Biophysics, 2008. **3**(2): p. 146-154.
47. Weissig, V., T.K. Pettinger, and N. Murdock, *Nanopharmaceuticals (part 1): products on the market.* Int J Nanomedicine, 2014. **9**: p. 4357-73.
48. Mansour, H.M., C. Park, and R. Bawa, *Design and development of approved nanopharmaceutical products*, in *Handbook of Clinical Nanomedicine*, R. Bawa, G.F. Audette, and I. Rubinstein, Editors. 2014. p. 1-33.
49. Bawa, R., *FDA and Nanotech: Baby Steps Lead to Regulatory Uncertainty*, in *Bio-Nanotechnology*. 2013, Blackwell Publishing Ltd. p. 720-732.
50. Bawarski, W.E., et al., *Emerging nanopharmaceuticals.* Nanomedicine: Nanotechnology, Biology and Medicine, 2008. **4**(4): p. 273-282.
51. Loxley, A., *Solid Lipid Nanoparticles for the Delivery of Pharmaceutical Actives.* Drug Delivery Technology, 2009. **9**.
52. Silva, A.C., *Solid lipid nanoparticles (SLN) for oral delivery of Risperidone*, in *Faculty of Pharmacy*. 2012, University of Porto.
53. Mehnert, W. and K. Mäder, *Solid lipid nanoparticles: Production, characterization and applications.* Advanced Drug Delivery Reviews, 2001. **47**(2–3): p. 165-196.
54. Ruktanonchai, U., et al., *The effect of cetyl palmitate crystallinity on physical properties of gamma-oryzanol encapsulated in solid lipid nanoparticles.* Nanotechnology, 2008. **19**(9): p. 095701.
55. Tamjidi, F., et al., *Nanostructured lipid carriers (NLC): A potential delivery system for bioactive food molecules.* Innovative Food Science & Emerging Technologies, 2013. **19**: p. 29-43.
56. Garud, A., D. Singh, and N. Garud, *Solid Lipid Nanoparticles (SLN): Method, Characterization and Applications.* International Current Pharmaceutical Journal, 2012. **1**: p. 384-393.
57. Souto, E.B., et al., *Nanopartículas de lipídios sólidos: métodos clássicos de produção laboratorial*. Quím. Nova, 2011. **34**: p. 1762-1769.
58. Freitas, C. and R.H. Mullera, *Spray-drying of solid lipid nanoparticles (SLN TM).* Eur J Pharm Biopharm, 1998. **46**(2): p. 145-51.
59. Nasrollahi, S.A., A.R. Abbasian, and E.S. Farboud, *In vitro comparison of simple tretinoin-cream and cream loaded with tretinoin-SLN.* journal of Pharmaceutical Technology and Drug Research, 2013. **2**(1).

60. Kamble, M., et al., *SOLID LIPID NANOPARTICLES AND NANOSTRUCTURED LIPID CARRIERS – AN OVERVIEW.* INTERNATIONAL JOURNAL OF PHARMACEUTICAL, CHEMICAL AND BIOLOGICAL SCIENCES, 2012. **2**: p. 681-691.
61. Uner, M. and G. Yener, *Importance of solid lipid nanoparticles (SLN) in various administration routes and future perspectives.* Int J Nanomedicine, 2007. **2**(3): p. 289-300.
62. Park, K., *Transport of nanostructured lipid carriers across the intestinal barrier.* J Control Release, 2013. **166**(2): p. 195.
63. Fahning, B.M. and E.B. Lobão, *Nanotecnologia aplicada a fármacos*, in *Faculdade Católica Salesiana do Espírito Santo*. 2011: Vitória. p. 98.
64. Yang, S., et al., *Body Distribution of Camptothecin Solid Lipid Nanoparticles After Oral Administration.* Pharmaceutical Research, 1999. **16**(5): p. 751-757.
65. Zara, G.P., et al., *PHARMACOKINETICS OF DOXORUBICIN INCORPORATED IN SOLID LIPID NANOSPHERES (SLN).* Pharmacological Research, 1999. **40**(3): p. 281-286.
66. Ryan, J.A. *Introduction to animal cell culture.* 2008 10-09-2015]; Available from: http://download.bioon.com/view/upload/month_0806/20080626_a9b77d7f680657adb5cffghuKfNApqmK.attach.pdf.
67. Cruz, M., et al., *Modelos experimentais em oncologia: O contributo da cultura de células para o conhecimento da biologia do cancro.* Revista Portuguesa de Pneumologia, 2009. **15**(04): p. 669-682.
68. Daguano, K.M., C. Santos, and S.O. Rogero, *Citotoxicity analysis of bioceramics for use in systems of implantations.* Matéria (Rio J.) 2007. **12**: p. 134 – 139.
69. Kroll, A., et al., *Current in vitro methods in nanoparticle risk assessment: limitations and challenges.* Eur J Pharm Biopharm, 2009. **72**(2): p. 370-7.
70. Wissing, S.A., O. Kayser, and R.H. Muller, *Solid lipid nanoparticles for parenteral drug delivery.* Adv Drug Deliv Rev, 2004. **56**(9): p. 1257-72.
71. Tzachev, C.T. and H.L. Svilenov, *Lipid Nanoparticles at the Current Stage and Prospects – A Review Article.* International Journal of Pharmaceutical Sciences Review and Research, 2013. **18**: p. 103-115.
72. *A Basic Guide to Particle Characterization*, M.I. Worldwide, Editor. 2012. p. 1-25.
73. *Dynamic light scattering*. 2014 [cited 2014 19-05-2014]; Available from: https://en.wikipedia.org/wiki/Dynamic_light_scattering.
74. Martins, S., *Drug delivery across blood-brain barrier by means of intravenous administration of lipid nanoparticles*, in *Faculty of Pharmacy* 2012, University of Porto.
75. Neves, A.R., et al., *Novel resveratrol nanodelivery systems based on lipid nanoparticles to enhance its oral bioavailability.* Int J Nanomedicine, 2013. **8**: p. 177-87.
76. *A basic guide to particle characterization*, M.I. Worldwide, Editor. 2015. p. 1-24.
77. *Cryogenic Specimen Preparation Principles*. 2015 [cited 2015 12-05-2015]; Available from: http://www.emsdiasum.com/microscopy/technical/datasheet/cryosem_adv.aspx.
78. *Cryo-scanning electron microscope (Cryo-SEM)*. 2013 12-05-2015]; Available from: http://www.ammrf.org.au/myscope/sem/background/practical/types/cryo-sem.php
79. *Zeta Potential: A Complete Course in 5 Minutes*, Z.-M. Inc., Editor. p. 1-8.
80. *PRINCIPIO DELL'ELECTROPHORETIC LIGHT SCATTERING.* 23-05-2014]; Available from: http://alfatest.it/pagina.php?p=71.
81. *Differential Scanning Calorimetry (DSC): FREQUENTLY ASKED QUESTIONS*, in *A Beginner's Guide*, I. PerkinElmer, Editor. 2014: Waltham, MA 02451 USA. p. 1-9.
82. *TA INSTRUMENTS DIFFERENTIAL SCANNING CALORIMETER (DSC).* p. 1-10.
83. Gill, P., T.T. Moghadam, and B. Ranjbar, *Differential Scanning Calorimetry Techniques: Applications in Biology and Nanoscience.* Journal of Biomolecular Techniques : JBT, 2010. **21**(4): p. 167-193.

84. *High Pressure Liquid Chromatography*, T. Isco, Editor. 2012: Lincoln, Nebraska, 68501 USA.
85. Ribani, M., et al., *VALIDAÇÃO EM MÉTODOS CROMATOGRÁFICOS E ELETROFORÉTICOS.* Química Nova, 2004. **27**: p. 771-780.
86. Administration, U.S.F.a.D., *Reviewer Guidance: Validation of Chromatographic Methods*, C.f.D.E.a.R. (CDER), Editor. 1994: Rockville.
87. (ICH), I.C.o.H., *Validation of Analytical Procedures: Text and Methodology, Q2 (R1) (CPMP/ICH/381/95).* European Medicines Agency, 1995: p. 1-15.
88. *DESENVOLVIMENTO DE MÉTODOS ANALÍTICOS DE HPLC NA INDÚSTRIA FARMACÊUTICA*, BioPharmacos, Editor. 2009. p. 1-13.
89. Eloy, J.O., et al., *Desenvolvimento e validação de um método analítico por CLAE para quantificação de ácido ursólico em dispersões sólidas.* Química Nova, 2012. **35**: p. 1036-1040.
90. Das, S., W.K. Ng, and R.B. Tan, *Sucrose ester stabilized solid lipid nanoparticles and nanostructured lipid carriers: I. Effect of formulation variables on the physicochemical properties, drug release and stability of clotrimazole-loaded nanoparticles.* Nanotechnology, 2014. **25**(10): p. 105101.
91. Bernhart, E., et al., *Interference with distinct steps of sphingolipid synthesis and signaling attenuates proliferation of U87MG glioma cells.* Biochemical Pharmacology, 2015. **96**(2): p. 119-130.
92. *Subculture of Adherent Cell Lines*, in *Fundamental Techniques in Cell Culture*. 2010: Laboratory Handbook-2nd Edition.
93. Alves, E.A. and A.C. Guimarães, *Cultivo celular*, in *Conceitos e Métodos para a Formação de Profissionais em Laboratórios de Saúde*, E. Molinaro, L. Caputo, and R. Amendoeira, Editors. 2010. p. 215-253.
94. Garcia, R.C., *Efeitos neurodegenerativos da metilecgonidina e da cocaína em cultura celular primária de hipocampo.*, in *Faculdade de Ciências Farmacêuticas*. 2009, Universidade de São Paulo: São Paulo. p. 114.
95. Wållberg, F., *Flow cytometry for bioprocess control.*, in *Department of Biotechnology*. 2004: Stockholm, Sweden.
96. Biosciences, B., *Introduction to Flow Cytometry: A Learning Guide*. 2000. p. 1-52.
97. Bernhart, E., et al., *Interference with distinct steps of sphingolipid synthesis and signaling attenuates proliferation of U87MG glioma cells.* Biochem Pharmacol, 2015. **96**(2): p. 119-30.
98. Panopoulos, A., et al., *Glioblastoma motility occurs in the absence of actin polymer.* Mol Biol Cell, 2011. **22**(13): p. 2212-20.
99. Chaturvedi, S.P. and V. Kumar, *Production Techniques of Lipid Nanoparticles: A Review.* Research Journal of Pharmaceutical, Biological and Chemical Sciences, 2012. **3**(3): p. 525-541.
100. Souto, E.B., J.F. Fangueiro, and R.H. Müller, *Fundamentals of Pharmaceutical Nanoscience,*. Springer New York Heidelberg Dordrecht London ed. 2013.
101. Gomes, M.J., et al., *Lipid nanoparticles for topical and transdermal application for alopecia treatment: development, physicochemical characterization, and in vitro release and penetration studies.* Int J Nanomedicine, 2014. **9**: p. 1231-42.
102. Xie, S., et al., *Preparation, characterization and pharmacokinetics of enrofloxacin-loaded solid lipid nanoparticles: influences of fatty acids.* Colloids Surf B Biointerfaces, 2011. **83**(2): p. 382-7.
103. Rosa, N., *Development of Nanoparticles Loaded with Bioactive Compounds for Application as Nutraceuticals*, in *Faculty of Engineering*. 2011, University of Porto. p. 94.
104. Pizzol, C.D., et al., *Influence of Surfactant and Lipid Type on the Physicochemical Properties and Biocompatibility of Solid Lipid Nanoparticles.* International Journal of Environmental Research and Public Health, 2014. **11**(8): p. 8581-8596.

105. Balakrishnan, V., et al., *In Vitro Evaluation of Cytotoxicity of Colloidal Amorphous Silica Nanoparticles Designed for Drug Delivery on Human Cell Lines.* Journal of Nanomaterials, 2013. **2013**: p. 1-8.